ESTIMATION OF THE RADIAL VARIATION OF SEISMIC VELOCITIES AND DENSITY IN THE EARTH

Thesis by

Thomas Hillman Jordan

In Partial Fulfillment of the Requirements

for the Degree of

Doctor of Philosophy

California Institute of Technology

Pasadena, California

1973

(Submitted August 4, 1972)

ACKNOWLEDGMENTS

The work presented in this thesis is the result of my long and fruitful association with Dr. Don L. Anderson. Without his constant guidance and unwaivering support this research could not have been completed. His broad knowledge was my most valuable resource. Dr. Freeman Gilbert impressed on me the need for a systematic approach to the inverse problem. My frequent discussions with him were a source of ideas and encouragement.

To my colleague, Mr. J. Bernard Minster, I owe a special word of gratitude. He has worked with me on many aspects of this research, and his contribution to the theory presented in Chapter 2 has been substantial.

Mr. Martin Smith coded the normal mode routines and helped me during the initial stages of this research. Mr. Bruce Julian kindly provided me with his travel-time routines. Miss Robin Springer, Mr. Michael Abrams, and Mr. Laszlo Lenches assisted in the preparation of the manuscript.

This research was supported by the Advanced Research Projects Agency of the Department of Defense and was monitored by the Air Force Office of Scientific Research under contract F44620-72-C-0078.

ABSTRACT

An inversion procedure is developed to estimate the radial variations of compressional velocity, shear velocity, and density in the Earth. The radial distributions are defined as spherically symmetric averages of the actual distributions in the laterally heterogeneous Earth, and the nature of the averaging implied by averaging certain sets of eigenperiod and travel-time data is examined. For travel-time data, the spherical averaging yields the Terrestrial Monopole if the data sample a distribution derived from a uniform distribution of sources and receivers. Since this is difficult to obtain for absolute times, differential travel times are used to constrain the velocities. It is shown that the bias inherent in available sets of differential travel-time data is considerably less than that in equivalent sets of absolute travel-time data, if the phase combination is suitably chosen. Observations are presented for the phase combinations PcP-P, ScS-S, P'(AB)-P'(DF), and P'(BC)-P'(DF).

The inversion algorithm developed is based on a linear approximation to the perturbation equations and is shown to provide a stable method for estimating the radial distributions of velocities and density from a finite number of inaccurate data. The linear inversion theory presented is complete; it allows one to estimate the resolving power of the data and the resolvability of specified features in the model.

Three estimates of the radial distributions are derived using an extensive set of eigenperiod and travel-time data. One model, designated model B1, fits 127 of the 177 eigenperiods of the Dziewonski-Gilbert set within their formal 95% confidence intervals. This model satisfies extensive sets of auxillary data as well.

It is shown from resolving power calculations that little information is lost by using differential travel times in lieu of absolute times. It is demonstrated that the nature of the averaging in the estimation procedure for given sets of gross Earth data can be improved by judicious specification of the norm on the space of models.

TABLE OF CONTENTS

LIST OF FIGURES

LIST OF TABLES

Chapter 1

INTRODUCTION

1.1 Statement of the problem. This thesis addresses the problem of estimating the average radial distributions of compressional velocity, shear velocity, and density in the Earth from the observations of the Earth's mass, moment of inertia, body wave travel times, and periods of free oscillation.

1.2 Motivation. Seismological investigation of the structure of the Earth began with Oldham's correct identification of compressional, shear, and surface waves on seismograms of the Assam earthquake of 1897. Application of the theory of elastic wave propagation to the problem of interpreting seismological data proceeded rapidly, culminating with the publication of the Jeffreys-Bullen and Gutenberg-Richter tables. Bullen [1963, p.3] remarks:

> The period from 1911 to 1940 saw the application of seismological data to problems of the Earth's internal structure to a quite remarkable degree. The period started with the vaguest notions about a molten central core and finished with well-determined values of the density, pressure, compressibility, rigidity, and gravity throughout practically the whole Earth.

Despite the progress made in the first part of this century, the problem of describing the variations of elastic parameters and density in the Earth remains an area of vigorous geophysical research. The interest in refining the descriptions currently available is not motivated by some misplaced concern for detail. Rather, it is dictated by the critical dependence on these parameters of nearly every inference about the composition and state of the Earth's interior. Much of the attention recently refocused on the problem of Earth structure has been stimulated by three technological advances: the extension of the observable seismic bandwidth to ultra-long periods, the development of laboratory techniques for measuring material properties at high pressures and temperatures, and the advent of the computer.

Ultra-long period seismology, heralded by Benioff's design of the strain seismometer, has provided an important new source of data, the periods of the Earth's free oscillation. Prior to mid-century, the only direct information about the density distribution in the Earth came from measurements of the Earth's gravity field and dynamic response. In particular, Bullen's classical density models were constrained only by the mean density and moment of inertia. The measurements of surface-wave velocities commencing in the 1950's and the reliable observations of free oscillation periods reported since the great Chilian earthquake of 1960 have yielded valuable independent constraints on the possible variations of density.

Additional impetus has come from our increasing knowledge of the behavior of materials at pressures and temperatures appropriate to the Earth's deep interior. To infer the Earth's composition and state, we must compare the density and velocity distributions found from geophysical data with observed material behavior at known conditions. Recent improvements in the precision and range of static compression, ultrasonic, and shock-wave experiments have set the stage for this comparison.

Finally, the problem of refining the estimates of Earth structure is feasibly approached only with the aid of modern computing systems. To evaluate the success of any model, the data functionals for that model must be calculated and compared with observations. This can be a laborious task. For example, calculating the eigenperiod of a spheroidal mode requires many numerical integrations of a sixth-order system of differential equations; hand computation of the currently well-observed eigenperiods for even one realistic Earth model is a lifetime effort. However, it takes only a few minutes on a fast computer.

1.3 Approach. To date, efforts towards modeling physical parameters in the Earth have involved only very simple, usually one-dimensional representations. A useful and often adequate approximation is to assume that the Earth behaves as a spherically symmetric, non-rotating, elastic and isotropic body to small mechanical excitations in the seismic frequency band (10^{-4} Hz - 10 Hz). We shall adopt these assumptions, thus allowing us to select an Earth model by specifying the compressional velocity, shear velocity, and density as functions of radius alone.

With these assumptions, it becomes feasible to solve the forward problem for a number of gross Earth data functionals (data functionals that depend on the radial variations) for which data are available. These include the Earth's mass and moment, its eigenperiods, and the ray-theoretical travel times of signals propagating through its interior. Our approach to the inverse problem of estimating the model given estimates of these data functionals follows closely the treatment of Backus and Gilbert [1967, 1968, 1969, 1970]. The inversion theory used is developed in Chapter 2.

Of course, the observations reflect the fact that the Earth is a rotating, laterally-varying body. The precision with which the data can now be measured is such that contamination by these departures from our assumptions can cause serious incompatibility and bias. We shall try to reduce these effects by using averaged sets of free oscillation and travel-time data. The motivation for this is discussed in Chapter 3.

Unfortunately, with the present-day distribution of seismic sources and receivers it is not possible to sample uniformly the velocity structure of the Earth's upper layers using body waves. For this reason averaged sets of absolute travel-time data generally are biased. At teleseismic distances this bias enters into the distance-time expression as approximately a constant term, called by seismologists the "baseline error". To reduce as much as possible the baseline error without eliminating the valuable information contained in travel-time data, we shall use in the inversion calculations differential travel times; that is, the differences between the arrival times of two body phases. If the phase combinations measured are judiciously chosen, the differential times will be relatively unbiased. In particular, baseline errors will cancel.

In Chapter 4 the use of differential travel times as gross Earth data is discussed. We also present in this chapter some observations of differential travel times useful in constraining the radial variations of seismic velocities.

These observations are combined in Chapter 5 with eigenperiod data and the observed mass and moment of inertia to derive estimates of the radial velocity and density distributions. Emphasis is placed on the construction of reasonable, but simple representations which are used to initiate the iterative inversion algorithm. This algorithm uses the inversion theory presented in Chapter 2 to provide a perturbation to the starting model which, in a sense that is well-defined, is the "smallest" necessary to satisfy the data. Therefore, the resulting representations will deviate in some least way from the starting model.

Chapter 2

INVERSION THEORY

2.1 Introduction. The task of deducing the constraints provided by observables on the variations of physical parameters in the Earth has been called the geophysical inverse problem. The mathematical formulation of this problem characterizes possible variations as entities in an abstract function space, each entity representing an Earth model. In particular a spherically symmetric, non-rotating, linearly elastic, and isotropic (SNREI[1]) Earth can be described by specifying the compressional velocity, the shear velocity, and the density as functions of radius. An observation is the value of a functional defined on this space of Earth models. Examples include the Earth's mass and moment of inertia, the measured travel times of seismic waves, and the observed periods of free oscillation. We will assume that the forward problem for each data functional has been solved: given any interesting Earth model the value of the data functional can be computed. In general the relationship between the data functional and the model is nonlinear.

Since the distributions of physical parameters are continuous on some interval and the number of data obtainable is necessarily finite, the inverse problem generally has no unique solution. Furthermore, the observations used as data are invariably contaminated by errors; only estimates of the values of data functionals for the

---

[1] The notation is due to Dahlen [1968].

Earth are available. Inaccuracies act to increase the ensemble of acceptable models. These circumstances, unfortunate for the geophysicist, make the problem mathematically interesting and motivate the inversion theory presented in this chapter.

A variety of techniques, both theoretical and computational, have been applied towards the solution of the geophysical inverse problem. One potentially powerful technique is the Monte Carlo method described in the geophysical context by Keilis-Borok and Yanovskaya [1967] and applied to the determination of SNREI Earth models by Press [1968,1970,1972]. Monte Carlo calculations utilize a random selection procedure to generate arbitrary models, test the models against a set of data, and display those that satisfy the data sufficiently well. The idea is to sample uniformly some region of the model space thought to contain the best representation of the Earth and generate a fairly complete catalogue of acceptable models. Properties of the real Earth would then be those common to this entire ensemble.

In practice Monte Carlo techniques face severe limitations. Even with the most advanced computing systems, the calculations are laborious and time consuming; the number of trials necessary to sample even very restricted regions of the model space is large. The more efficient algorithms such as the one used by Press [1972] require a sieve-like series of tests against the data: at each of several steps models are rejected or retained depending on how well they satisfy some subset of the data. It is not clear in what way these algorithms sample the model space.

A supposed advantage of the Monte Carlo method is that nonlinear data functionals can be used directly without resorting to linear estimation. However, for geophysical inverse problems that use mode data, complete recalculation of the eigenfrequencies for each generated model is economically unfeasible. Instead, first-order variational parameters are used [Press, 1972], eliminating the advantage of Monte Carlo over the linear prediction method.

At the present time the linear prediction method offers the most efficient and informative approach to the solution of the geophysical inverse problem. Basically, this method employs an iterative perturbation algorithm that approximates the difference between the sought representation of the Earth and some initial model as a particular solution to the finite system of linear, inhomogeneous, integral equations relating changes in the model to first-order changes in the data. The data functionals are computed for the starting model and subtracted from the observed data; the system of perturbation equations is solved, and the calculated perturbation is added to the starting model. This process is iterated until the data are satisfied. For the one-dimensional case, this algorithm is simply Newton's method.

The first-order approximation reduces the nonlinear problem to the problem of solving an underdetermined system of linear equations. A general and extensive theory for the solution of the underconstrained linear inverse problem for inaccurately known data has been developed by Backus and Gilbert [1967,1968,1970] in an important series of papers. The central concept in this theory is the following: although the exact solution cannot be computed because the information provided by the data is insufficient, it is possible to estimate accurately <u>linear averages</u> of the desired model. The task to which their theory is addressed is the constuction of an optimal inverse filter from the constraints imposed by the observations, through which the correct solution may be viewed. They show that there exists a tradeoff between the ability to resolve detail and the accuracy with which this detail can be estimated. These concepts represent a major contribution to the theory of linear estimation and will see wide use outside the geophysical inverse problem.

Presented here is a variation on the Backus-Gilbert theory that incorporates the stochastic inverse theory of Franklin [1970]. A particular, unique solution to the linear system is obtained by minimizing a specified quadratic measure of error. This quadratic form is the sum of two terms, a measure of the resolution of the estimate and a measure of its accuracy, parameterized to yield a Backus-Gilbert-type tradeoff curve. The generalized inverse of Penrose [1955] and Moore [1920] and the stochastic inverse of Franklin [1970] are shown to lie on this tradeoff curve, the stochastic inverse being, in one sense, an optimal point. Any particular solution computed by selecting a point on the tradeoff curve is shown to be an estimate of the correct solution convolved with a projection-like smoothing operator, termed here the response operator of the linear system. Convolving the response operator with delta functions yields Backus-Gilbert-type averaging kernels (except that they are not constrained to be unimodular).

One important aspect of the approach presented here is that the model space is generalized to a Hilbert space with a fairly arbitrary norm, or measure of length. In the application to the construction of velocity and density profiles in the Earth (Chapter 5) the operator defining the norm is chosen to be a "roughing" operator, i.e., the inverse of a smoothing operator. The advantages of generalizing the norm in this way are severalfold. Most importantly, it allows one to introduce information about the solution not directly contained in the data. The "rougher" the norm is, the smoother the particular solution will be. If one is confident, say, that the variation of elastic parameters in some region of the Earth is well-behaved, then the method allows a solution embodying this information (or prejudice) to be constructed. The roughing can be discontinuous - a convenient way to allow for the possibility, or reality, of discontinuities in the model. Also, by manipulating the norm on the model space one can control to some degree the localization of the averaging kernels. Finally, if the roughing operator is chosen to be unbounded (see section 2.6), then the Fréchet kernels for travel times, which are not square-integrable, are members of the model space (this is shown in section 4.2).

Necessarily this introduction has been heuristic and vague. The presentation in the remaining sections of this chapter will be more formal and assumes that the reader has a basic understanding of the Backus-Gilbert theory (see Gilbert [1972] for an elementary treatment).

2.2 Hilbert spaces of Earth models. A model of a spherically symmetric Earth of radius R is an ordered multiple of functions on the closed interval $[0,R]$. For example, each SNREI Earth model is described by the function triple $[v_p(r), v_s(r), \rho(r)]$, $0 \le r \le R$, where v_p is the compressional velocity, v_s is the shear velocity, and ρ is the density. Although constuction of SNREI Earth models is our ultimate goal, for the purposes of notational simplicity we retain in this chapter a general definition: a spherically symmetric Earth model $\mathbf{m}$ is an M-tuple of real-valued, piecewise-continuous functions $[m_1(r), m_2(r), \ldots, m_M(r)]$ defined and integrable on the interval $[0,R]$. The model $\mathbf{m}$ is a member of a vector space $\mathfrak{M}$ over the field of real numbers $\mathbf{R}$ if the vector sum of two models $\mathbf{m}+\mathbf{m}'$ is taken equal to $[m_1(r) + m_1'(r), m_2(r) + m_2'(r), \ldots, m_M(r) + m_M'(r)]$. Formally $\mathfrak{M}$ is the Cartesian product of M vector spaces, $\mathfrak{M} = \mathfrak{M}_1 \otimes \mathfrak{M}_2 \otimes \cdots \otimes \mathfrak{M}_M$. Each $\mathfrak{M}_i$, $i = 1,2,\ldots,M$, is the vector space over $\mathbf{R}$ of real, piecewise-continuous functions integrable with respect to a weight $w_i(r)$ on the interval $[0,R]$. The weighting function $w_i(r)$ must be strictly positive on $[0,R]$ but is otherwise arbitrary.[2]

A linear operator $\mathbf{L}: \mathfrak{M} \to \mathfrak{V}$ is a single-valued, linear mapping of $\mathfrak{M}$ into a vector space $\mathfrak{V}$. Any linear operator of interest to us here can be represented as an M x 1 array of linear operators

---

[2] Backus and Gilbert in their original 1967 paper used the volume measure $w_i(r) \propto r^2$. In this case the measure is singular at the origin; the domain of definition must be restricted to the semi-open interval $(0,R]$, and $\mathfrak{M}$ consists of functions regular at the origin. In subsequent papers by these authors [1968,1970] and in Chapter 5 of this work, $w_i(r)$ is chosen to be a constant.

$[\,\mathbf{L}_i : \mathfrak{M}_i \rightarrow \mathfrak{V};\ i = 1,2,\ldots,M]$, each characterized by a vector-valued integral kernel $L_i(r)$. For any $\mathbf{m} \in \mathfrak{M}$ the element $\mathbf{L}\cdot\mathbf{m} \in \mathfrak{V}$ can be computed by integration:

$$(2.2.1) \qquad \mathbf{L}\cdot\mathbf{m} = \sum_{i=1}^{M} \mathbf{L}_i\,\mathbf{m}_i = \sum_{i=1}^{M} \int_0^R L_i(r)\; m_i(r)\; w_i(r)\; dr$$

The weighting functions $w_i(r)$ should be chosen to render this product dimensionally homogeneous.

Much of the analysis in this chapter will involve manipulation of linear operators that map the model space into itself. Any interesting linear operator $\mathbf{L}: \mathfrak{M} \rightarrow \mathfrak{M}$ can be represented as an M x M array of operators $[\,\mathbf{L}_{ij}: \mathfrak{M}_i \rightarrow \mathfrak{M}_j;\ i,j = 1,2,\ldots,M]$ with scalar-valued integral kernels $L_{ij}(r,r')$. If $\mathbf{L}$ has eigenvalues (scalars λ such that $\mathbf{L}\cdot\psi = \lambda\psi$), then, because $\mathfrak{M}$ is defined over $\mathbf{R}$, they must be real.[3]

A class of operators whose eigenvalues are always real are the symmetric operators, for which $L(r,r') = L(r',r)$.[4] If the transpose of $\mathbf{L}$, denoted $\mathbf{L}^*$, is defined as the operator with kernel $L^*(r,r') = L(r',r)$, then $\mathbf{L}$ is symmetric if and only if $\mathbf{L} = \mathbf{L}^*$.

Associated with every symmetric operator $\mathbf{L}: \mathfrak{M} \rightarrow \mathfrak{M}$ is a unique, symmetric bilinear functional

$$(2.2.2) \qquad \lambda(\mathbf{m},\mathbf{m}') = \sum_{i,j=1}^{M} \int_0^R \int_0^R m_i(r) L_{ij}(r,r') m_j'(r') \cdot w_i(r)dr\; w_j(r')dr',$$

---

[3] Although the spaces we will consider are all real, the theory can be extended in a straightforward manner to spaces defined over the field of complex numbers, permitting the eigenvalues to be complex.

[4] Most statements made here are proved in Courant and Hilbert [1937].

and a unique quadratic form

$$\lambda(\mathbf{m}) = \lambda(\mathbf{m}, \mathbf{m}). \tag{2.2.3}$$

A symmetric operator and its corresponding bilinear and quadratic forms are said to be positive definite, positive semi-definite, or indefinite depending on whether $\lambda(\mathbf{m}) > 0$, $\lambda(\mathbf{m}) \geq 0$, or $\lambda(\mathbf{m}) \gtrless 0$ for all $\mathbf{m} \neq 0$.

Any symmetric, positive definite bilinear functional can be used as an inner product on $\mathfrak{M}$. The vector space $\mathfrak{M}$ with an inner product

$$\mathbf{m} \overset{L}{\cdot} \mathbf{m}' \equiv \lambda(\mathbf{m}, \mathbf{m}') \tag{2.2.4}$$

defines an inner product space $\mathfrak{M}_L$ which can be completed to a Hilbert space. The norm associated with this inner product is

$$||\mathbf{m}||_L \equiv \lambda^{1/2}(\mathbf{m}). \tag{2.2.5}$$

Any $\mathbf{m} \in \mathfrak{M}$ is a member of $\mathfrak{M}_L$ if

$$||\mathbf{m}||_L < \infty . \tag{2.2.6}$$

The super- and subscription of the inner product, the norm, and the Hilbert space are dropped for the special case $\mathbf{L} = \mathbf{I}$, the identity operator on $\mathfrak{M} : \mathbf{m} \cdot \mathbf{m}' \equiv \mathbf{m} \cdot \mathbf{I} \cdot \mathbf{m}' = \sum_i \int_0^R m_i(r)\, m_i'(r)\, w_i(r)\, dr$ and $||\mathbf{m}|| = (\mathbf{m} \cdot \mathbf{m})^{1/2}$.

For our purposes (indeed, for most physical problems) quadratic convergence is sufficient for the identification of vectors. That is, a sequence of vectors $\{\mathbf{m}_\alpha : \alpha = 1,2,\ldots\}$, members of $\mathfrak{M}$, is said to converge to the element $\mathbf{m} \in \mathfrak{M}$ if $\lim_{\alpha \to 0} ||\mathbf{m} - \mathbf{m}_\alpha|| = 0$.

2.3 The perturbation equations. Interesting data functionals such as the mass, moment of inertia, eigenfrequencies, and travel times of an SNREI Earth model are each Fréchet-differentiable. Paraphrasing Backus and Gilbert [1967, p.249] in our own notation, we say that a data functional D on $\mathfrak{M}$ is Fréchet-differentiable at a point $\mathbf{m}$ in $\mathfrak{M}$ if there exists a member $\mathbf{a}$ of $\mathfrak{M}$, determined by D and $\mathbf{m}$, such that for any member $\delta\mathbf{m}$ of $\mathfrak{M}$

$$(2.3.1) \qquad D(\mathbf{m}+\delta\mathbf{m}) = D(\mathbf{m}) + \mathbf{a}\cdot\delta\mathbf{m} + \varepsilon(\delta\mathbf{m})$$

where $\varepsilon(\delta\mathbf{m})\,||\delta\mathbf{m}||^{-1}$ approaches zero uniformly as $\delta\mathbf{m}$ approaches zero. The vector $\mathbf{a}$ is called the Fréchet kernel of D.

Associated with each ordered set $\mathscr{D}^N$ of N Fréchet-differentiable data functionals and each Earth model $\mathbf{m}$ are the linear perturbation equations

$$(2.3.2) \qquad \mathbf{a}_i\cdot\delta\mathbf{m} = \delta D_i \equiv D_i(\mathbf{m}+\delta\mathbf{m}) - D_i(\mathbf{m}), \quad i = 1,2,\ldots,N,$$

which are correct to first order in $\delta\mathbf{m}$. These equations can be written

$$(2.3.3) \qquad \mathbf{A}\cdot\delta\mathbf{m} = \delta\mathbf{d},$$

where $\mathbf{A} = \begin{bmatrix} \mathbf{a}_1 \\ \cdot \\ \cdot \\ \cdot \\ \mathbf{a}_N \end{bmatrix}$ and $\delta\mathbf{d} = \begin{bmatrix} \delta D_1 \\ \cdot \\ \cdot \\ \cdot \\ \delta D_N \end{bmatrix}$. The operator $\mathbf{A}$ maps a change in the model into a change in the data. This can be made accurate enough by making $\delta\mathbf{m}$ small enough. The vector $\delta\mathbf{d}$ is a member of the N-dimensional Euclidian space $\mathbf{E}^N$ associated with the set $\mathscr{D}^N$. The inner product between two vectors $\mathbf{d}$ and $\mathbf{d}'$ in E^N is written $\mathbf{d}\,\mathbf{d}'$ and equals $\sum_{i=1}^{N} \upsilon_i d_i d_i'$, the υ_i, $i = 1,2,..,N$, being positive weights rendering the inner product dimensionally homogeneous.

Suppose $\epsilon(\delta\mathbf{m}) \in E^N$ is the vector representing the error committed in the linear approximation (2.3.3). Then the constraint

$$(2.3.4) \qquad ||\epsilon(\delta\mathbf{m})|| < \xi, \ \xi > 0,$$

which limits the error to an open ball in E^N about the origin, defines for each point $\mathbf{m} \in \mathfrak{M}$ a subset of $\mathfrak{M}$ that is, in general, multiply connected. We will define the domain of $\mathbf{A}$ to be $\mathcal{D}(\xi,\mathbf{m})$, the simply connected part of this subset that includes the origin. All perturbations in $\mathcal{D}(\xi,\mathbf{m})$ map into a region $\mathcal{R}(\xi,\mathbf{m}) \subset E^N$, the range of $\mathbf{A}$, with an error whose norm is less than ξ. A vector $\mathbf{m}' \in \mathcal{D}(\xi,\mathbf{m}) + \mathbf{m}$ is said to be ξ-near $\mathbf{m}$.[5] Obviously, $\mathcal{R}(\xi,\mathbf{m}) \subset \mathfrak{R}(\mathbf{A})$, the range space of $\mathbf{A}$ (spanned by the eigenvectors of $\mathbf{A} \cdot \mathbf{A}^*$).

Given a set of N observations $\mathbf{d}_0$ and a starting model $\mathbf{m}_s$, we define $\delta\mathbf{d} = \mathbf{d}_0 - \mathbf{d}(\mathbf{m}_s)$. Now the linear inverse problem can be formally stated:

We seek to estimate the difference $\delta\mathbf{m}_0$ between the representation $\mathbf{m}_0$ of the "real" Earth and the initial guess $\mathbf{m}_s$ by an application of some bounded linear operator $\mathbf{L}: E^N \rightarrow \mathfrak{M}$ to the data residual vector $\delta\mathbf{d}$.

If $\mathbf{m}_0$ is an exact representation of the Earth, if the functionals in $\mathscr{D}^N$ depend linearly on the model, and if the data are perfectly

---

[5] This is a variation on the terminology used by Backus and Gilbert [1970, p.125].

known, then $\delta\mathbf{m}_0$ can be expected to satisfy equation (2.3.3).[6] If the set $\mathscr{D}^N$ contains nonlinear data functionals (such as travel times and eigenfrequencies) and if $\mathbf{m}_0$ is ξ-near $\mathbf{m}_s$, then $\delta\mathbf{m}_0$ can be expected to satisfy (2.3.3) with an error of norm less than ξ, again assuming $\mathbf{d}_0$ and $\mathbf{m}_0$ are exact. Thus, in the nonlinear case, the success of the estimate will depend largely upon proper specification of the starting model.

2.4 The generalized inverse. For finite N the problem of computing the solution to (2.3.3) is ill-posed in the sense that the solution is not unique. In fact, it is obvious that $\mathbf{A}$ possesses a null manifold $\mathfrak{N}(\mathbf{A})$ of infinite dimension. If $\mathbf{h}\in\mathfrak{N}(\mathbf{A})$, then it solves the homogeneous equation $\mathbf{A}\cdot\mathbf{h} = 0$. The general solution to equation (2.3.3) can be written

$$(2.4.1) \qquad \delta\mathbf{m} = \overline{\delta\mathbf{m}} + \sum_{n=1}^{\infty} \alpha_n \mathbf{h}_n,$$

where $\overline{\delta\mathbf{m}}$ is any particular solution to (2.3.3), $\{\mathbf{h}_n : n = 1,2,\ldots\}$ is a basis for $\mathfrak{N}(\mathbf{A})$, and the coefficients α_n, $n = 1,2,\ldots$, are arbitrary scalars. If $\mathfrak{R}(\mathbf{A}^*)$ is the range space of $\mathbf{A}^*$, the space spanned by the set of Fréchet kernels $\{\mathbf{a}_i : i = 1,2,\ldots,N\}$, then $\mathfrak{M}$ is the direct sum of $\mathfrak{N}(\mathbf{A})$ and $\mathfrak{R}(\mathbf{A}^*)$.

One particular and interesting solution to (2.3.3) is given by the generalized inverse of $\mathbf{A}$ [Moore, 1920; Tseng, 1949; Bjerhammar, 1952; Penrose 1955]. The operator $\mathbf{A}$ has a unique generalized inverse

---

[6] Implicit in this statement is the assumption that $\mathbf{d}_0\in\mathfrak{R}(\mathbf{A})$.

$A^{\dagger}: E^N \rightarrow \mathfrak{M}$ such that

$$(2.4.2) \qquad \begin{aligned} A \cdot A^{\dagger} &= P_{\mathfrak{R}(A)}, \\ A^{\dagger} A &= P_{\mathfrak{R}(A^*)}, \end{aligned}$$

where $P_{\mathfrak{R}(A)}$ is the orthogonal projection operator mapping E^N onto $\mathfrak{R}(A)$, and $P_{\mathfrak{R}(A^*)}$ is the orthogonal projection operator mapping $\mathfrak{M}$ onto $\mathfrak{R}(A^*)$.[7] The estimate

$$(2.4.3) \qquad \overline{\delta \mathbf{m}} = A^{\dagger}\, \delta d$$

is the unique solution that minimizes the norm $||\delta\mathbf{m}||$. Substituting (2.3.3) into (2.4.3) and using (2.4.2) we obtain

$$(2.4.4) \qquad \overline{\delta \mathbf{m}} = A^{\dagger} A \cdot \delta d = P_{\mathfrak{R}(A^*)} \cdot \delta \mathbf{m}.$$

Therefore, the solution given by the generalized inverse corresponds to the orthogonal projection of any solution, in particular $\delta\mathbf{m}_0$, onto the subspace $\mathfrak{R}(A^*)$.

Using equations (2.4.2) one can easily show that

$$(2.4.5) \qquad A^{\dagger} = A^*(A \cdot A^*)^{\dagger},$$

reducing the computation of $A^{\dagger}$ to determining the generalized inverse of a symmetric, positive semi-definite operator on E^N. If A has rank N, $A \cdot A^*$ is positive definite and $(A \cdot A^*)^{\dagger} = (A \cdot A^*)^{-1}$. Otherwise, $A \cdot A^*$ can be diagonalized by an orthogonal transformation $U: E^N \rightarrow E^N$; $A \cdot A^* = U \Delta U^*$ where $\Delta = \mathrm{diag}(\mu_1^2, \mu_2^2, \ldots, \mu_N^2)$ and the ith column of U, $\mathbf{u}_i$, solves the eigenvalue equation

---

[7] P is an orthogonal projection operator if $P \cdot P = P$ and $P^* = P$.

$$\mathbf{A} \cdot \mathbf{A}^* \mathbf{u}_i = \mu_i^2 \mathbf{u}_i, \; i = 1,2,\ldots,N. \tag{2.4.6}$$

Then, $(\mathbf{A} \cdot \mathbf{A}^*)^\dagger = \mathbf{U}\Delta^\dagger \mathbf{U}^*$. Since $\mathbf{A} \cdot \mathbf{A}^*$ is degenerate, some of the μ_i^2's, say N - K of them, will be zero, and $\dim[\mathfrak{R}(\mathbf{A}\cdot\mathbf{A}^*)] = K$. The generalized inverse of $\mathbf{A}\cdot\mathbf{A}^*$ is easily computed by ordering the eigenvalues so that $\mu_i^2 \leq \mu_j^2$ if $i > j$. Then,

$$(\mathbf{A} \cdot \mathbf{A}^*)^\dagger = \sum_{i=1}^{K} \mu_i^{-2} \; \mathbf{u}_i \, \mathbf{u}_i^*. \tag{2.4.7}$$ [8]

The dyadic $\mathbf{u}_i\mathbf{u}_i^* : \mathbf{E}^N \to \mathbf{E}^N$ is the linear operator defined by $(\mathbf{u}_i \; \mathbf{u}_i^*)\,\mathbf{v} = (\mathbf{u}_i\mathbf{v})\,\mathbf{u}_i, \; \mathbf{v}\in\mathbf{E}^N$.

The form of equation (2.4.4) illustrates an important point: Since the data kernels are not a complete set, the value of a component $\delta\mathbf{m}_{0i}, i = 1,2,\ldots,M$, of $\delta\mathbf{m}_0$ at a point $r\in[0,R]$ cannot be determined. Rather, a linear average

$$\overline{\delta m}_i(r) = \sum_{j=1}^{M} \int_0^R P_{ij}(r,r') \; \delta m_{0j}(r') \; w_j(r') \; dr' \tag{2.4.8}$$

is obtained. It is desirable to compute an average which is <u>localized</u> at each point. Roughly speaking, this means that we want the ith term in this sum to dominate and the contributions to this term to be small away from the point r.[9] As we add more linearly independent data to the data set, the kernel $P_{ij}(r,r')$ should look more like the identity kernel $\delta_{ij}\;\delta(r-r')$, where δ_{ij} is the Kronecker delta and $\delta(r-r')$ is

---

[8] This approach is suggested by Penrose [1955, p.408]. See also the discussions by Lanczos [1961], Wiggins [1972], and Jackson [1972].

[9] Backus and Gilbert [1968] provide an exhaustive discussion.

is the Dirac delta distribution. The kernel $P_{ij}(r,r')$ with i and r fixed is an example of an averaging kernel [Backus and Gilbert, 1968], except that it is not constrained to be unimodular.

In practice, considerations of localization limit the usefulness of the generalized inverse. Backus and Gilbert [1968] examined the kernels of the operator $P_{\mathbb{R}(\mathbf{A}^*)}$ and found that, for typical sets of eigenfrequency data, the linear averaging associated with this projection was not as localized as averaging kernels obtained by minimizing the integral of the absolute value of the kernel times the weighting function $(r - r')^2$. The former had better resolution, i.e., the minimum scale length of features not appreciably damped by the averaging was smaller, but had substantially larger sidebands than the latter.

Furthermore, the inverse (2.4.3) was derived under the assumption that the data are perfectly well known. Actually $\delta\mathbf{d}$ is only an estimate of the vector $\mathbf{A} \cdot \delta\mathbf{m}_0$ that has been corrupted by errors or "noise" entering through observational errors, finite sampling, computational inaccuracies, etc. Neglecting this error can yield model estimates with large statistical uncertainties [Backus and Gilbert, 1970].

These limitations of the generalized inverse can be overcome by appealing to a stochastic formulation of the linear inverse problem.

2.5 The stochastic inverse. The equation corresponding to (2.3.3) for inaccurate data can be cast in the form

$$(2.5.1) \qquad \mathbf{A} \cdot \delta\mathbf{m} + \mathbf{n} = \delta\mathbf{d} ,$$

where $\mathbf{n} \in E^N$ is a vector containing the components of noise. Since these components have some unknown scalar value, the error is described only in terms of its statistics. Following Franklin [1970] we consider (2.5.1) to be a sample of the stochastic equation

$$(2.5.2) \qquad \mathbf{A} \cdot \mathbf{p}_s + \mathbf{p}_n = \mathbf{p}_d ,$$

where $\mathbf{p}_s$ is the stochastic process describing the solution and is defined over $\mathfrak{M}$; $\mathbf{p}_n$ is the noise process, and $\mathbf{p}_d$ is the data process, both defined over E^N. In its stochastic formulation the inverse problem becomes to construct the best linear unbiased estimate of the solution process $\mathbf{p}_s$ as an application of some linear operator to the data process $\mathbf{p}_d$.

We digress briefly on the properties of stochastic processes that shall be needed for this section.[10] The process $\mathbf{p}_x$ defined over a real, separable Hilbert space $\mathfrak{U}$ maps an element $\mathbf{u}$ of $\mathfrak{U}$ into the random variable $\mathbf{p}_x \mathbf{u}$. If E{ } is the expectation operator, then the mean $m_x(\mathbf{u})$ of $\mathbf{p}_x\mathbf{u}$ always equals $E\{ \mathbf{p}_x \mathbf{u} \}$ and is a linear functional on $\mathfrak{U}$. The variance of this random variable, since it is the expectation of a square, is a positive semi-definite quadratic form on $\mathfrak{U}$; $\sigma_x{}^2(\mathbf{u}) = E\{ (\mathbf{p}_x\mathbf{u} - m_x(\mathbf{u}))^2\} = \mathbf{u}\, C_{xx} \mathbf{u}$. The linear operator $C_{xx}: \mathfrak{U} \rightarrow \mathfrak{U}$ is called the autocorrelation operator of the process $\mathbf{p}_x$. Similarly, for two processes $\mathbf{p}_x$ and $\mathbf{p}_y$ defined over $\mathfrak{U}$ and $\mathfrak{V}$ respectively,

---

[10] The reader may refer to Doob [1953] for details and proofs.

there exists a $C_{xy}: \mathfrak{V} \to \mathfrak{U}$, called the cross-correlation operator of $\mathbf{p}_x$ and $\mathbf{p}_y$, such that $E\{(\mathbf{p}_x\mathbf{u} - m_x(\mathbf{u}))(\mathbf{p}_y\mathbf{v} - m_y(\mathbf{v}))\} = \mathbf{u}\, C_{xy}\, \mathbf{v}$. Evidently, $C_{yx} = C_{xy}^*$.

Since on all spaces quadratic convergence identifies vectors, two stochastic processes $\mathbf{p}_x$ and $\mathbf{p}_{x'}$ defined over $\mathfrak{U}$ are taken to be identical if $m_x = m_{x'}$ and $C_{xx} = C_{x'x'}$; all distributions are equivalently normal. Then a process $\mathbf{p}_x$ can be represented by the decomposition $\sum_n a_n \mathbf{u}_n$, where $\{\mathbf{u}_n : n = 1,2,\ldots\}$ is some orthonormal basis for $\mathfrak{U}$ and $\{a_n : n = 1,2,\ldots\}$ is a set of independent Gaussian random variables. The Karhunin-Loève theorem [Loève, 1955, p.478] asserts that $\mathbf{u}_n$ is an eigenvector of C_{xx} and that α_n^2, the variance of the variable a_n, is its eigenvalue:

$$C_{xx} = \sum_n \alpha_n^2\, \mathbf{u}_n \mathbf{u}_n^*. \tag{2.5.3}$$

Returning to the inverse problem, we seek a linear operator $B: \mathbf{E}^N \to \mathfrak{M}$ such that the process

$$\overline{\mathbf{p}_s} = B\mathbf{p}_d \tag{2.5.4}$$

is the best linear unbiased estimate of $\mathbf{p}_s$ given equation (2.5.2) and the Gaussian statistics of $\mathbf{p}_s$ and $\mathbf{p}_n$.

Any bias can be removed at the outset by subtracting from $\mathbf{p}_s$ and $\mathbf{p}_n$ their expectations, $E\{\mathbf{p}_s\}$ and $E\{\mathbf{p}_n\}$, which are supposed known. We assume this has been done, so that each process in (2.5.2) has zero mean. This will insure that the estimate is unbiased, i.e., $E\{(\mathbf{p}_s - \overline{\mathbf{p}_s}) \cdot \mathbf{g}\} = 0$ for all $\mathbf{g} \in \mathfrak{M}$.

The process $\overline{p_s}$ is said to be the best linear estimate of p_s if it minimizes the variance $\varepsilon^2(g) \equiv E\{[(p_s - \overline{p_s}) \cdot g]^2\}$ for all $g \in \mathfrak{M}$. As shown by Franklin [1970], this can be done if the autocorrelation operator C_{dd} is positive definite. Substitution using (2.5.4) and expansion of the autocorrelation operator of $p_s - \overline{p_s}$ yields

$$\varepsilon^2(g) = g \cdot C_{ss} \cdot g - 2\, g \cdot C_{sd} B^* \cdot g + g \cdot B C_{dd} B^* \cdot g. \tag{2.5.5}$$

The first and second variations of the quadratic functional ε^2 with respect to a variation of the vector $f \equiv B^* \cdot g$ are

$$\begin{aligned} \delta(\varepsilon^2) &= 2(f C_{dd} - g \cdot C_{sd})\, \delta f\,, \\ \delta^2(\varepsilon^2) &= 2(f C_{dd} - g \cdot C_{sd})\, \delta^2 f + \delta f\, C_{dd}\, \delta f\,. \end{aligned} \tag{2.5.6}$$

The functional ε^2 is stationary if and only if $\delta(\varepsilon^2) = 0$ for all arbitrary variations δf. Therefore the linear combination $C_{dd} f - C_{ds} \cdot g$ is required to be zero for all $g \in \mathfrak{M}$. This is true if and only if $B = C_{sd}\, C_{dd}^{-1}$. With this choice the second variation $\delta^2(\varepsilon^2)$ reduces to the positive definite quadratic form $\delta f\, C_{dd}\, \delta f$, and the stationary point is a minimum. Therefore the best linear estimate of p_s is

$$\overline{p_s} = C_{sd}\, C_{dd}^{-1}\, p_d. \tag{2.5.7}$$

The correlation operators in (2.5.7) can be expanded in terms of the correlation operators for p_s and p_n, which are supposed known:

$$\begin{aligned} C_{sd} &= C_{ss} \cdot A^* + C_{sn}\,, \\ C_{dd} &= A \cdot C_{ss} \cdot A^* + A \cdot C_{sn} + C_{ns} \cdot A^* + C_{nn}\,. \end{aligned} \tag{2.5.8}$$

It is convenient and usually reasonable to assume that the solution and noise processes are uncorrelated, i.e., $C_{sn} = 0$. With this assumption equations (2.5.8) simplify to

$$C_{sd} = C_{ss} \cdot A^* ,$$
(2.5.9)
$$C_{dd} = A \cdot C_{ss} \cdot A^* + C_{nn} .$$

Using (2.5.9) in equation (2.5.7), we obtain for a sample $\delta \mathbf{d}$ of $\mathbf{p}_d$ the estimate

(2.5.10)
$$\overline{\delta m} = C_{ss} \cdot A^* (A \cdot C_{ss} \cdot A^* + C_{nn})^{-1} \delta \mathbf{d} .$$

The operator in this equation will be called the stochastic inverse of A.

The statistical information embodied in an emsemble of samples can be used to estimate the autocorrelation operators C_{ss} and C_{nn} appearing in (2.5.10). For example, suppose $\{ \mathbf{d}_1, \mathbf{d}_2, \ldots, \mathbf{d}_L \}$ is a set of L independent observations of the data functionals and assume that the sample mean $\overline{\mathbf{d}} = \frac{1}{L} \sum_{i=1}^{L} \mathbf{d}_i$ is an unbiased estimator of $\mathbf{d}_0$. Then the sample variance matrix

(2.5.11)
$$\mathbf{V} = \frac{1}{L-1} \sum_{i=1}^{L} \sum_{j=1}^{L} (\mathbf{d}_i - \overline{\mathbf{d}})(\mathbf{d}_j - \overline{\mathbf{d}})^*$$

is an unbiased estimator of C_{nn} . If the data components are statistically independent, then, in the limit $L \to \infty$, $\mathbf{V}$ converges to the diagonal form

(2.5.12)
$$C_{nn} = \begin{bmatrix} \sigma_1^2 & \cdot & \cdot & \cdot & 0 \\ \cdot & \cdot & & & \cdot \\ \cdot & & \cdot & & \cdot \\ \cdot & & & \cdot & \cdot \\ 0 & \cdot & \cdot & \cdot & \sigma_N^2 \end{bmatrix} .$$

When all the variances σ_i^2, $i = 1,2,\ldots,N$, are nonzero, $\mathbf{C}_{nn}$ will be positive definite, thus insuring that $\mathbf{C}_{dd}$ be positive definite as we have assumed.

If independent samples of p_s are available, a similar procedure can be used to construct an estimate of the autocorrelation operator $\mathbf{C}_{ss}$. In the geophysical inverse problem this is not the case. Answering questions raised by this fact will be the purpose of the next section.

Of course, using information about the solution and noise processes in deriving an estimate of the solution is not a new idea; its roots lie in the linear filtering and prediction theories of Kolmogoroff and Wiener [Wiener, 1949]. In fact, equation (2.5.10) is analogous to the results of Wiener's theory for the construction of the optimum infinite-lag smoothing filter [Davenport and Root, 1958] and has been explicitly obtained by Strand and Westwater [1968]. It reduces to Twomey's [1963] results for the special case $\mathbf{C}_{ss} = \mathbf{I}$, $\mathbf{C}_{nn} = \gamma\mathbf{I}$.

2.6 Specification of the solution autocorrelation operator. As outlined in the previous section, the statistics formed from an ensemble of samples can be used to estimate the autocorrelation operator of a stochastic process. However, at least in the inverse problem that concerns us, this approach cannot be applied to the construction of the solution autocorrelation operator $\mathbf{C}_{ss}$ appearing in (2.5.10). The Earth itself is presumably unique, and the mind twists to imagine what a sample ensemble of p_s might be (the radial variations of elastic parameters in a number of Earth-like planets taken at random from our galaxy perhaps?). The resulting notions are generally absurd, and we dismiss the possibility that the probability distribution of p_s is describable in terms of the limits of relative frequencies. Then we must ask, what is the significance of characterizing the solution as a sample of a Gaussian process with zero expectation and an autocorrelation operator C_{ss} in this estimation procedure?

To begin to answer this question, we must first examine the behavior of the stochastic inverse in the limit of zero noise. One measure of the size of the noise is the operator norm $||C_{nn}||$, equal to the largest eigenvalue of C_{nn}. Suppose for the moment that p_s is a "white" process, i.e., $C_{ss} = I$. We assert that by requiring $||C_{nn}||$ to be small enough the solution given by the stochastic inverse $A^s = A^*(A\cdot A^* + C_{nn})^{-1}$ can be made arbitrarily close to the solution given by the generalized inverse $A^\dagger$. Put more formally, for any $\varepsilon > 0$ there exists a positive number $\gamma(\varepsilon)$ such that, if $||C_{nn}|| < \gamma(\varepsilon)$, then, for all $\delta d \neq 0$, $||A^\dagger\, \delta d - A^s\, \delta d||^2 < \varepsilon\, ||\delta d||^2$. To show this we first note that $\gamma(\varepsilon) I - C_{nn}$ will be positive definite, so it is sufficient to find a $\gamma(\varepsilon)$ such that

$$(2.6.1)\qquad ||[(A\cdot A^*)^\dagger - (A\cdot A^* + \gamma I)^{-1}]^* A\cdot A^*[(A\cdot A^*)^\dagger - (A\cdot A^* + \gamma I)^{-1}]|| < \varepsilon.$$

Equation (2.4.7) and the completeness relation

$$(2.6.2)\qquad I = \sum_{i=1}^{N} u_i\, u_i^*$$

can be substituted into (2.6.1). Computation shows that the resulting inequality is true when

$$\gamma(\varepsilon) < \mu_K^2 \frac{\mu_K\sqrt{\varepsilon}}{1 - \mu_K\sqrt{\varepsilon}}, \tag{2.6.3}$$

thus proving the assertion by construction. Using the terminology of A. N. Tikhonov [1963a, 1963b], we say that the stochastic inverse solution $A^s\delta d$ <u>regularizes</u> the generalized inverse solution (2.4.3).

Identical arguments can be made to show that equation (2.5.10) regularizes the computation of

$$\overline{\delta m} = C_{ss} \cdot A^*(A \cdot C_{ss} \cdot A^*)^\dagger \, \delta d . \tag{2.6.4}$$

This solution has a simple geometrical interpretation. Assume that C_{ss} is positive definite and define L to be the inverse of C_{ss}: $L = C_{ss}^{-1}$. C_{ss} is idempotent with respect to the product defined in (2.2.4); that is, $C_{ss} \overset{L}{\cdot} C_{ss} = C_{ss}$. In fact, C_{ss} is the identity operator on $\mathfrak{M}_L$. Let $A_L = A \cdot C_{ss}$, so that equation (2.3.3) becomes

$$A_L \overset{L}{\cdot} \delta m = \delta d . \tag{2.6.5}$$

Substituting (2.6.5) into (2.6.4) we obtain

$$\overline{\delta m} = A_L^*(A_L \overset{L}{\cdot} A_L^*)^\dagger A_L \overset{L}{\cdot} \delta m. \tag{2.6.6}$$

The operator $P^L_{\mathfrak{R}(A_L^*)} \equiv A_L^*(A_L \overset{L}{\cdot} A_L^*)^\dagger A_L$ is an orthogonal projection operator on $\mathfrak{M}_L$ in the sense that $P^L_{\mathfrak{R}(A_L^*)} \overset{L}{\cdot} P^L_{\mathfrak{R}(A_L^*)} = P^L_{\mathfrak{R}(A_L^*)}$ and $P^{L*}_{\mathfrak{R}(A_L^*)} = P^L_{\mathfrak{R}(A_L^*)}$. Therefore, for perfectly known data, the solution (2.6.4) is the symmetric projection of any solution, in particular δm_0, onto the manifold $\mathfrak{R}(A_L^*) \subset \mathfrak{M}_L$, the inner product on $\mathfrak{M}_L$ being defined by (2.2.4). $A_L^\dagger \equiv A_L^*(A_L \overset{L}{\cdot} A_L^*)^\dagger$ is the generalized inverse of A_L.

As pointed out in §2.1, it will be useful to prescribe the solution autocorrelation operator as a smoothing operator, or, looked at another way, to prescribe the inner product on the model space in terms of a "roughing" operator, the inverse of a smoothing operator. The arguments in the preceeding paragraph were intended to suggest that these viewpoints are identical. The rationale for such a choice can come from either of two considerations: we may wish to incorporate _a priori_ assumptions about the smoothness of the solution, or we may wish to manipulate averaging kernels so that they are, say, more localized.

To clarify what is meant by choosing the solution autocorrelation operator to be a smoothing operator, we write C_{ss} in terms of its Karhunin-Loève expansion,

$$C_{ss} = \sum_{n=1}^{\infty} \kappa_n^2 \ \psi_n \psi_n^*, \tag{2.6.7}$$

and assume that the set of eigenvectors $\{\psi_n : n = 1,2,...\}$ has been ordered so that, if ψ_i is smoother (say, has fewer zero crossings) than ψ_j, then $i < j$. We will call C_{ss} a smoothing operator if $\kappa_i^2 > \kappa_j^2$ for all $i < j$. Note that the definition implies that any smoothing operator is positive definite. This definition is not the most general one, but it will be convenient for our purposes.

If C_{ss} is a smoothing operator, then

$$L \equiv C_{ss}^{-1} = \sum_{n=1}^{\infty} \kappa_n^{-2} \psi_n \psi_n^* \tag{2.6.8}$$

is a "roughing" operator in the sense that rougher eigenvectors have larger eigenvalues. $\mathbf{L}$ can be used to define an ordering on the model space: a model $\mathbf{m}$ is said to be smoother than a model $\mathbf{m}'$ if

$$\frac{||\mathbf{m}||_L}{||\mathbf{m}||} < \frac{||\mathbf{m}'||_L}{||\mathbf{m}'||} . \tag{2.6.9}$$

Since they are orthogonal projections, the solution (2.4.3) minimizes $||\delta\mathbf{m}||$ and the solution (2.6.4) minimizes $||\delta\mathbf{m}||_L$. Therefore, with $\mathbf{C}_{ss}$ chosen as a smoothing operator, (2.6.4) provides a smoother solution than the generalized inverse.[11]

Since a member of the model space $\mathfrak{M}$ is an M-tuple of functions on the interval $[0,R]$, defining $\mathbf{C}_{ss}$ to be a smoothing operator does not make much sense. Basically the ordering of the eigenvectors of a smoothing operator requires characterizing them by generalized wavenumbers, or numbers of zero crossings. But the total number of zero crossings of a vector in $\mathfrak{M}$ does not really coincide with our notion of its smoothness: Suppose $\psi(r) = [\sin M\pi r/R, 0,\ldots, 0]$ (M terms) and $\psi'(r) = [\sin 2\pi r/R, \sin 2\pi r/R,\ldots, \sin 2\pi r/R]$ (M terms) where $M > 2$. Now ψ has fewer $(M-1)$ zero crossings than $\psi'(M)$, but intuitively ψ is not smoother than ψ'.

To avoid this difficulty comparisons of smoothness will be made component by component. In the example given above ψ_1 ($\psi_1(r)=\sin M\pi r/R$) is less smooth than ψ_1', but ψ_2 is smoother than ψ_2'. One form of the solution autocorrelation operator that is compatible with this decision is

---

[11] This assumes that the solutions are distinct. They will be identical when the eigenvectors of $\mathbf{C}_{ss}$ and $\mathbf{A}^*\mathbf{A}$ are the same.

(2.6.10)
$$C_{ss} = \begin{bmatrix} C_1 & 0 & \cdots & 0 \\ 0 & C_2 & \cdots & 0 \\ \cdot & \cdot & & \cdot \\ \cdot & \cdot & & \cdot \\ \cdot & \cdot & & \cdot \\ 0 & 0 & \cdots & C_M \end{bmatrix}.$$

Now $C_i: \mathfrak{M}_i \to \mathfrak{M}_i$ can be chosen to be a smoothing operator on $\mathfrak{M}_i$, $i = 1,2,\ldots,M$. In this case C_{ss} will still be positive definite but will not always be a smoothing operator in the strict sense that we have defined the term. If the process p_s is considered to be an M-tuple of processes $[\, p_1, p_2, \ldots, p_M]$, each p_i being defined over $\mathfrak{M}_i$, then equation (2.6.10) implies that $E\{(p_i m_i)(p_j m_j)\} = 0$ if $i \neq j$ for all $m_i \in \mathfrak{M}_i$ and all $m_j \in \mathfrak{M}_j$. The component processes are thus uncorrelated.

An example of the type of smoothing operator that is useful in the practical applications of this theory (such as Chapter 5) can be obtained as the solution to a second-order inhomogeneous differential equation with homogeneous boundary conditions. Consider the problem of constructing a smoothing operator C on the space of functions real-valued and continuous on the interval $[a,b]$, $0 < a < b \leq R$:[12]

Let $\Lambda(r)$ be a differential operator of the Sturm-Liouville type; $\Lambda(r) = \frac{d}{dr}\left[p(r)\,\frac{d}{dr}\right] - q(r)$, $r \in [a,b]$. The differential equation with homogeneous boundary conditions

(2.6.11)
$$\begin{aligned} \Lambda(r)s(r) + k^2 w(r)s(r) &= 0, \\ \left[\frac{d}{dr}\,s(r) + \alpha s(r)\right]_{r=a} &= 0, \end{aligned}$$

[12] The interval $[a,b]$ is used instead of $[0,R]$ to allow the construction of autocorrelation operators for functions (processes) expected to be piecewise-continuous. See Chapter 5 .

(2.6.11 cont.) $$\left[\frac{d}{dr}\, s(r) + \beta s(r)\right]_{r=b} = 0$$

generates a set of eigenfunctions $\{s_n : n = 1,2,\ldots\}$, taken to be normalized, that is complete on the interval [a,b] [Morse and Feshbach, 1953]. The eigenvalues k_n^2, $n = 1,2,\ldots$, can be ordered as a continuously increasing sequence with $k_1^2 < k_2^2 < \cdots < k_n^2 < \cdots$. With this ordering the number of nodes in the eigenfunctions on the interval [a,b] also forms a continuously increasing sequence [Morse and Feshbach, 1953, p.722]. We specify the kernel of $\mathbf{C}$ in the following form:

(2.6.12) $$C(r,r') = \sum_{n=1}^{\infty} \kappa_n^{\,2}\, s_n(r)\, s_n(r').$$

For $\mathbf{C}$ to be a smoothing operator the sequence of spectral coefficients $\{\kappa_1^{\,2},\kappa_2^{\,2},\ldots,\kappa_n^{\,2},\ldots\}$ should be continuously decreasing. This will be true if, for a given scalar value of the parameter k,

(2.6.13) $$\kappa_n^{\,2} = \frac{k^2}{k^2 + k_n^{\,2}}\,.$$

Particularized in this way $\mathbf{C}$ has the desirable properties that a) its norm is less than or equal to 1, and b) it converges in quadratic mean to the identity operator as k goes to infinity. That is,

(2.6.14a) $$||\mathbf{C}|| \le 1,$$

(2.6.14b) $$\lim_{k\to\infty} ||(\mathbf{I} - \mathbf{C})\cdot \mathbf{f}|| = 0.$$

The parameter k is simply the mean wave-number of $\mathbf{C}$. It can be easily verified that for this choice of spectral coefficients the kernel of $\mathbf{C}$ satisfies the inhomogeneous system

$$
(2.6.15) \qquad
\begin{aligned}
&[w(r) - k^{-2}\Lambda(r)]\, C(r,r') = \delta(r-r'),\\
&\left[\frac{d}{dr} C(r,r') + \alpha C(r,r')\right]_{r=a} = 0,\\
&\left[\frac{d}{dr} C(r,r') + \beta C(r,r')\right]_{r=b} = 0.
\end{aligned}
$$

As an example we solve this system for the special case $w(r) = p(r) = r^2$, $q(r) = 0$. In this case (2.6.15) has a regular singular point at $r = 0$. Solutions to the equations (2.6.11) are the spherical Bessel functions of angular order zero. Solving (2.6.15) we find

$$
(2.6.16) \qquad C(r,r') = \frac{k}{2rr'}\left\{ e^{-k|r-r'|} + D^{-1}[A\, e^{-k(b-a)} \cosh k(r-r') + B \cosh k(a+b-r-r') + C \sinh k(a+b-r-r')] \right\},
$$

where
$$
\begin{aligned}
A &= [1 - a(k+\alpha)][1 + b(k-\beta)],\\
B &= \alpha a + \beta b - [k^2 - k(\alpha+\beta) + \alpha\beta]ab - 1,\\
C &= k(b-a),\\
D &= [1 - \alpha a - \beta b + (\alpha\beta - k^2)ab]\sinh k(a-b)\\
&\quad - k[b - a + (\beta-\alpha)ab]\cosh k(a-b).
\end{aligned}
$$

Fig. 2.1 shows $C(r,r')$ given by (2.6.16) on the interval (0,1] centered at $r' = 0.5$ for the case $\alpha^{-1} = \beta^{-1} = 0$. In this figure the kernel is displayed for k values of 5, 20, and 50.

2.7 The tradeoff curve. The Backus-Gilbert theory of linear estimation [Backus and Gilbert, 1970] suggests that for the problem described in §2.5 - the estimation of a function given the values of a set of linear data functionals corrupted by noise - there exists a tradeoff between the ability to resolve detail and the reliability of the estimate. In

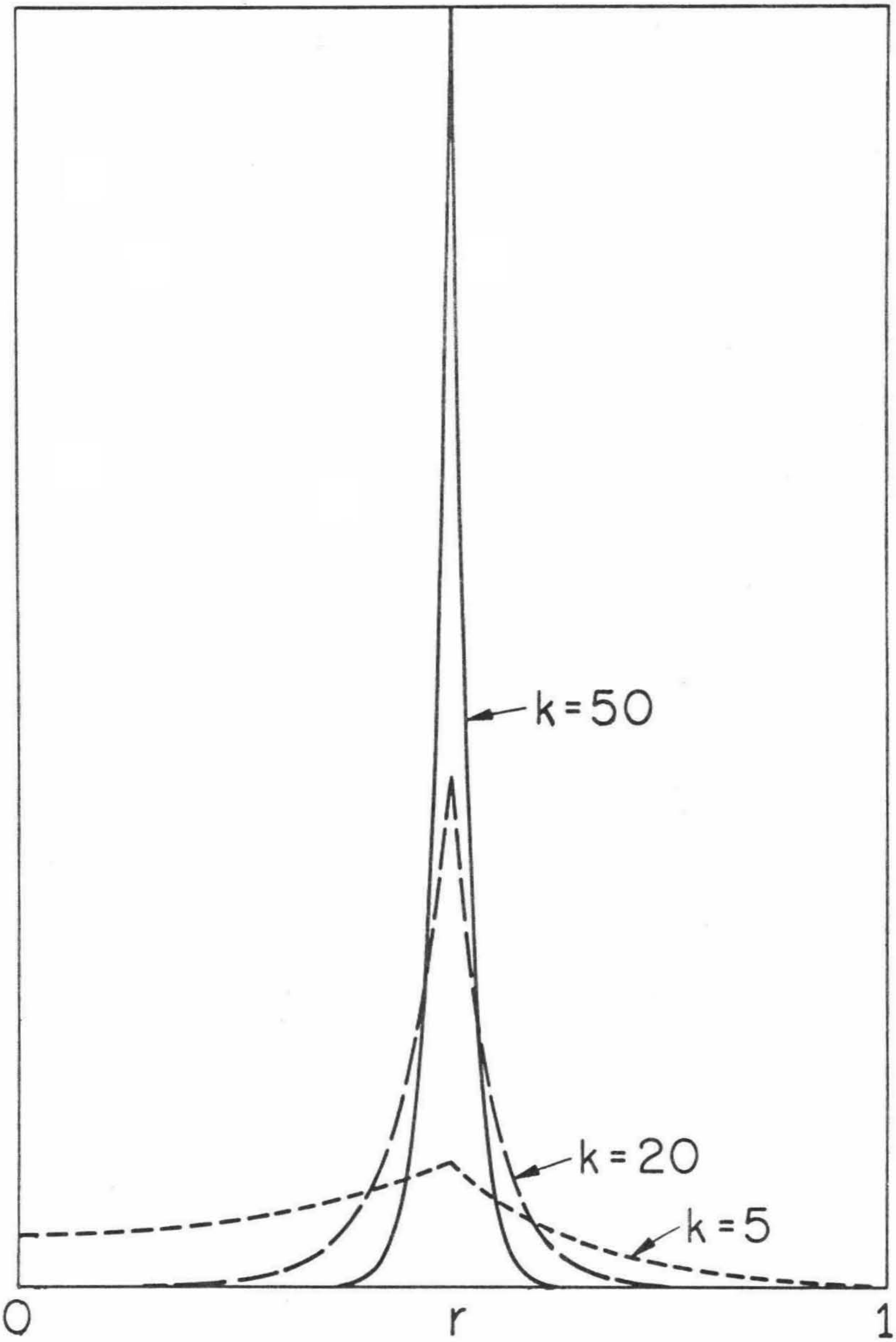

Figure 2.1. The kernel $c\ (r,r')$ given by equation (2.6.16) on the interval (0,1] centered at $r'=1/2$ for the case $\alpha^{-1}=\beta^{-1}=0$.

this section we construct a Backus-Gilbert-type tradeoff curve on which the generalized inverse (§2.4) and the stochastic inverse (§2.5) are represented as discrete points. It is shown that the stochastic inverse is an optimal point. The generalized inner product $\sim \overset{L}{\cdot} \sim$ and norm $||\sim||_L$ introduced in §2.6 are retained throughout the analysis and are assumed to be dimensionless quantities.

An estimate $\overline{\delta \mathbf{m}}$ of the function $\delta \mathbf{m}_0$ satisfying

$$(2.7.1) \qquad \mathbf{A}_L \overset{L}{\cdot} \delta \mathbf{m}_0 + \mathbf{n} = \delta \mathbf{d}$$

is sought given $\mathbf{A}_L, \delta \mathbf{d}$, and the statistics of a Gaussian noise process $\mathbf{p}_n$ from which $\mathbf{n}$ is a sample. The process $\mathbf{p}_n$ is assumed to have zero expectation and a positive definite autocorrelation operator $\mathbf{C}_{nn}$. The null space $\mathfrak{N}(\mathbf{A})$ is populated by those members $\mathbf{h}$ of $\mathfrak{M}_L$ for which $\mathbf{A}_L \overset{L}{\cdot} \mathbf{h} = 0$. Since the data contain no information about the components of $\delta \mathbf{m}_0$ in $\mathfrak{N}(\mathbf{A})$, the estimate $\overline{\delta \mathbf{m}}$ is required to belong to the range space $\mathfrak{R}(\mathbf{A}^*) = \mathfrak{M}_L - \mathfrak{N}(\mathbf{A})$. This is equivalent to constraining $\overline{\delta \mathbf{m}}$ to be a linear combination of the data kernels:

$$(2.7.2) \qquad \overline{\delta \mathbf{m}} = \mathbf{A}_L^* \mathbf{b}, \text{ for some } \mathbf{b} \in \mathbf{E}^N.$$

The vector $\mathbf{b}$ is to be determined by minimizing an appropriate scalar measure of the error of estimation.

One obvious measure of the error of estimation of $\delta \mathbf{m}_0$ is the norm of the difference between $\delta \mathbf{m}_0$ and $\overline{\delta \mathbf{m}}$. Define

$$(2.7.3) \qquad \varepsilon_1^{\,2}(\mathbf{b}) = ||\delta \mathbf{m}_0 - \mathbf{A}_L^* \mathbf{b}||_L^2.$$

The subspaces $\mathfrak{N}(A)$ and $\mathfrak{R}(A^*)$ are orthogonal, so it is clear that the projection of $\delta\mathbf{m}_0$ onto $\mathfrak{N}(A)$ contributes to ${\varepsilon_1}^2$ its full squared norm regardless of the choice of $\mathbf{b}$. In fact, ${\varepsilon_1}^2$ is minimized at the value $||\mathbf{P}^L_{\mathfrak{N}(A)} \overset{L}{\cdot} \delta\mathbf{m}_0||^2_L$ for $\mathbf{b} = (A_L \overset{L}{\cdot} A^*_L)^\dagger A_L \overset{L}{\cdot} \delta\mathbf{m}_0$. This is the solution (2.6.6).

Therfore, if the data were perfectly accurate, the best linear estimate of the vector $\delta\mathbf{m}_0$ would result from the application of the generalized inverse $A^\dagger_L = A^*_L(A_L \overset{L}{\cdot} A^*_L)^\dagger$ to the data sample vector $\delta\mathbf{d}$. However $\mathbf{n} \neq 0$ implies an uncertainty in $\delta\mathbf{d}$ and, correspondingly, in $\overline{\delta\mathbf{m}}$. A measure of the uncertainty of any estimate of the form (2.7.2) due to noise in the data is the variance ${\varepsilon_2}^2$ of the projection of $\mathbf{p}_n$ onto $\mathbf{b}$. By definition,

$$(2.7.4) \qquad {\varepsilon_2}^2(\mathbf{b}) = \mathbf{b}\, C_{nn}\, \mathbf{b}\,.$$

Minimizing this error with respect to a variation of $\mathbf{b}$ yields the trivial solution $\mathbf{b} = 0$.

In general the two measures of error ${\varepsilon_1}^2$ and ${\varepsilon_2}^2$ compete: ${\varepsilon_1}^2$ is minimized when ${\varepsilon_2}^2$ is largest and vice versa. To explore the possibilities for some sort of compromise, we consider the quadratic measure of error

$$(2.7.5) \qquad \varepsilon^2(\theta, \mathbf{b}) = {\varepsilon_1}^2(\mathbf{b}) \cos\theta + {\varepsilon_2}^2(\mathbf{b}) \sin\theta$$

composed of a weighted sum of the two measures of error. The weighting is parameterized by an angle θ that will be allowed to vary on the interval $[0, \pi/2]$, so that $\varepsilon^2(0, \mathbf{b}) = {\varepsilon_1}^2(\mathbf{b})$ and $\varepsilon^2(\pi/2, \mathbf{b}) = {\varepsilon_2}^2(\mathbf{b})$.

For a fixed $\theta > 0$, $\varepsilon^2(\theta, \mathbf{b})$ can be minimized with respect to a variation of the vector $\mathbf{b}$. The first and second variations are

$$\begin{aligned}
\delta(\varepsilon^2) &= 2[\mathbf{b}\, A_L \overset{L}{\cdot} A_L^* - \delta\mathbf{m}_0 \overset{L}{\cdot} A_L^*]\, \delta\mathbf{b} \cos\theta + 2\, \mathbf{b}\, C_{nn} \delta\mathbf{b} \sin\theta, \\
\delta^2(\varepsilon^2) &= [\delta\mathbf{b} A_L \overset{L}{\cdot} A_L^* \delta\mathbf{b} + 2(\mathbf{b} A_L \overset{L}{\cdot} A_L^* - \delta\mathbf{m}_0 \overset{L}{\cdot} A_L^*)\delta^2\mathbf{b}\,] \cos\theta \\
&\quad + [\delta\mathbf{b}\, C_{nn} \delta\mathbf{b} + 2\mathbf{b}\, C_{nn} \delta^2\mathbf{b}\,] \sin\theta.
\end{aligned} \tag{2.7.6}$$

For the functional $\varepsilon^2(\theta, \mathbf{b})$ to be stationary it is required that

$$(A_L \overset{L}{\cdot} A_L^* + \tan\theta\, C_{nn})\,\mathbf{b} = A_L \overset{L}{\cdot} \delta\mathbf{m}_0. \tag{2.7.7}$$

If $\theta > 0$, then $A_L \overset{L}{\cdot} A_L^* + \tan\theta\, C_{nn}$ is positive definite, and the unique $\mathbf{b}$ that makes $\varepsilon^2(\theta, \mathbf{b})$ stationary is

$$\mathbf{b}(\theta) = (A_L \overset{L}{\cdot} A_L^* + \tan\theta\, C_{nn})^{-1} A_L \overset{L}{\cdot} \delta\mathbf{m}_0. \tag{2.7.8}$$

This stationary point is a minimum because the second variation reduces to the positive definite quadratic form

$$\delta^2(\varepsilon^2) = \delta\mathbf{b}\, (A_L \overset{L}{\cdot} A_L^* \cos\theta + C_{nn} \sin\theta)\,\delta\mathbf{b}\,. \tag{2.7.9}$$

If $\theta = 0$ and A_L has rank $K < N$, then there exists an $(N-K)$-dimensional manifold of solutions to (2.7.7), and the stationary point is not unique. To obtain a unique solution we may constrain $\mathbf{b}$ and its variations to lie in the subspace $\mathfrak{R}(A_L \overset{L}{\cdot} A_L^*) = \mathfrak{R}(A) \subset E^N$. Then the choice of $\mathbf{b}$ that minimizes (2.7.5) is given by the generalized inverse

$$\mathbf{b}(0) = (A_L \overset{L}{\cdot} A_L^*)^{\dagger} A_L \overset{L}{\cdot} \delta\mathbf{m}_0. \tag{2.7.10}$$

This choice is the natural one, because, as was shown in §2.6, the estimate (2.7.2) substituting for $\mathbf{b}$ using (2.7.8) regularizes the computation of the generalized inverse solution obtained from (2.7.10) along the path $\theta \to 0$. Realizing that the generalized inverse of a positive definite operator is just its ordinary inverse, we can write

$$\mathbf{b}(\theta) = (\mathbf{A}_L \overset{L}{\cdot} \mathbf{A}_L^* + \tan\theta\ \mathbf{C}_{nn})^{\dagger} \mathbf{A}_L \overset{L}{\cdot} \delta\mathbf{m}_0, \tag{2.7.11}$$

for any $\theta \in [0,\pi/2]$.

Replacing the vector $\mathbf{A}_L \overset{L}{\cdot} \delta\mathbf{m}_0$ by its best estimate $\delta\mathbf{d}$ and substituting (2.7.11) into equation (2.7.2) yields for the best linear estimate of $\delta\mathbf{m}_0$ the equation

$$\overline{\delta\mathbf{m}}(\theta) = \mathbf{A}_L^*(\mathbf{A}_L \overset{L}{\cdot} \mathbf{A}_L^* + \tan\theta\ \mathbf{C}_{nn})^{\dagger}\ \delta\mathbf{d}\ . \tag{2.7.12}$$

Special cases of (2.7.12) include the generalized inverse ($\theta = 0$) and the stochastic inverse ($\theta = \pi/4$).

The estimate $\mathbf{b}(\theta)$ can be put into (2.7.3) and (2.7.4) to obtain $\varepsilon_1^{\,2}$ and $\varepsilon_2^{\,2}$ as functions of θ:

$$\begin{aligned} \varepsilon_1^{\,2}(\theta) &= \|\delta\mathbf{m}_0 - \mathbf{R}(\theta) \overset{L}{\cdot} \delta\mathbf{m}_0\|_L^{\,2}, \\ \varepsilon_2^{\,2}(\theta) &= \delta\mathbf{m}_0 \overset{L}{\cdot} \mathbf{V}(\theta) \overset{L}{\cdot} \delta\mathbf{m}_0. \end{aligned} \tag{2.7.13}$$

The operators $\mathbf{R}(\theta)$ and $\mathbf{V}(\theta)$ appearing in these expressions are defined by the equations

$$\begin{aligned} \mathbf{R}(\theta) &= \mathbf{A}_L^*\ \mathbf{Q}^{\dagger}(\theta)\ \mathbf{A}_L\ , \\ \mathbf{V}(\theta) &= \mathbf{A}_L^*\ \mathbf{Q}^{\dagger}(\theta)\ \mathbf{C}_{nn}\mathbf{Q}^{\dagger}(\theta)\ \mathbf{A}_L\ , \\ \mathbf{Q}(\theta) &= \mathbf{A}_L \overset{L}{\cdot} \mathbf{A}_L^* + \tan\theta\ \mathbf{C}_{nn}\ . \end{aligned} \tag{2.7.14}$$

Both $\mathbf{R}(\theta)$ and $\mathbf{V}(\theta)$ are positive semi-definite, symmetric operators mapping $\mathfrak{M}$ onto $\mathfrak{R}(A^*)$.

For $\delta\mathbf{m}_0$ fixed, equations (2.7.13) determine a curve in the positive quadrant of the $\varepsilon_1{}^2 - \varepsilon_2{}^2$ plane that is parameterized by the angle θ. Backus and Gilbert [1970] have termed such graphs <u>tradeoff curves</u>. They have constructed tradeoff curves for the problem of estimating the scalar quantity $\delta m_0(r)$ (r fixed). The tradeoff curve given by equations (2.7.13) is for the problem of estimating the vector quantity $\delta\mathbf{m}_0$. Nevertheless, the qualitative features of these curves are essentially the same. For any $\theta \in (0,\pi/2)$, the expressions for $\varepsilon_1{}^2$ and $\varepsilon_2{}^2$ can be differentiated with respect to θ:

$$\text{(2.7.15)} \qquad \begin{aligned} \frac{d\varepsilon_1{}^2}{d\theta} &= 2\,\delta\mathbf{m}_0 \overset{L}{\cdot} \frac{d}{d\theta} \overset{L}{\cdot} [\,\mathbf{R} - \mathbf{C}_{ss}] \overset{L}{\cdot} \delta\mathbf{m}_0 \,, \\ \frac{d\varepsilon_2{}^2}{d\theta} &= 2\,\delta\mathbf{m}_0 \overset{L}{\cdot} \mathbf{A}_L^* \frac{d\mathbf{Q}^{-1}}{d\theta}\, \mathbf{C}_{nn}\, \mathbf{Q}^{-1}\, \mathbf{A}_L \overset{L}{\cdot} \delta\mathbf{m}_0 \,. \end{aligned}$$

Now, since $\frac{d}{d\theta}[\mathbf{Q}\,\mathbf{Q}^{-1}] = \frac{d}{d\theta}[\,\mathbf{I}\,] = 0$, we can write

$$\text{(2.7.16)} \qquad \frac{d\mathbf{Q}^{-1}}{d\theta} = -\,\mathbf{Q}^{-1}\frac{d\mathbf{Q}}{d\theta}\,\mathbf{Q}^{-1}.$$

The derivative of $\mathbf{Q}(\theta)$ can be computed from (2.7.14):

$$\text{(2.7.17)} \qquad \frac{d\mathbf{Q}}{d\theta} = \mathbf{C}_{nn}\ \sec^2\theta.$$

Using (2.7.14), (2.7.16), and (2.7.17) in (2.7.15), we find that

$$\text{(2.7.18)} \qquad \frac{d\varepsilon_1{}^2}{d\theta} = 2\,\delta\mathbf{m}_0 \overset{L}{\cdot} \mathbf{V}(\theta) \overset{L}{\cdot} [\,\mathbf{C}_{ss} - \mathbf{R}(\theta)] \overset{L}{\cdot} \delta\mathbf{m}_0\ \sec^2\theta,$$

and that

$$(2.7.19) \qquad \frac{d\varepsilon_2^{\,2}}{d\theta} = -2\,\delta m_0 \overset{L}{\cdot} A_L^* Q^{-1} C_{nn} Q^{-1} C_{nn} Q^{-1} A_L^* \overset{L}{\cdot} \delta m_0 \;\sec^2\theta .$$

C_{nn} is assumed to be positive definite, and it will be shown in §2.8 that, for a finite number of data, the operator $[\, C_{ss} - R(\theta)]$ is positive definite. Therefore, for any $\delta m_0 \notin \mathfrak{N}(A)$,

$$(2.7.20) \qquad \frac{d\varepsilon_1^{\,2}}{d\theta} > 0, \qquad \frac{d\varepsilon_2^{\,2}}{d\theta} > 0.$$

Now,

$$V(\theta) \overset{L}{\cdot} [\, C_{ss} - R(\theta)] =$$

$$A_L^* Q^{-1}(\theta)\, C_{nn}\, Q^{-1}(\theta)\, [\, Q(\theta) - A_L^* \overset{L}{\cdot} A_L] Q^{-1}(\theta)\, A_L = $$

$$A_L^* Q^{-1}(\theta)\, C_{nn}\, Q^{-1}(\theta)\, C_{nn}\, Q^{-1}(\theta)\, A_L \tan\theta .$$

Using this equation in equation (2.7.18) and dividing the results into (2.7.19), we obtain

$$(2.7.21) \qquad \frac{d[\varepsilon_2^{\,2}]}{d[\varepsilon_1^{\,2}]} = -\cot\theta .$$

Equation (2.7.21) can be differentiated with respect to $\varepsilon_1^{\,2}$ to yield

$$(2.7.22) \qquad \frac{d^2[\varepsilon_2^{\,2}]}{d[\varepsilon_1^{\,2}]^2} = \csc^2\theta \left[\frac{d\,\theta}{d[\varepsilon_1^{\,2}]}\right].$$

The inequality (2.7.20) implies that this derivative is positive.

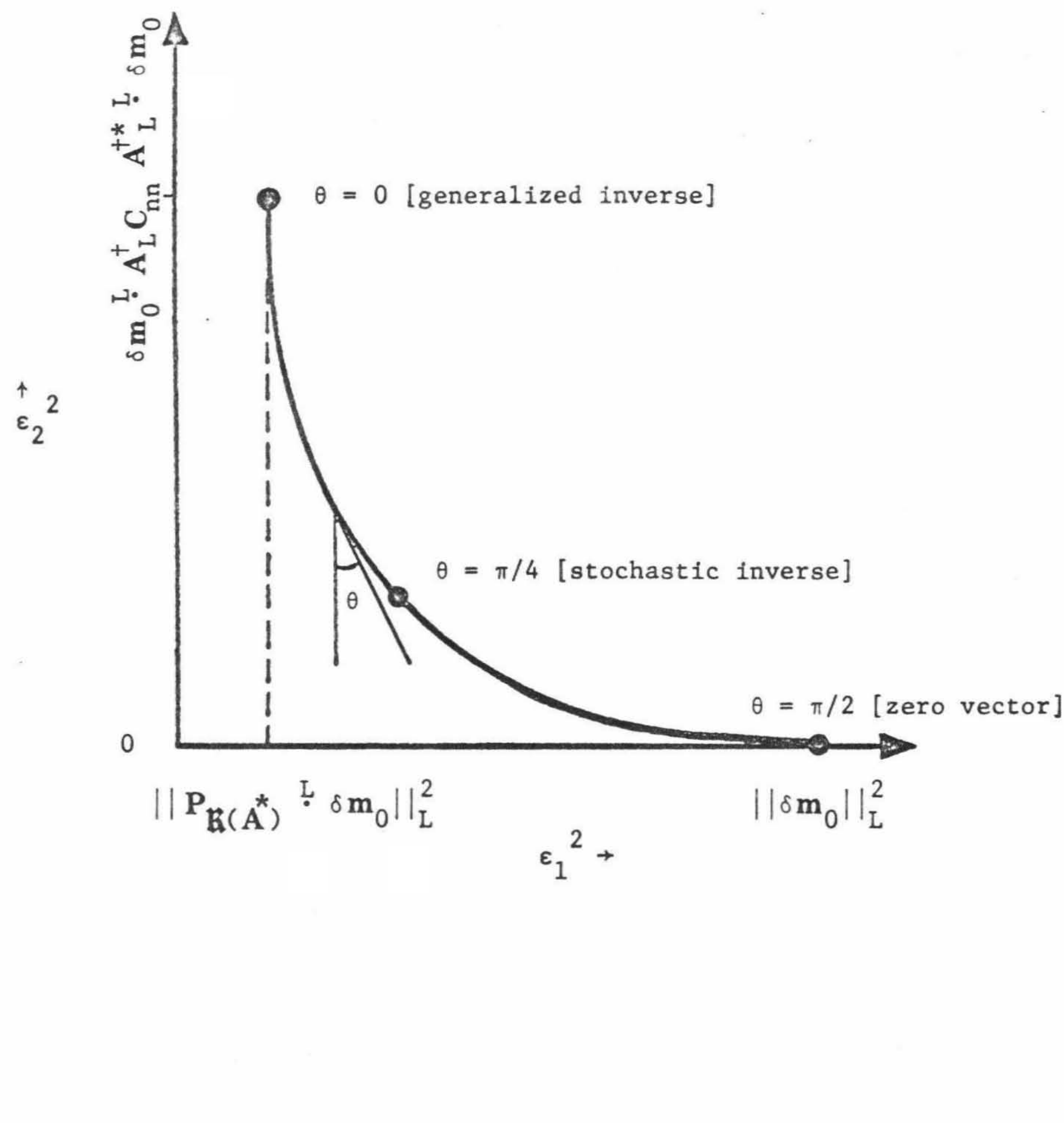

Figure 2.2. Schematic geometry of the tradeoff curve.

From (2.7.20), (2.7.21), and (2.7.22), we infer that the tradeoff curve between ε_1^2 and ε_2^2 is monotonically decreasing and convex towards the origin and that θ is the acute angle between the tangent to the tradeoff curve and the ε_2^2 axis. Therefore,

$$
(2.7.23)\qquad
\begin{aligned}
\inf_{0<\theta<\pi/2} \varepsilon_1^2(\theta) &= \varepsilon_1^2(0) = \| \mathbf{P}_{\mathbb{R}(\mathbf{A}^*)} \overset{L}{\cdot} \delta\mathbf{m}_0 \|_L^2 ,\\
\sup_{0<\theta<\pi/2} \varepsilon_1^2(\theta) &= \varepsilon_1^2(\pi/2) = \|\delta\mathbf{m}_0\|_L^2 ,\\
\inf_{0<\theta<\pi/2} \varepsilon_2^2(\theta) &= \varepsilon_2^2(\pi/2) = 0 ,\\
\sup_{0<\theta<\pi/2} \varepsilon_2^2(\theta) &= \varepsilon_2^2(0) = \delta\mathbf{m}_0 \overset{L}{\cdot} \mathbf{A}_L^{\dagger}\mathbf{C}_{nn}\, \mathbf{A}_L^{\dagger *} \overset{L}{\cdot} \delta\mathbf{m}_0 \ .
\end{aligned}
$$

A schematic diagram of this tradeoff curve is pictured in Figure 2.2. The qualitative features of this diagram are essentially identical to those of Figure 3 of Backus and Gilbert [1970, p.144].

Backus and Gilbert [1970] point out that it is best to avoid solutions corresponding to extremal values of θ. Clearly, the generalized inverse solution [eq.(2.6.4)] is a poor choice on the tradeoff curve. According to Gilbert [1972, p.146], " the place to be is down at the corner." This optimal point can be defined by the equation

$$
(2.7.24)\qquad \frac{d[\varepsilon_2^2]}{d[\varepsilon_1^2]} = -1 \ .
$$

We see from equation (2.7.21) that this point corresponds to the solution (2.5.10) obtained from the stochastic inverse.

2.8 <u>The response operator</u>. For the estimate $\overline{\delta \mathbf{m}}(\theta)$ to be useful, we must be able to evaluate how successfully it approximates the desired solution $\delta \mathbf{m}_0$. Substituting equation (2.7.11) into equation (2.7.2) we obtain

$$\overline{\delta \mathbf{m}}(\theta) \;=\; \mathbf{R}(\theta) \overset{L}{\cdot} \delta \mathbf{m}_0 . \tag{2.8.1}$$

This result is a generalization of equation (2.4.4). The operator $\mathbf{R}(\theta)$ represents the filter through which we "see" $\delta \mathbf{m}_0$. It is optimal in the sense that it minimizes the quadratic form ε^2. We shall call $\mathbf{R}(\theta)$ the <u>response operator</u>. For $\theta = 0$, the response operator reduces to the projection operator $\mathbf{P}^L_{\mathfrak{R}(A_L^*)}$ defined in §2.6. For $\theta = \pi/4$, the response operator equals the autocorrelation operator of the process $\overline{\mathbf{p}_s}$ given by (2.5.7).

Given $\mathbf{R}(\theta)$ and any $\mathbf{g} \in \mathfrak{M}_L$, we define the <u>relative success of estimation</u> η_L^2 of the vector $\mathbf{g}$ at θ by the equation

$$\eta_L^2(\theta, \mathbf{g}) \;=\; \frac{\mathbf{g} \overset{L}{\cdot} \mathbf{R}(\theta) \overset{L}{\cdot} \mathbf{g}}{\mathbf{g} \overset{L}{\cdot} \mathbf{g}} . \tag{2.8.2}$$

It can be easily seen that $0 \le \eta_L^2(\theta, \mathbf{g}) \le 1$ for all $\mathbf{g}$. Let $\mathbf{f} = (A_L \overset{L}{\cdot} A_L^*)^\dagger A_L \overset{L}{\cdot} \mathbf{g}$, so that $\mathbf{g} = A_L^* \mathbf{f} + \mathbf{P}^L_{\mathfrak{N}(A_L)} \overset{L}{\cdot} \mathbf{g}$. Since $\mathbf{R}(\theta)$ is positive semi-definite, $\eta_L^2 \ge 0$. Furthermore, since $\mathfrak{N}(\mathbf{R}) = \mathfrak{N}(A_L)$, it is clear that $\eta_L^2 \le \mathbf{f} A_L \overset{L}{\cdot} A_L^* \mathbf{Q}^\dagger A_L \overset{L}{\cdot} A_L^* \mathbf{f} / \mathbf{f} A_L \overset{L}{\cdot} A_L^* \mathbf{f}$. Now the term on the right of this expression will be always less than or equal to 1 if $\| \mathbf{Q}^\dagger A_L \overset{L}{\cdot} A_L^* \mathbf{f} \| \le \| \mathbf{f} \|$. This inequality holds because $\| A_L \overset{L}{\cdot} A_L^* \| \le \| \mathbf{Q} \|$, and we can therefore replace $A_L \overset{L}{\cdot} A_L^*$ by $\mathbf{Q}$.

Thus we conclude that $\eta_L^2 \leq 1$. This implies that $\mathbf{C}_{ss} - \mathbf{R}(\theta)$ is a positive semi-definite operator, a fact we used in the previous section.

Suppose that $R(r,r_0)$ is the kernel of $\mathbf{R}(\theta)$. From (2.8.1) we see that that this kernel with r_0 fixed is an averaging kernel in $\mathfrak{M}_L$; that is, defines a vector in $\mathfrak{M}_L$ whose L-product with $\delta \mathbf{m}_0$ is the estimate $\overline{\delta m}(r_0)$. In the limit of infinite resolution this kernel will approach the kernel $C_{ss}(r,r_0)$. Equivalent averaging kernels in the space $\mathfrak{M}$ are obtained by applying $\mathbf{R}$ to the operator $\mathbf{I}$. Define

$$\mathscr{A} = \mathbf{R}(\theta) \overset{L}{\cdot} \mathbf{I} \tag{2.8.3}$$

In the limit of infinite resolution the kernel of $\mathscr{A}$ approaches the kernel $I(r,r_0)$ which consists of delta functions. $\mathscr{A}$ and $\mathbf{R}(\theta)$ are equivalent in the sense that

$$\mathscr{A} \cdot \delta \mathbf{m}_0 = \mathbf{R}(\theta) \overset{L}{\cdot} \delta \mathbf{m}_0 . \tag{2.8.4}$$

It is usually more convenient to work with $\mathscr{A}$, since it does not require comparison with $\mathbf{C}_{ss}$. We note that $\mathscr{A}$ is not symmetric.

2.9 The variance operator. In the previous section we saw that the response operator $\mathbf{R}(\theta)$ is a representation of the inverse filter used to calculate the estimate $\overline{\delta \mathbf{m}}$. Examination of this operator (or, equivalently, the operator $\mathscr{A}$) allows one to judge the nature of the averaging required in the estimation of the solution $\delta \mathbf{m}_0$. Any features of the solution lost in this averaging are said to be unresolvable. The components in the null space of $\mathbf{A}$ will obviously be unresolvable, and, due to the fact that the data are contaminated by errors, it is possible that a component of the solution in the range space of $\mathbf{A}$ is unresolvable as well.

A simple quantitative criterion for the resolvability of any vector in the model space can be established in terms of the operator $\mathbf{V}(\theta)$ defined in (2.7.14). This operator represents a transformation of the error autocorrelation operator $\mathbf{C}_{nn}$ into the model space. The eigenvalues of $\mathbf{V}(\theta)$ represent the variances of the errors induced on the model space by errors in the data along directions given by its eigenvectors, motivating us to call $\mathbf{V}(\theta)$ the <u>variance</u> <u>operator</u>. If ξ^2 is an eigenvalue of $\mathbf{V}(\theta)$ associated with the eigenvector $\mathbf{v}$, then the probability that the errors in the data will give rise to an error in the estimate along the direction $\mathbf{v}$ with a magnitude less than $1.96\ \xi$ is 95%. This follows from the fact that the errors are normally distributed and that, for a normal distribution, the integrated probability in the interval [$-1.96 \times$ the standard deviation, $+1.96 \times$ standard deviation] about the mean is 95%. In general, let $k(c)$ be the factor associated with the confidence coefficient c, so that $k(95\%) = 1.96$.

Now, since the errors are normally distributed, the question of the resolvability of vectors in $\mathfrak{M}$ can be posed as the problem of deciding between two simple hypotheses. Let $\mathbf{m}$ and $\mathbf{m}'$ be two vectors in $\mathfrak{M}$, and let us ask, are these two vectors resolvable by the observations? Quite obviously, they will not be if the difference between them $\delta\mathbf{m} = \mathbf{m} - \mathbf{m}'$ is the zero vector. In the usual fashion of statistical inference [Freeman, 1963] we set up a null hypothesis:

the vector $\delta\mathbf{m}$ is the zero vector, and an alternative hypothesis: the vector $\delta\mathbf{m}$ is not the zero vector. If, on the basis of some criterion, we can reject the null hypothesis, then we shall say that $\delta\mathbf{m}$ is resolvable.

The most obvious criterion is the following: we reject the null hypothesis if the projection of $\delta\mathbf{m}$ onto $\mathfrak{R}(\mathbf{A}^*)$ lies outside the hyperellipse $\mathscr{E}[\mathbf{V}(\theta)] \subset \mathfrak{R}(\mathbf{A}^*)$ whose principal axes are along the eigenvectors $\mathbf{v}_n$ of $\mathbf{V}(\theta)$ and have lengths $k(c)\ \xi_n$, where c is some chosen confidence coefficient. Translating this geometrical criterion into an algebraic statement, we say that $\delta\mathbf{m}$ is resolvable with a confidence c if

$$\delta\mathbf{m} \cdot \mathbf{V}^{\dagger}(\theta) \cdot \delta\mathbf{m} > k^2(c). \tag{2.9.1}$$

The form of the resolvability criterion given in equation (2.9.1) requires that the error autocorrelation operator $\mathbf{C}_{nn}$ be nonsingular. In fact, because the generalized inverse of $\mathbf{V}(\theta)$ appears in this expression, the computation will be unstable if the error induced on the model space is very small.

Chapter 3

SPHERICALLY SYMMETRIC AVERAGES OF THE EARTH'S VELOCITY AND DENSITY DISTRIBUTIONS

3.1 Introduction. For most seismological purposes, wave propagation in the Earth can be adequately described by specifying the compressional and shear velocities and density at each point in the Earth's interior. At the present time, however, the inverse problem of modeling these three quantities from the observations of wave propagation becomes feasible only if the distributions are taken to be spherically symmetric. For models involving more than one spatial dimension, the foward computation of such data functionals as travel times and eigenperiods is difficult and incredibly laborious. More importantly, the available observations do not contain enough usable information about aspherical variations of velocity and density to warrant inversion. For these reasons we restrict our attention to Earth models that are spherically symmetric.

Approximate spherical symmetry is to be expected. For an isolated, stationary, self-gravitating fluid in its equilibrium configuration, surfaces of constant density, pressure, and therefore velocity are spherical and concentric about its center of mass. Because the strength of the Earth is much less than the hydrostatic pressure throughout most of its interior, its state of stress is very nearly hydrostatic. If the state of the Earth's interior is close to equilibrium, then the density distribution should be approximately spherically symmetric, since the other body forces are small compared to the force of selfgravity. Realizing that velocity variations are intimately related to density variations through their dependence on pressure, we should expect approximate spherical symmetry in the velocities as well.

In the early years of seismology, spherical symmetry proved to be an adequate assumption for the purposes of modeling the velocities and density. Indeed, it was not until the 1930's that the errors in travel time observations were reduced to the point that corrections for the Earth's ellipticity were warranted. These corrections, up to four seconds for some phases, were published in the form of tables by Bullen in 1937. Apart from the Earth's ellipticity of figure, which was sufficiently well predicted by hydrostatic theory, aspherical variations for the most part appeared to be confined to the Earth's crust. The existence of lateral differences in the uppermost layers explained reasonably well the fluctuations in travel times at short distances and the differences in surface wave dispersion. The consistency of travel times at distances greater than 20°, evidenced by the similarity of the Jeffreys-Bullen and Gutenberg-Richter tables, provided a strong argument for the spherical symmetry of velocities in the lower mantle and core.

Predictably, modern refinements and diversification of seismic techniques have reduced the standard error of one observation to where most of the scatter in travel times can be attributed to lateral heterogeneity. This is also true for many of the eigenperiods greater than 300 seconds. It now appears that the entire upper mantle is laterally variable and that heterogeneities persist at least to the depth of the core-mantle interface. In the light of these facts, we must reexamine the appropriateness of requiring a spherically symmetric representation of the Earth to satisfy data contaminated by the effects of lateral heterogeneities.

Most authors working on the radial variations of velocity using travel times have tried to eliminate lateral effects either by averaging the data or by applying direct corrections for them. The latter procedure is exemplified by the use of station corrections [Herrin and Taggart, 1968]. Unfortunately, this method is limited; it only accounts for anomalies in the vicinity of the receiver - usually only in the form of a constant correction for all distances and azimuths. Some work has progressed on correcting for source anomalies underneath the Aleutian arc using nuclear explosion data and three-dimensional ray tracing techniques [Sorrells et al.,1971; Jacob,1972], but the wide application of this method has been prevented by its complexity and a lack of data.

Applying direct corrections to free oscillation data is even more tedious. McGinley [1968] has treated the effect of some lateral structures on torsional oscillations using perturbation theory, and Dahlen [1968, 1969] has formulated the general first-order perturbation theory for both spheroidal and torsional oscillations using Rayleigh's principle. However, the calculations are too complex and the regional structure of the Earth is too unknown to permit any simple correction to be made to the eigenperiod data.

A more reasonable procedure is to treat the fluctuations due to lateral variations as another source of error and simply eliminate them by averaging. This has been the procedure of most investigators since the early work of Jeffreys. It is clear that averaged data contain information about some sort of spherically averaged representation of the Earth. For any estimates to be useful we must know the approximate nature of the spherical averaging, as well as the kind of data distribution required to insure that the sample averages estimate without bias data functionals of this spherically symmetric representation.

Two averaging theorems which provide this information exist, one for eigenfrequencies, due to Gilbert, and one for travel times. The purpose of this chapter is to state these theorems.

3.2 <u>The Terrestrial Monopole</u>. Suppose $v_p(r,\theta,\phi)$ is the compressional velocity, $v_s(r,\theta,\phi)$ is the shear velocity, and $\rho(r,\theta,\phi)$ is the density in the Earth expressed in spherical coordinates with an origin at the Earth's center of mass. Then the spherically symmetric distributions

(3.2.1) $$\begin{bmatrix} v_{p0}(r) \\ v_{s0}(r) \\ \rho_0(r) \end{bmatrix} = \frac{1}{4\pi}\int_0^{2\pi}\int_0^{\pi} \begin{bmatrix} v_p(r,\theta,\phi) \\ v_s(r,\theta,\phi) \\ \rho\ (r,\theta,\phi) \end{bmatrix} \sin\theta\, d\theta\, d\phi$$

constitute what Gilbert [1972] has termed the Terrestrial Monopole. The velocity and density distributions in the Earth can each be written as the sum of two terms:

$$(3.2.2)\qquad \begin{bmatrix} v_p(r,\theta,\phi) \\ v_s(r,\theta,\phi) \\ \rho\ (r,\theta,\phi) \end{bmatrix} = \begin{bmatrix} v_{p0}(r) \\ v_{s0}(r) \\ \rho_0\ (r) \end{bmatrix} + \begin{bmatrix} \delta v_p(r,\theta,\phi) \\ \delta v_s(r,\theta,\phi) \\ \delta\rho\ (r,\theta,\phi) \end{bmatrix}.$$

The terms δv_p, δv_s, and $\delta\rho$ represent the departures from spherical symmetry and average to zero on spheres of constant radius r. If the Earth is nearly spherically symmetric, then these terms will be small compared to v_p, v_s, and ρ.

3.3 Gilbert's averaging theorem for eigenfrequencies. Because of rotational symmetry, an eigenfrequency of angular order ℓ belonging to to the Terrestrial Monopole is $(2\ell + 1)$-fold degenerate. The effect of adding aspherical perturbations as in equation (3.2.2) is to remove this degeneracy. Gilbert [1972] has shown that, to first order in δv_p, δv_s, and $\delta\rho$, the arithmetic average of singlet eigenfrequencies in a mode multiplet split by lateral heterogeneities is the degenerate multiplet eigenfrequency of the Terrestrial Monopole. This result is a direct consequence of the zero sum rule of degenerate perturbation theory and is true for all first-order aspherical perturbations, including those due to rotation and ellipticity.[1]

As Gilbert [1972] points out, this implies that, if the distribution of source and receiver parameters is such that the probability of picking a particular frequency as the "peak frequency" of a mode multiplet has a density equal to the density of singlets at that fre -

[1] Dahlen [1968, p.364] had shown this for ellipticity.

quency, then the average of many observed peaks is an unbiased estimate of the eigenfrequency belonging to the Terrestrial Monopole.

Because of this averaging theorem, the construction of the Terrestrial Monopole is a logical goal of gross Earth inversion studies that use mode data.

3.4 An averaging theorem for travel times. At the present time, the body of reliable eigenperiod data samples only sparsely those modes with periods less than 300 seconds. Below 300 seconds the normal mode spectrum of the Earth is densely populated, and the identification of individual lines is difficult. Until this deficiency is remedied,[2] better estimates of the density and seismic velocities in the Earth will be obtained by the simultaneous inversion of both eigenperiod and travel-time data. However, for the results of any inversion to have meaning, the sets of averaged eigenperiod data and averaged travel-time data must be consistent in the sense that they average the velocity distributions in roughly the same way.

Most seismologists have seemed contented to define the "average" radial velocity distribution in the Earth to be the one obtained by the inversion of travel-time averages. Quotes are often used around the word average to indicate that the nature of the averaging depends on the distribution of sources and receivers [e.g. Freedman, 1968, p.1270]; there is the general realization that often regions of high seismicity (tectonic regions) and high station density (continental

---

[2] Dziewonski and Gilbert (personal communication) have turned their attention to this problem and have met with some success.

platforms) receive undue weight and bias this averaging. Intuitively, the average velocity distribution corresponds to the travel-time curve obtained by averaging many observations, each measured from a source-receiver pair located at random on the Earth's surface.

These intuitive notions have a solid basis in the following theorem: To first order in δv (P or S), the ray-theoretical surface-focus travel times between source-receiver pairs at constant angular distance Δ are distributed with a mean equal to the travel time T_0 at distance Δ through the Terrestrial Monopole, provided the distributions of sources and receivers on the surface of the Earth are uniform.

This result follows directly from Fermat's principle of stationary time. To first order, perturbations of the travel times due to variations in the path are negligible. As a consequence, an integration over all source-receiver geometries to get the mean yields $T_0(\Delta)$ plus terms containing areal averages of δv, which are zero. A more complete discussion of the proof is given in Appendix 1.

To a good approximation, unbiased estimates of both the travel times and eigenperiods of the Terrestrial Monopole are attainable, making their simultaneous inversion feasible. In practice, the hypothesis of this averaging theorem is difficult to satisfy for absolute travel times - the distributions of sources and receivers on the Earth's surface are certainly not uniform. This motivates the use of differential travel times, discussed in Chapter 4.

Importantly, since no equivalent averaging theorems exist at this time for amplitude, $dT/d\Delta$, and group velocity data functionals, the averages of their observations cannot be as simply interpreted as the averages of travel-time and eigenperiod data. For these reasons we have excluded them from the data sets used in our calculations.

3.5 Other spherically symmetric representations. Abrupt discontinuities are well-established features of the Earth's velocity and density distributions. The Earth's surface and core-mantle interface are the most obvious examples. Since the radii of these discontinuities are variable due to the effects of rotation, lateral heterogeneities, and non-hydrostatic stress differences, averaging over spheres of constant radius to obtain the Terrestrial Monopole " smears them out "; sharp discontinuities become zones of transition. For example, it is observed that the core-mantle boundary reflects considerable compressional energy propagating at periods as low as 1 second. Kanamori [1967] estimates from the spectral amplitudes of PcP phases that a major transition must occur in a layer less than 1 kilometer thick. Now, the ellipticity of the core-mantle interface is about 0.003, so that spherical averaging [equation (3.2.1)] yields a transition region approximately 10 km thick. Large amplitude lateral variations in the radius of this boundary would yield a correspondingly thicker transition zone. This sort of spherically symmetric representation can be inconvenient in theoretical and numerical calculations.

If the variations in the radii of discontinuities are small compared to the radius of the Earth, spherically symmetric averages can be defined which preserve these discontinuities and still allow one to make use of the first-order averaging theorems. The prescription is simple: the radii of the discontinuities are first averaged over the sphere, and the resulting distributions are averaged as in equation (3.2.1). Of course, we expect that the difference between this averaged representation and the Terrestrial Monopole will be negligible, at least to first order.

Chapter 4

DIFFERENTIAL TRAVEL TIMES AS GROSS EARTH DATA

4.1 Introduction. A differential travel time is simply the difference between the times of arrival of any two body phases radiated from the same source and recorded at the same station. For example, if the travel time of the phase PcP at distance Δ is $T_{PcP}(\Delta)$ and if the time of P is $T_P(\Delta)$, then the differential travel time of the phase combination PcP-P equals $T_{PcP}(\Delta) - T_P(\Delta)$ and is denoted $T_{PcP-P}(\Delta)$.

Differential travel times have been used for some time by seismologists for locating earthquakes. The differential times of certain phase combinations yield directly good first approximations to the origin time (S-P), the depth (pP-P, sP-P), and the distance (PcP-P, PKKP-P) of an earthquake, and they are often tabulated for use at observatories.

Use has been made of differential times in the construction and verification of absolute travel-time curves. Gutenberg and Richter [1934] used PKKP-P, P'P'-P, and P'P'P'-P times to get the absolute times of PKKP, P'P', and P'P'P'. These phases were recorded only after deep events with poorly constrained hypocenters, and the differential times were relatively insensitive to the depth of focus. In more recent studies, Hales and Roberts [1970 b, 1971] used the differential times of SKS-S, SKKS-SKS, and SKKKS-SKKS to construct travel-time curves for S and K. Bolt [1968] presented some readings of the time $T_{P'(AB)-P'(DF)}$ to check his determination of the absolute times for the phase P'(AB).

Although differential times have been employed in the study of absolute travel times, the direct use of them to infer the velocity structure has been limited to locating reflectors. If the velocity distribution above a discontinuity is known, then the time between the arrivals of the direct and reflected waves yields an estimate of the depth of the discontinuity. Hales and Roberts [1970 b] used a shear velocity model for the mantle and the differential times of ScS-S to estimate the depth of the core-mantle boundary.

The purpose of this chapter is 1) to demonstrate that the differential travel times of particular phase combinations are an excellent source of gross Earth data and are relatively uncontaminated by the systematic errors that corrupt absolute travel time data, and 2) to present some observations of T_{PcP-P}, T_{ScS-S}, $T_{P'(AB)-P'(DF)}$, and $T_{P'(BC)-P'(DF)}$. The observations are included in the data sets used in Chapter 5 to derive estimates of the radial variation of seismic velocities and density. We begin with a general discussion on the inversion of travel-time data.

4.2 Inversion of travel-time data. The classical work of Herglotz [1907] and Wiechert [1910] established a constructive existence and uniqueness theorem for the solution of the travel-time inverse problem in a radially stratified medium, subject to certain assumptions. Their method has been used extensively in seismology to construct profiles of elastic-wave velocities in the Earth from the observations of travel times. A number of authors [Slichter, 1932; Gerver and Markushevich, 1967; Backus and Gilbert, 1969; Johnson, 1971] have pointed out the various inadequacies of this theory in its application to real data and the real Earth. To be strictly valid, the Herglotz-Wiechert procedure requires that the velocity gradient dv/dr be everywhere less than v/r and that the ray-parameter - distance relationship be perfectly well known at almost all distances. Of course, in practice neither requirement can be realized. Only a finite number of data can be obtained, and both shadow zones in the Earth and errors in the data do exist.

These reasons motivate the use of a linear theory, such as the one in Chapter 2, to solve the inverse problem. The linear formulation, equation (2.3.3), utilizes the spherically symmetric Fréchet kernels to relate changes in the model to changes in the data functionals. For travel times the spherically symmetric Fréchet kernel is given by equation (A1.2.5). Using (A1.1.4) and (A1.2.3), we see that this kernel can be written

$$(4.2.1) \qquad a(r) = \sum_{i=1}^{n+1} \frac{-\eta(r)}{v_0^2(r)\,(\eta^2(r)-p^2)^{1/2}}\, H[\varepsilon_i(r-\rho_{i-1})] \cdot H[\varepsilon_i(\rho_i-r)], \quad 0 \leq r \leq R,$$

where $\eta(r) = r/v_0(r)$ and p is the parameter of the ray. If any of the turning radii ρ_i, $i = 1,2,\ldots,n$, equal the classical turning radius $\rho = p\, v_0(\rho)$, then the kernel has a square-root singularity at $r = \rho$.

We can easily show that this singularity is integrable. That is, it can be shown

$$I[a] \equiv \int_0^R a(r)\, dr < \infty . \tag{4.2.2}$$

The integral I[a] is an improper integral of the second kind, and according to Gradshteyn and Ryzhik [1965], the integral is bounded if there exists a scalar $\alpha < 1$ such that

$$\lim_{r \to \rho} [(r - \rho)^{\alpha} a(r)] < \infty . \tag{4.2.3}$$

Now, $a(r) \propto (r - [v_0(r)/v_0(\rho)]\, \rho)^{-1/2}$, the other factors being always bounded, so that (4.2.3) is true if $\alpha \geq 1/2$ and if v_0 is continuous at ρ. Therefore, the integral exists at all but isolated values of p.

Although a(r) is integrable, its square obviously is not. This means that the Fréchet kernel relating changes in velocity to first-order changes in travel time is not a member of the Hilbert space of square-integrable functions, a fact that is the source of some theoretical difficulty. The linear theory requires that the Fréchet kernels belong to the space of Earth models. Since Backus and Gilbert [1967] take this to be the Hilbert space of square-integrable functions, travel time data cannot be inverted directly for velocity using their procedure. To avoid this difficulty, Backus and Gilbert [1969] and Johnson [1971] integrate the perturbation equation [equation (2.3.2)] by parts, yielding an equation relating a change in a <u>derivative</u> of velocity to a change in travel-time. The Fréchet kernel in this new equation is an integral of a(r) and is square-integrable. As Johnson [1971] points out, this procedure is an example of what

Backus [1970b] has called a linear quelling by integration.

The fact that a(r) is not square-integrable presents no difficulty if the inner product on the model space is suitably chosen.[1] The Fréchet kernel a(r) relates a spherically symmetric velocity variation $\delta v(r)$ to its corresponding first-order perturbation δT in travel time by the equation

$$\int_0^R a(r)\ \delta v(r)\ dr \quad = \quad \delta T. \tag{4.2.4}$$

If the inner product on the model space is defined as the bilinear form associated with the positive definite symmetric kernel $L(r,r')$, then we noted in §2.6 that the Fréchet kernel is

$$a_L(r) \quad = \quad \int_0^R L^{-1}(r,r')\ a(r')\ dr', \tag{4.2.5}$$

so that the perturbation equation (4.2.4) becomes

$$\int_0^R \int_0^R a_L(r)\ L(r,r')\ \delta v(r')\ dr\ dr' \quad = \quad \delta T\ . \tag{4.2.6}$$

Now, the kernel $a_L(r)$ belongs to the model space if

$$\int_0^R \int_0^R a_L(r)\ L(r,r')\ a_L(r')\ dr\ dr' \quad < \quad \infty\ . \tag{4.2.7}$$

This inequality is satisfied if the integral

$$\int_0^R \int_0^R a(r)\ C(r,r')\ a(r')\ dr\ dr' \tag{4.2.8}$$

is bounded, where $C(r,r') \equiv L^{-1}(r,r')$. It is easy to show that

---

[1] Generalization of the inner product on the model space is discussed in Chapter 2. The notation used in this section is compatible with the notation used in Chapter 2 if $M = 1$ and $w(r) = 1$.

(4.2.8) is bounded if we specify $C(r,r')$ by the expansion

$$C(r,r') = \sum_{n=1}^{\infty} \frac{k^2}{k^2 + n^2\pi^2} s_n(r)\, s_n(r'), \tag{4.2.9}$$

where $s_n(r) = 2^{-1/2} \sin n\pi r$ for all positive integers n.[2] Substituting (4.2.9) into (4.2.8), we obtain

$$\sum_{n=1}^{\infty} \frac{k^2}{k^2 + n^2\pi^2} \left[\int_0^R a(r)\, s_n(r)\, dr \right]^2, \tag{4.2.10}$$

which we assert is bounded. The assertion is verified by noting that the integral in the brackets is always less than or equal to $2^{-1/2}\, I[a]$, a constant for all n. Therefore, (4.2.10) converges as n^{-2}, and $a_L(r)$ belongs to the model space.

Since the characteristic wave-number k_n of the system (2.6.11) is always proportional to n, the travel-time Fréchet kernel (4.2.1) will belong to any model space for which $C(r,r')$ $\left(= L^{-1}(r,r')\right)$ satisfies the system (2.6.15). In the terminology of Backus [1970b], equation (4.2.5) is a linear quelling by convolution.

Travel-time data can thus be inverted using the theory developed in Chapter 2.

4.3 <u>A comparison of systematic errors in absolute and differential travel times</u>. Because a differential travel time is a linear combination of absolute travel times, the theory presented in the previous section and the averaging theorem for travel times given in §3.4 for

---

[2] It can be shown that $C(r,r')$ satisfies (2.6.15) with $p(r) = w(r) = 1$, $q(r) = 0$. Since $j_0(r) = (\sin r)/r$, $C(r,r')$ equals the product of the kernel given in (2.6.16) and the factor rr'.

absolute times can be applied verbatum to differential times. In this section we argue that the systematic errors in particular differential travel times are generally much less than the systematic errors in the corresponding absolute travel times. For this reason differential travel-time data will be used in lieu of absolute travel-time data in the numerical inversions presented in Chapter 5.

The statistical uncertainties in estimating mean travel times calculated from sample dispersion are generally small, as low as ±0.06 seconds (standard error in the mean) for direct teleseismic P waves in the 1968 Tables [Arnold, 1968]. For Gaussian processes the standard error in the mean is inversely proportional to the square-root of the sample size, and it can be arbitrarily reduced simply by increasing the number of measurements. But statistics of this type adequately measure the error only if the error process has zero mean - the sample mean must be an unbiased statistic. Most likely, however, sample averages of existing travel-time data are severely biased by systematic errors introduced in the mislocation of earthquakes, incorrect identification of arrival times, poor sampling of lateral heterogeneities, the inadequacies of ray theory, etc.

Because we cannot easily account for their effect on model estimates, these systematic errors must be reduced to insignificance. Obviously, systematic errors are not reduced simply by increasing the sample size. If independently estimated, they can be subtracted. For travel times this procedure involves estimating source and station anomalies, calculating corrections for ellipticity, and the like.

The difficulties involved with this approach were mentioned in §3.1. An alternative is to use differential travel times. The idea is the following: A differential travel time is the difference between two absolute travel times. If the absolute times are systematically in error by the same amount, their difference will be an unbiased quantity.

The relative effect of some systematic errors on the differential times of PcP-P, ScS-S, P'(AB)-P'(DF), and P'(BC)-P'(DF) and on their corresponding absolute times for an earthquake 600 km deep can be evaluated using Table 4.1. (Further discussion of these phase combinations and some observations of their differential travel times are presented in the next section.) We consider the following sources of systematic error:

Origin time and location errors. Before the use of nuclear explosions as sources and before the advent of the WWSSN, origin time and location errors were the most serious concern of seismologists. These errors are now much reduced. However, locating earthquakes and modifying travel-time tables is still a "bootstrap" procedure and is susceptible to bias. Of course, for differential travel times, origin time errors cancel uniquely. The difference in travel time δT resulting from a mislocation $\delta\Delta$ in angular distance and δh in depth is given approximately by the formula

$$(4.3.1) \qquad \delta T = \left[\frac{\partial T}{\partial \Delta}\right] \delta\Delta + \left[\frac{\partial T}{\partial h}\right] \delta h \ .$$

The values of the derivatives in (4.3.1) have been computed for several

Table 4.1

Parameters for estimating the sensitivity of travel times to bias

X	Y	Δ	$\partial T/\partial\Delta$ (sec/deg)			$\partial T/\partial h$ (sec/100km)			seconds above 600 km		
		(deg)	X	Y	X-Y	X	Y	X-Y	X	Y	|X-Y|
PcP	P	30^o	2.6	8.5	-5.9	9.2	4.9	5.3	72	102	30
		70^o	4.3	5.9	-1.6	8.6	8.6	0	76	90	14
ScS	S	30^o	4.9	15.4	-10.5	17.1	8.8	8.3	130	182	52
		80^o	8.3	10.0	-1.7	15.5	14.5	1.0	137	143	6
P'(AB)	P'(DF)	145^o	3.9	1.7	2.2	9.0	9.6	-0.6	74	72	2
		175^o	4.4	0.1	4.3	8.8	9.9	-1.1	76	71	5
P'(BC)	P'(DF)	145^o	2.6	1.7	0.9	9.4	9.6	-0.2	72	72	0
		155^o	2.2	1.3	0.9	9.5	9.7	-0.2	72	71	1

phases from the Jeffreys-Bullen Tables and listed in Table 4.1. With few exceptions, these values are less for the differential times. For example, at 70° the error in T_P due to an epicentral mislocation of 0.1° is about 0.6 seconds [$\partial T_P/\partial\Delta = 5.9$ sec/deg], whereas the corresponding error in T_{PcP-P} is only about 0.2 seconds [$\partial T_{PcP-P}/\partial\Delta = -1.6$ sec/deg]. At the same distance the error in T_P due to a 10 km error in the depth of focus is 0.9 seconds [$\partial T_P/\partial h = 8.6$ sec/100 km]. The corresponding error in the time of PcP-P is less than .01 seconds. For differential times, the greatest absolute values of [$\partial T/\partial\Delta$] and [$\partial T/\partial h$] given in the table are those of ScS-S at 30° (10.5 sec/deg and 8.3 sec/100 km, respectively). Even so, both of these values are less than the corresponding values for S at the same distance (15.4 and 8.8).

Sampling bias. Because seismic sources are generally in tectonic regions and because most receivers are on continental platforms, the uniform distributions of sources and receivers required by the first-order averaging theorem [§3.4] are not available. In particular, there is a paucity of observations that sample the upper mantle under ocean basins. This sampling bias is now probably the most serious source of systematic errors in the measurements of absolute travel times. Fortunately, severe lateral heterogeneity seems for the most part confined to the crust and upper mantle. Phases with high apparent velocities travel along nearly vertical paths through this region, so that for some range of (low) $dT/d\Delta$'s sampling bias will appear in the travel time curve as approximately a constant term. This constant error is termed the baseline error. Of course, the baseline error for phases propagating as compressional waves through the upper mantle will be different (generally smaller) than for shear phases. We observe that differential travel times of high apparent velocity phases travelling through the upper mantle in the same mode of propagation are relatively insensitive to variations in upper mantle structure. Quite obviously, simple baseline errors cancel. Table 4.1 gives some indication of how insensitive several phase combinations are. For example, the phase PcP arriving at an angular distance of 30° from a source 600 km deep spends about 72 seconds traversing the upper 600 km of the mantle; at the same distance the phase P spends about 102 seconds. Therefore, a 1% variation in velocity averaged over the upper mantle will change the travel time by about 0.7 seconds for PcP and 1.0 second for P. However, the same variation will affect their differential travel time by only 0.3 seconds. This reduction is even more dramatic for the other combinations and distances listed in the table.

Reading errors. Much of the art of seismology involves extracting signals from a background of noise. In this task, no substitute has yet been found for the seismologist's eye. However, every seismologist is aware that picking emergent arrivals late, especially phases that are not first arrivals, can be a source of considerable bias in travel-time measurements. If two phases have the same waveform, then their differential travel time can be measured between any two correlatable features of the signal, such as peaks or zero-crossings. This advantage of differential travel times has been used to reduce reading errors and improve time resolution. Hales and Roberts [1970b], for instance, read the differential times of ScS-S by correlating peaks. However, this procedure must be used with caution since unknown effects due to propagation and source can distort one signal relative to another and introduce systematic errors.

We have established in the discussion above that the susceptibility of a differential travel-time datum to bias will be small if

i) the difference between the ray parameters of the two phases is small,

ii) the modes of propagation through the upper mantle are the same,

iii) the ray paths through the upper mantle are similar,

iv) the waveforms are similar and well recorded on the same instrument.

4.4 Observations of differential travel times. In this section five sets of differential travel-time data are presented. These are listed in Table 4.2. Surface focus differential travel times of PcP-P were reduced from the published absolute travel times of PcP and P recorded from nuclear explosions and reported by Kogan [1960], Buchbinder [1965], Kanamori [1968], and Lambert et.al. [1968]. Differential travel times of core phases (relative to P'(DF)) were obtained from the data sets of Hai [1963] and Engdahl [1968] and supplemented by new readings from three deep-focus events in the Sunda Arc. In addition, two new sets of differential travel times for the phase combinations PcP-P and ScS-S were read from long-period records of the World Wide Standardized Seismographic Network using eleven deep-focus

Table 4.2

Observed sets of differential travel times

Phase combination	Distance range	Events used
PcP-P	25° - 80°	Explosions
PcP-P	25° - 70°	Deep earthquakes
ScS-S	25° - 85°	Deep earthquakes
P'(AB)-P'(DF)	145° - 180°	Deep earthquakes
P'(BC)-P'(DF)	145° - 160°	Deep earthquakes

earthquakes.

The earthquakes used in this study were restricted to events with focal depths greater than 500 km and magnitudes between 5.5 and 6.5. The reasons for this were several. Deep earthquakes in this magnitude range write exceptionally sharp seismograms, making them ideal for travel time studies.[3] Secondly, the ray paths for these events include only one transit through the heterogeneous upper mantle, reducing a source of possible bias. Thirdly, the records are uncontaminated by surface waves. This allows one to read the times of ScS-S at short distances. For normal-focus events, surface waves preceed ScS at distances less than 45°, and the reading of ScS-S is difficult [Hales and Roberts, 1970b]. Finally, simple geometrical considerations imply that these events will be well located [Mitronovas and Isacks, 1971].

---

[3] This fact was first noticed by Zoeppritz.

Table 4.3

Earthquakes used in the travel-time study

Designation	Date	Origin Time GMT	Latitude	Longitude	Depth	Mag	Source
Fiji A	4/10/65	22 32 46.0 ± .12	17.84 ± .028 S	178.70 ± .032 W	535 ± 4.5	5.7	ISS
		22 32 46.6	17.8	178.8	543	5.9	USCGS
					554 (pP-P)		ISS
New Hebrides	4/10/65	22 53 04.5 ± .11	13.45 ± .023 S	170.30 ± .026 E	641 ± 4.1	5.3	ISS
		22 53 04.8	13.4	170.3	644	6.2	USCGS
Mindanao	7/15/65	18 33 31.8 ± .10	7.64 ± .023 N	123.76 ± .031 E	605 ± 4.3	5.7	ISS
		18 33 30.7	7.7	123.8	590	6.0	USCGS
					592 (pP-P)		ISS
Peru-Brazil A	11/03/65	01 39 03.2 ± .09	9.04 ± .022 S	71.32 ± .032 W	587 ± 4.4	5.9	ISS
		01 39 03.1	9.1	71.4	593	6.2	USCGS
		01 39 03.3	9.05	71.34	590 ± 11		*
					589 (pP-P)		ISS
Fiji B	3/17/66	15 50 32.3 ± .26	21.08 ± .024 S	179.15 ± .026 W	627 ± 3.6	5.9	ISS
		15 50 33.1	21.1	179.2	639	6.2	USCGS
		15 50 33.0	21.12	179.24	639 ± 12		*
					633 (pP-P)		ISS
Argentina	12/20/66	12 26 53.6 ± .29	26.06 ± .020 S	63.10 ± .032 W	571 ± 3.8	5.8	ISS
		12 26 54.6	26.1	63.2	586	5.7	USCGS
					582 (pP-P)		ISS

*Engdahl [1968]

Table 4.3 (cont.)

Designation	Date	Origin Time GMT	Latitude	Longitude	Depth	Mag	Source
Peru-Brazil B	2/15/67	16 11 11.8 ± .25	9.05 ± .020 S	71.34 ± .024 W	598 ± 3.6	6.1	ISS
		16 11 11.5	9.07	71.38	595	6.1	USCGS
					597 (pP-P)		ISS
Java Sea A	3/24/67	09 00 20.0 ± .45	6.01 ± .025 S	112.33 ± .027 E	606 ± 6.2	5.9	ISS
		09 00 19.1	5.99	112.33	595	5.7	USCGS
					596 (pP-P)		ISS
Fiji C	10/09/67	17 21 48.7	21.07 S	179.27 W	643		†
		17 21 49.5	21.08	179.35	654	7.0	USCGS
		17 21 46.2 ± .33	21.10 ± .022	179.18 ± .019	605 ± 4.6	6.2	ISS
					633 (pP-P)		ISS
Java Sea B	1/30/68	03 44 24.8 ±	6.10 ± .020 S	113.36 ± .022 E	599 ± 5.2	6.0	ISS
		03 44 24.4	6.1	113.4	594	6.2	USCGS
					591 (pP-P)		ISS
Flores Sea	5/24/68	15 43 54.8 ± .53	6.84 ± .023 S	118.91 ± .028 E	618 ± 7.3	5.8	ISS
		15 43 54.2	6.8	118.9	609	6.0	USCGS
					618 (pP-P)		ISS
China	4/10/69	14 54 03.9	42.0 N	130.9 E	555	5.6	USCGS
Marianas	5/10/70	20 05 15.9	18.6 N	145.2 E	602	5.6	USCGS
Sea of Okhotsk	9/05/70	07 52 27.9	52.2 N	151.4 E	580	5.7	USCGS

† Mitronovas and Issacs [1971]

The thirteen deep-focus earthquakes used in this study are listed in Table 4.3. For the purposes of comparison, both ISS and USCGS locations are given, if available. In all cases the epicentral locations agree within 0.1°, and for all but one event the focal depths agree within 10 km. It can be judged from Table 4.1 that location errors of this magnitude will introduce errors in the differential travel times no greater than 1 second (for the extreme case of ScS-S at 30°). One event (Fiji C, 10/9/67) shows anomalous disagreement in the ISS and USCGS locations; the discrepancy in focal depth is nearly 50 km. Fortunately, this earthquake has been one subject of an intensive study by Mitronovas and Isacks [1971]. On the basis of their work, this anomaly can be attributed to the effect of including readings from certain anomalous stations for which the ray paths lie within the high-velocity lithospheric slab. The location we have used for this event is theirs, obtained by deleting these anomalous readings. They claim an accuracy of about ±5 km. For the other events we have used the ISS location if available and the USCGS location if not. In all cases we have used the location given in the top line of Table 4.3. All distances have been computed using geocentric coordinates.

We discuss below each data set individually:

PcP-P (surface focus). Observations of the travel times of PcP and P from nuclear explosions have been published by Kogan [1960] (South Pacific events), Buchbinder [1965] (BILBY event), Kanamori [1968] (LONGSHOT event), and Lambert et.al. (LONGSHOT event). All readings were made from records of short-period vertical seismometers. From these published values the differential times of PcP-P were computed, no corrections being applied. The data were residualed with respect to the Jeffreys-Bullen times, the residuals were divided into 5° cells, and the sample means and standard errors in the means were computed for cells centered at 30°, 35°, 40°, ... , 75° (from here on, a series of distances such as this will be abbreviated $30^\circ(5^\circ)75^\circ$). The distribution of residuals is given in Table 4.4. For every cell except

Table 4.4

Distribution of PcP-P residuals (surface focus)

Cell	Interval (sec)							
	-3	-2	-1	0	+1	+2	+3	
30°	1	0	2	8	4	0	0	0
35°	0	4	9	7	1	0	0	0
40°	0	1	8	6	3	0	2	0
45°	1	2	16	13	3	2	1	0
50°	0	1	6	10	6	3	0	0
55°	0	0	1	2	5	1	1	0
60°	1	0	0	5	4	0	2	0
65°	1	1	1	2	3	3	0	1
70°	2	1	0	0	1	1	1	1
75°	1	1	1	1	0	1	0	0

the last two, the residuals had a well-defined mode. Readings beyond 65° were few and showed considerable scatter. The sample mean and standard error in the mean were computed using the following formulae:

$$(4.4.1) \qquad \overline{T} = \frac{\Sigma\, w_i\, T_i}{\Sigma\, w_i}, \qquad s_m^2 = \frac{\Sigma\, w_i^2 (T_i - \overline{T})^2}{(\Sigma\, w_i)^2} .$$

In these expressions the w_i's are weights. It was decided to weight the readings given in Lambert et.al. only half as much as those in the other studies, because these readings showed appreciably more scatter. The means and standard errors in the means are given in Table 4.5.

Table 4.5

Observed surface focus PcP-P times

Distance (deg.)	Mean res. (sec.)	S.E.M. (sec.)	J.B.time (sec.)	Obs.time (sec.)
30	-0.5	0.18	182.4	181.9
35	-1.1	0.14	152.5	151.4
40	-0.7	0.22	125.8	125.1
45	-0.9	0.22	101.6	100.7
50	-0.4	0.19	80.3	79.9
55	+0.7	0.45	61.6	62.3
60	+0.2	0.33	45.9	46.1
65	+0.1	0.43	32.9	33.0
70	-0.3	1.11	22.4	22.1
75	-0.7	0.76	14.1	13.4

Figure 4.1 displays the observed residuals and the 5° cell means. The error bars represent one standard error in the mean.

PcP-P (deep focus). Records of fifteen deep-focus earthquakes from WWSSN stations in the distance range 25° - 75° from the source were examined for PcP phases. Two of the earthquakes were discarded because the P phases showed evidence of precursors, indicating a complex source function. PcP-P differential times were read exclusively from long-period, vertical components. Long-period records were used to insure

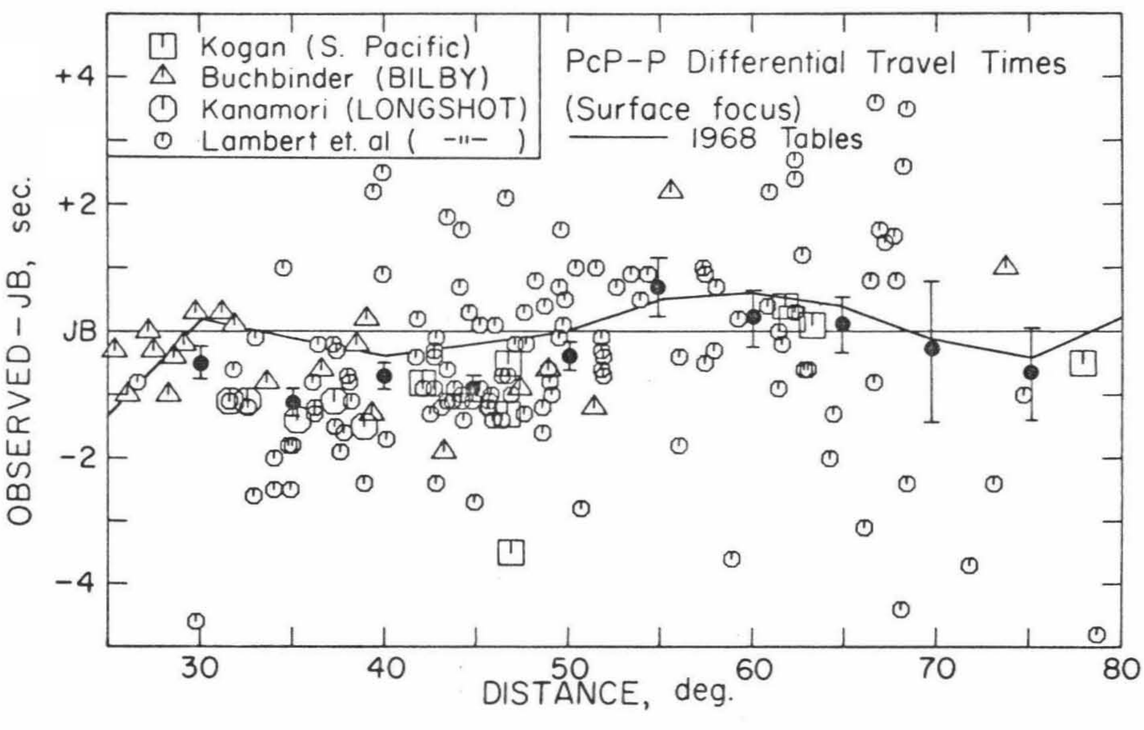

Figure 4.1. PcP-P differential travel times from nuclear explosion sources.

proper identification of the PcP phase. All readings were assigned a "quality", an integer between 0 and 5 inclusive, on the basis of sharpness of the onsets. The readings assigned a zero quality were dropped, eliminating all readings from three of the earthquakes. The measured PcP-P times from the remaining ten events are listed (with all the other data presented in this section) in Appendix 2. Figure 4.2 shows several records from the event designated Peru-Brazil B.

The procedure used to reduce these data was similar to the one described for the surface-focus PcP-P times: the times were residualed with respect to the appropriate J.B. travel time, the residuals were grouped into 5° cells, and means and standard errors in the means were computed. The distribution of residuals is given in the following table:

Table 4.6

Distribution of PcP-P residuals (deep focus)

Cell	Interval (sec)						
	-4	-3	-2	-1	0	+1	
30°	1	0	0	2	3	0	0
35°	1	1	1	0	1	1	0
40°	0	1	0	0	2	0	0
45°	0	1	1	2	7	3	0
50°	0	0	0	0	13	6	0
55°	0	0	0	1	2	2	0
60°	1	0	1	7	7	2	0
65°	0	0	2	7	1	3	0
70°	0	1	0	1	5	1	0

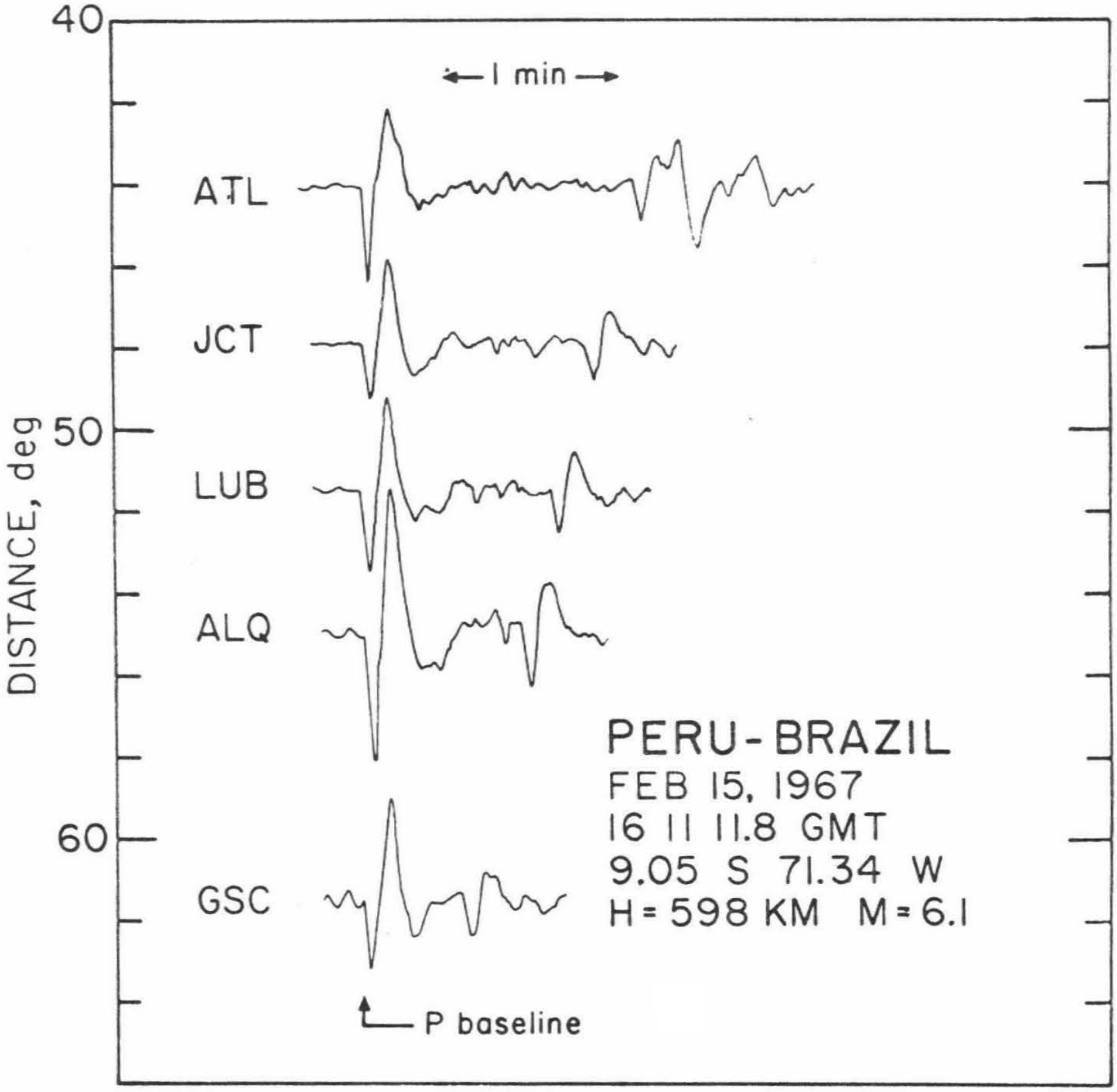

Figure 4.2. Examples of records from which PcP-P differential travel times have been measured.

The weighted means and standard errors in the means were computed for each cell using the formulae (4.4.1), the weights being set equal to the "quality" assigned to each reading. The results are given in Table 4.7.

Table 4.7

Observed deep-focus PcP-P times

For a 600 km focal depth

Distance (deg.)	Mean res. (sec.)	S.E.M. (sec.)	J.B.time (sec.)	Obs.time (sec.)
30	-0.9	0.27	163.1	162.2
35	-2.2	0.78	135.3	133.1
40	-1.2	0.81	110.3	109.1
45	-0.9	0.28	88.2	87.3
50	-0.1	0.06	68.9	68.8
55	+0.1	0.19	52.4	52.5
60	-1.0	0.23	38.5	37.5
65	-1.1	0.27	27.0	25.9
70	-0.7	0.25	17.9	17.2

The observed residuals and the cell means are displayed in Figure 4.4. For a focal depth of 600 km, the travel-time curves of the phases PcP, pP, and PP intersect at about 40°. Thus there are few observations and correspondingly large uncertainties in mean travel times in the distance range 35° - 40°.

Comparison of the mean PcP-P travel times for the two depths of focus shows that they are mutually consistent at a confidence level of 90%. The 1968 tables show the same general trend, although they are

Figure 4.3. Legend for figures 4.4 and 4.6

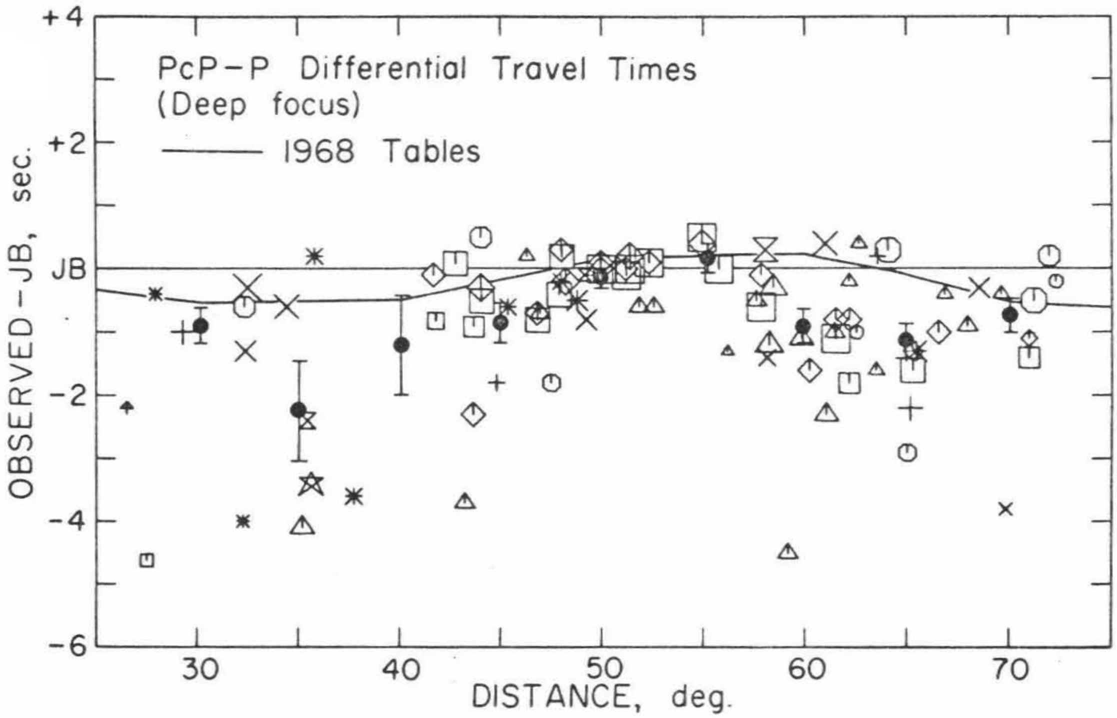

Figure 4.4. PcP-P residuals from deep-focus events. Black dots are the 5° cell means; error bars represent one standard error in the mean. Legend of events given in Figure 4.3.

up to one second later than the observed surface-focus times at distances in the range $30^\circ - 50^\circ$.

ScS-S (deep focus). Eleven of the deep-focus earthquakes listed in Table 4.3 (all except Java Sea B and Flores Sea) were used in the ScS-S study. All available records from WWSSN stations in the distance range 25° to 80° were read. The readings were assigned qualities ranging from 0 to 5 on the basis of the sharpness of the arrival, the similarities of the waveforms, and instrument polarization. Although both horizontal long-period instruments were used, SH polarization was preferred. This eliminates possible contamination by such SV polarized arrivals as SKS. Records of the Argentina event (12/20/66) from stations in the United States are reproduced in Figure 4.5. As before, all readings assigned a zero quality were discarded. There remained 193 observations. These are listed in Appendix 2.

Distributions of the residuals in 5° cells centered at the distances $30^\circ(5^\circ)80^\circ$ are listed in Table 4.8. Cell means and their computed standard errors can be found in Table 4.9, and they are plotted with the raw observations in Figure 4.6. Again, there are complications in the travel-time curve near 40° which make reading of the differential time difficult (in this case, due to the interference of sS and SS with ScS). The cell mean centered at 40° is displaced by about 1 1/2 seconds from the value obtained by interpolating nearby means, and this behavior can be attributed to these complications. In the inversion computations (Chapter 5) the standard error of this point was doubled.

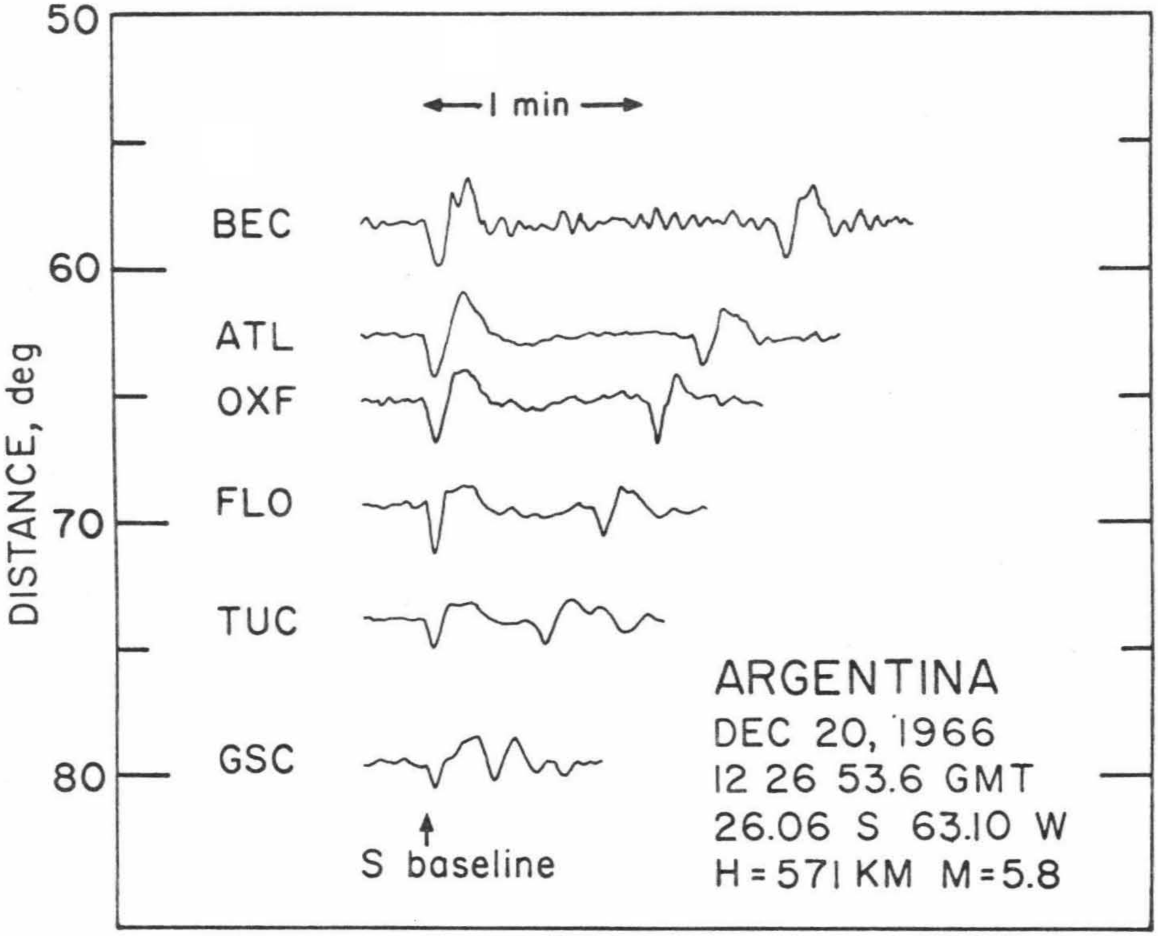

Figure 4.5. Examples of records from which ScS-S differential travel times have been measured.

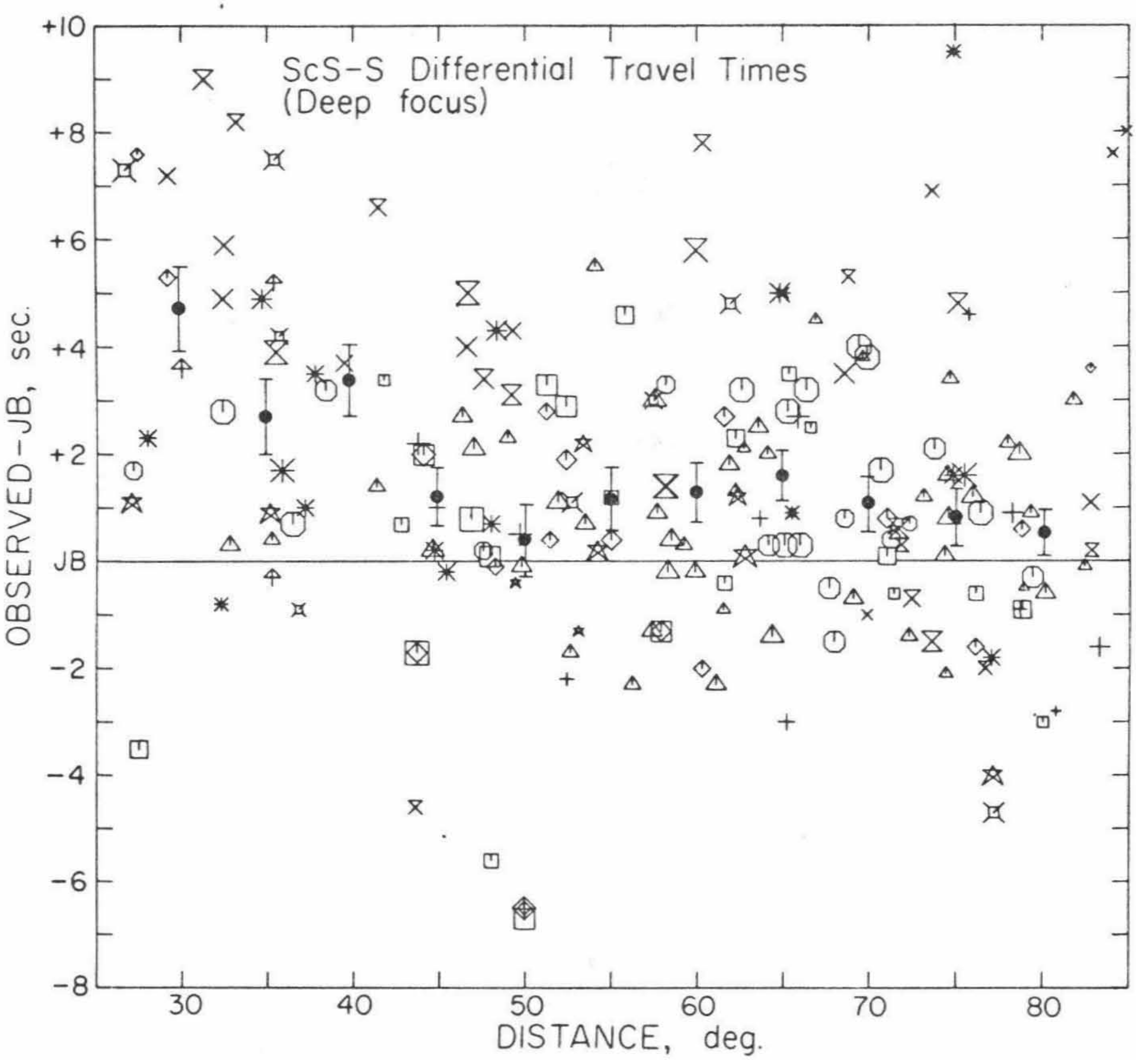

Figure 4.6. ScS-S residuals from deep-focus events. Black dots are the 5° cell means; error bars represent one standard error in the mean. Legend of events given in Figure 4.3.

Table 4.8

Distribution of ScS-S residuals (deep focus)

Cell	Interval (sec)								
	-6	-4	-2	0	+2	+4	+6	+8	
30°	0	0	0	1	0	3	3	1	1
35°	0	0	0	2	6	1	3	1	1
40°	0	0	0	0	2	4	0	1	0
45°	0	1	0	3	5	5	2	0	0
50°	3	1	1	3	6	6	2	0	0
55°	0	0	1	3	5	3	2	1	0
60°	0	0	2.	6	8	3	2	1	0
65°	0	0	1	1	7	9	3	0	0
70°	0	0	0	7	9	3	2	0	0
75°	0	2	2	4	8	2	2	1	1
80°	0	0	2	6	4	3	0	0	0

All cell means are positive J.B. residuals, indicating that either the shear velocity in the mantle is slower than the J.B. model, or else the depth to the core is greater. Several recent studies on the absolute travel times of PcP [Kogan, 1960; Taggart and Engdahl, 1968], as well as the differential times of PcP-P given here, require that the core radius be increased on the order of 10 km over the J.B. value of 3473 km. The latter possibility must therefore be rejected in favor of the former. More will be said about this in Chapter 5.

Hales and Roberts [1970b] have presented times of ScS-S corrected

Table 4.9

Observed deep-focus ScS-S times

Distance (deg.)	Mean res. (sec.)	S.E.M. (sec.)	J.B.time (sec.)	Obs.time (sec.)
30	+4.7	0.80	306.6	311.3
35	+2.7	0.71	256.7	259.4
40	+3.3	0.66	212.4	215.7
45	+1.2	0.52	173.1	174.3
50	+0.5	0.69	138.1	138.6
55	+1.2	0.58	107.3	108.5
60	+1.3	0.52	80.7	82.0
65	+1.6	0.44	58.1	59.7
70	+1.1	0.46	39.5	40.6
75	+0.8	0.60	24.7	25.5
80	+0.5	0.37	13.5	14.0

to a surface focus. From their observations they obtained 3486 km as the radius of the core. Comparison of our observations with theirs is difficult, since they list no travel times or J.B. residuals.

As can be seen from Table 4.8 or Figure 4.6, the differential travel times of ScS-S show a large scatter; the spread of the distribution at some distances exceeds 5 seconds. The scatter seems to be a genuine propagation effect; it does not correlate highly with the assigned qualities of the readings. A similarly large scatter was noted by Hales and Roberts [1970b]. They suggested the possibility that this scatter is due to lateral heterogeneity near or on the core-mantle boundary. To account for the observed scatter of 5 seconds or so by fluctuations of the core-mantle interface itself would require "bumps" on the order of 15 km in amplitude. Variations of this magnitude have been suggested by Hide [1966] and Hide and Horai [1968] to explain certain geomagnetic peculiarities and geoidal topography of low angular order. Phinney and Alexander [1966] found evidence from their observations of diffracted P waves of lateral heterogeneity at the core-mantle interface. Since several lines of independent evidence support this hypothesis, the possibility that lateral structure in this transition zone accounts for some of the scatter in the ScS-S data seems to be reasonable.

P'(AB)-P'(DF) and P'(BC)-P'(DF). It can be seen from an examination of Table 4.1 that the differential travel times of P' phase combinations are especially insensitive to the types of bias discussed in the previous section, a property which follows from the fact that these core phases are characterized by low values of $dT/d\Delta$. Since they also provide severe constraints on the possible variations of velocity in the core, the differential times of P' make excellent gross Earth data.

Several phase combinations were considered. The phase P'(DF) was chosen as the reference phase because it is a strong, clear arrival at all distances that other P' phases are observed (125° - 180°). For the Jeffreys model, there are two other branches of the P' travel-time curve, the AB branch and the BC branch. The AB branch represents the travel times of rays which bottom in the outer core and is well observed; it is a receding branch (has positive curvature) and terminates at the caustic B located at a distance of 143°. At distances greater than 143°, at least one other branch is observed. Jeffreys has labeled

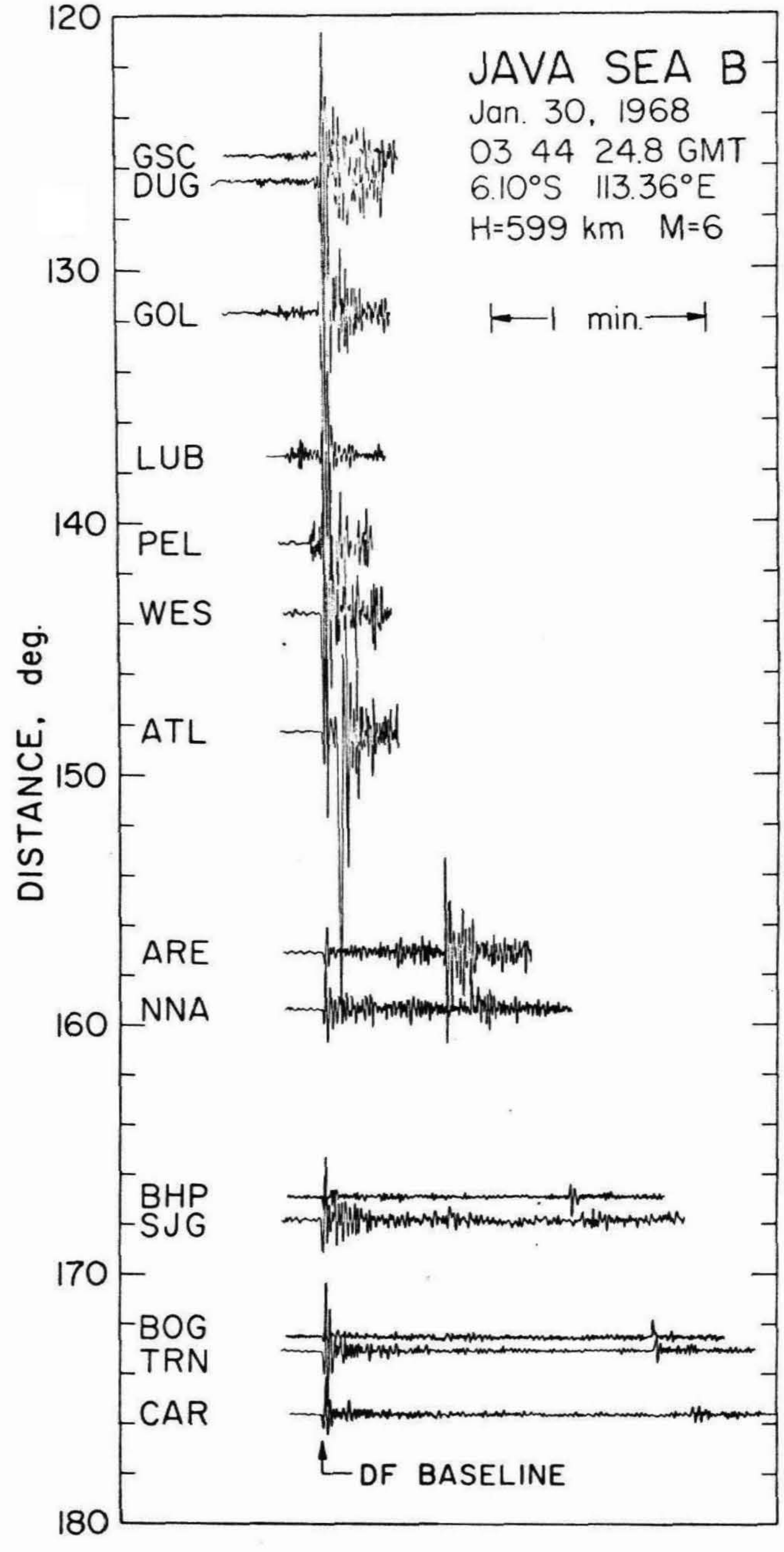

Figure 4.7. Examples of records from which P' differential travel times have been measured. Records at distances less than 143° show precursors.

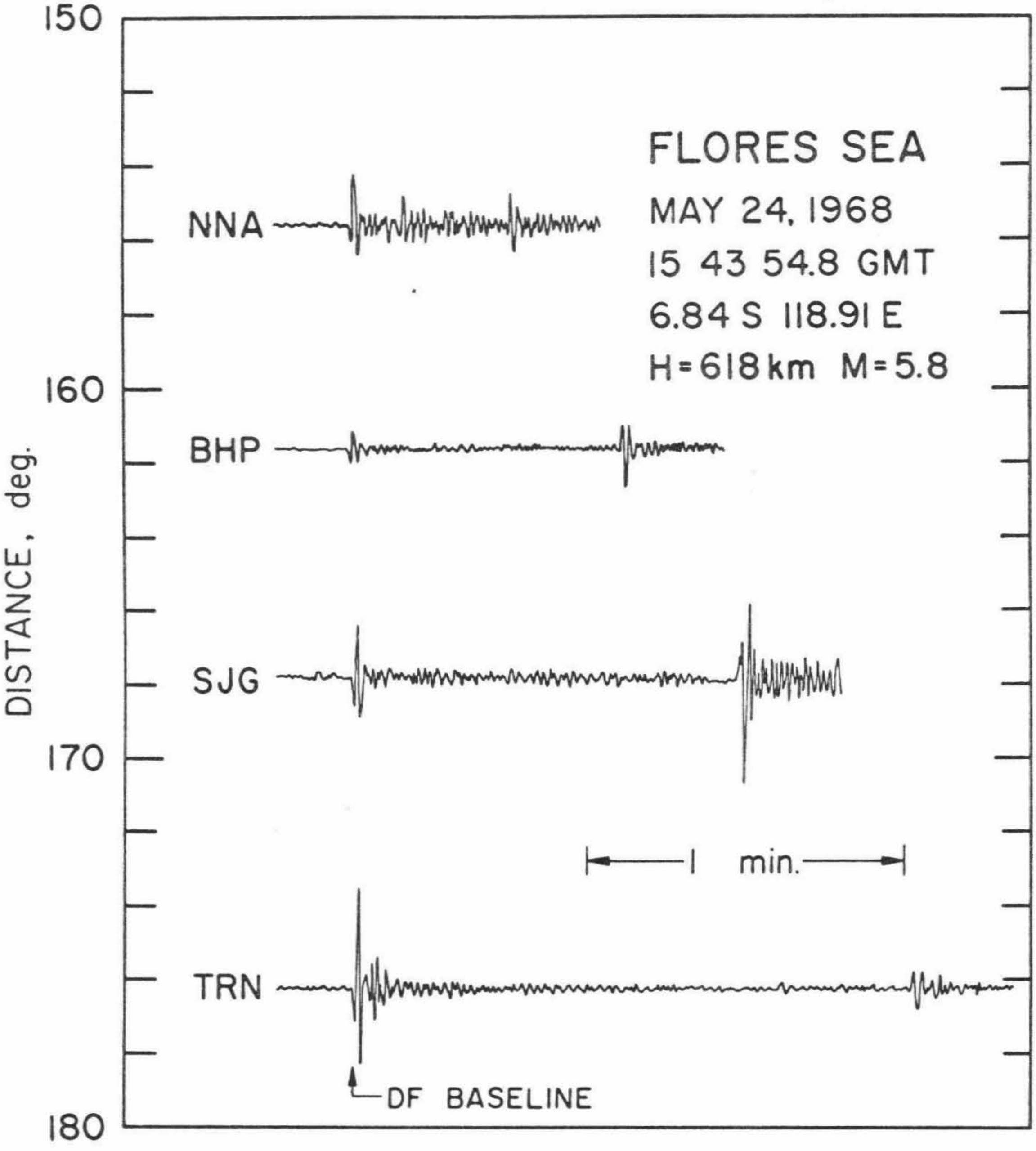

Figure 4.8. Examples of records from which P' differential travel times have been measured.

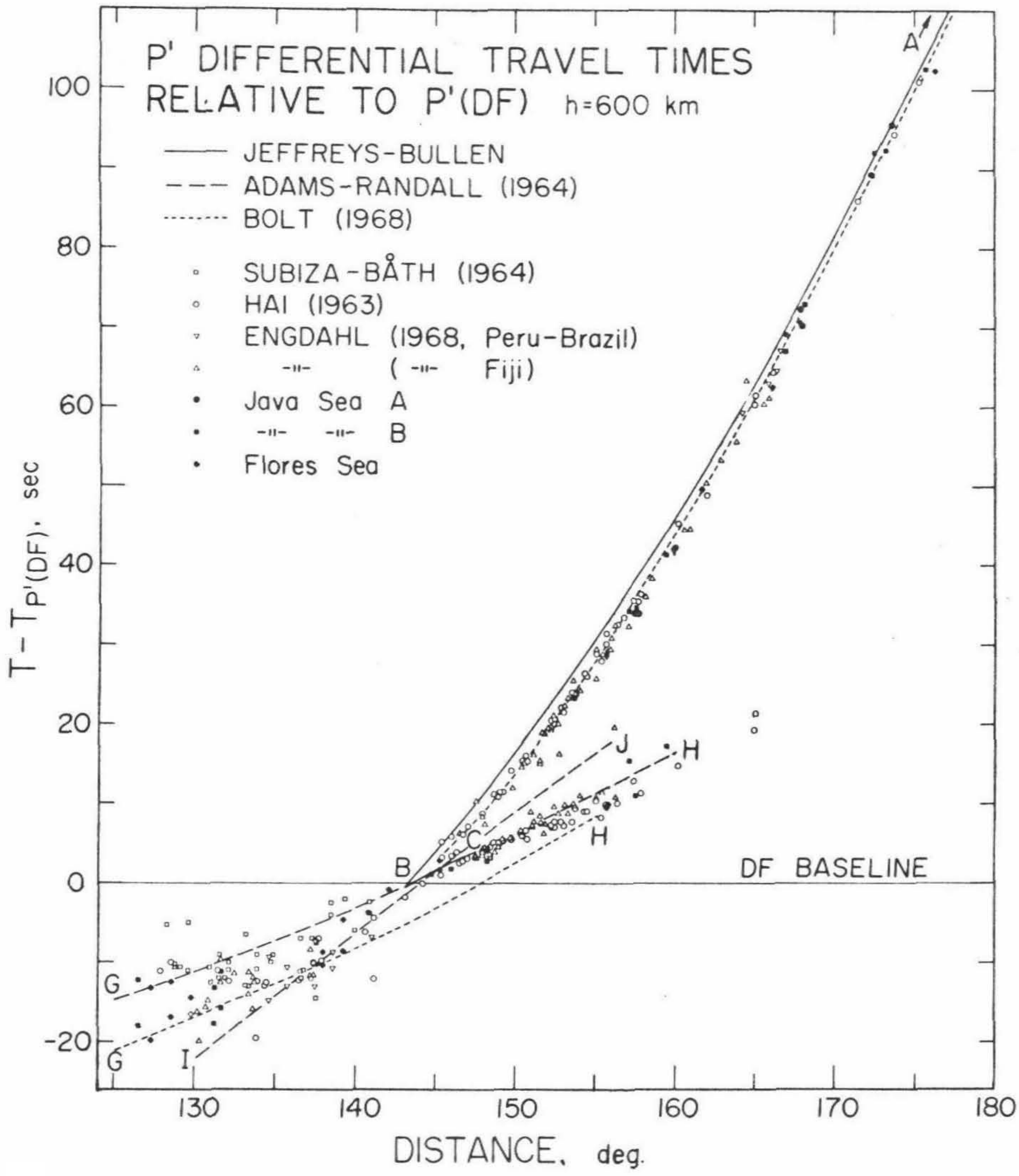

Figure 4.9. Plot of P' differential travel-time data.

this branch BC; in his model it represents rays bottoming below the B-caustic ray and above the inner core. Bolt [1959] has re-interpreted the arrivals beyond the caustic as members of a family constituting what he calls the GH branch. In his model there exists a transition region between the inner and outer cores in which these rays bottom, and it is separated from the outer core by a discontinuity. His interpretation was motivated by a series of small arrivals preceding P'(DF) at distances less than 143°. These precursors, originally studied by Gutenberg [1957], would, in Bolt's model, be refracted by the transition region - outer core discontinuity to distances near 125°. Recently, however, Haddon [1972] has proposed that these precursors might result from scattering off lateral heterogeneities in the vicinity of the core-mantle boundary. His arguement has been motivated by the anomalous curvature of this branch, pointed out by Buchbinder [1971], and the predominance of high frequencies in the precursors. Examples of these precursors from an event in the Sunda arc (Java Sea B) are shown in Figure 4.7.

To test Haddon's hypothesis, a simple model experiment was performed. Rays were traced through a two-dimensional Earth model consisting of a homogeneous mantle (v_p = 13 km/sec) surrounding a homogeneous core (v_p = 10 km/sec) separated by a "bumpy" boundary. The equation used to specify the radius of the boundary was $R_c = 3473 + \frac{A}{2} \sin n\pi\theta$. The rays were traced and the travel times computed for various values of the parameters n and A. The results for n = 20 and A = 0, 10, 20 km are pictured in Figure 4.10. It can be seen that the effect on the P'

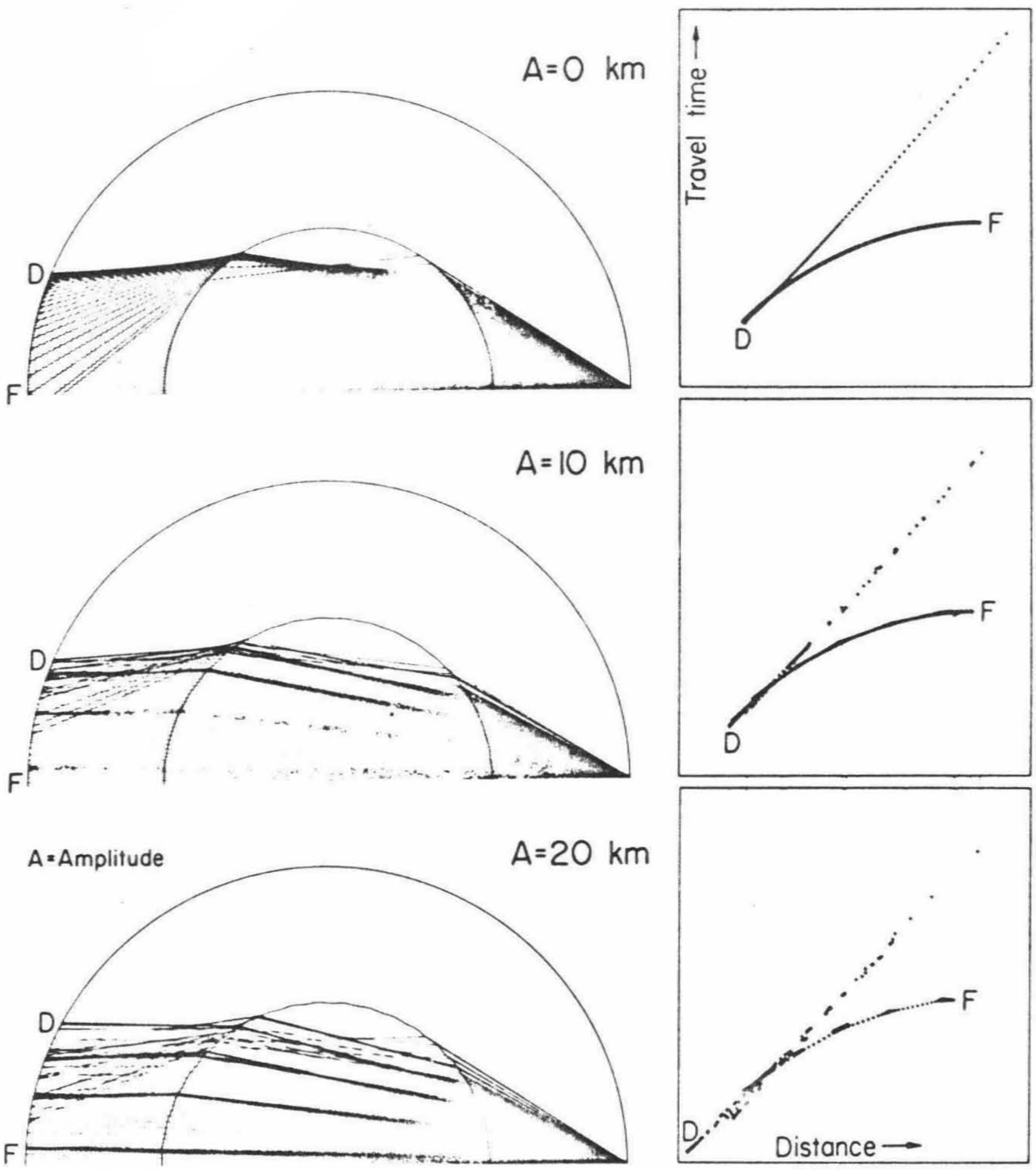

Figure 4.10. Model experiment showing the scattering of P' rays from bumps on the core-mantle boundary. Parameter A is the amplitude of bumps.

travel times is to introduce a number of arrivals as precursors to P'(DF) at distances less than the distance to the B caustic. Although the calculation is extremely crude, the resulting travel-time curve for A = 20 km looks surprisingly like the observations (compare with Figure 4.9 for example). This qualitative experiment confirms the plausibility of Haddon's hypothesis and lends further support to the speculation that the transition region between the mantle and core is laterally heterogeneous.

The observations of P' differential travel times shown in Figure 4.9 were computed from the raw readings of Engdahl [1968], who used the events designated Peru-Brazil A and Fiji B in Table 4.3, as well as Engdahl's [1968] compilation of Hai's [1963] times for a 600 km focal depth. Additional readings of precursor phases at distances less than 143° were taken from Subiza and Båth [1964]. To further supplement this data, times were read for three deep-focus earthquakes in the Sunda Arc from records written by short-period vertical component seismometers of the WWSSN. This geometry was advantageous because it provided a number of good readings of P'(AB)-P'(DF) near the antipode from stations situated in the Caribbean. Most of the readings were of very high quality. Examples of seismograms are shown in Figures 4.7 and 4.8.

All P' differential times were reduced to a 600 km focal depth using the J.B. Tables. Beyond 143° two branches are well delineated. The precursors to P'(DF) at distances less than 143° show their characteristic scatter. Neither the interpreation of Bolt [1968] nor the more complex model of Adams and Randall [1964], plotted with the obser-

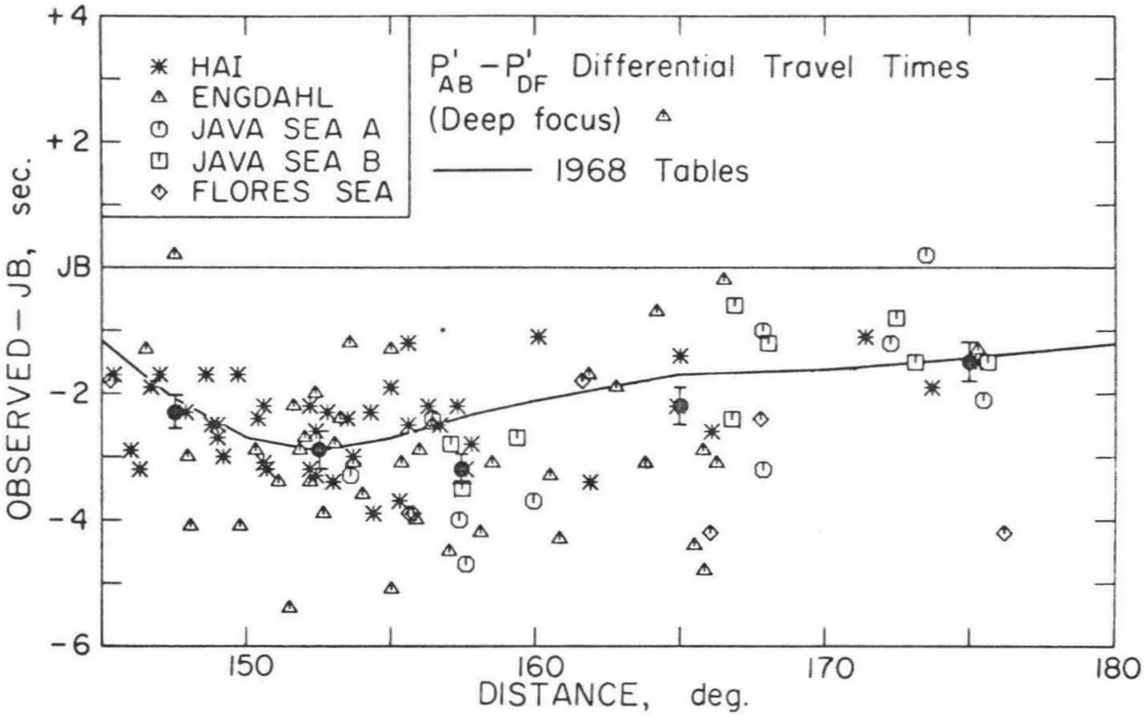

Figure 4.11. P'(AB) - P'(DF) residuals from deep-focus events. Black dots are cell means; error bars represent one standard error in the mean.

Table 4.10

Distribution of P'(AB)-P'(DF) residuals (deep focus)

Cell	Interval (sec)							
	-5	-4	-3	-2	-1	0	+1	
147.5°	0	2	3	5	7	0	1	0
152.5°	1	0	10	11	1	0	0	0
157.5°	1	5	8	10	2	0	0	0
165.0°	0	4	5	5	7	3	1	0
175.0°	0	1	0	1	7	1	1	0

vations in Figure 4.9, adequately explain these arrivals. Because of the possibility that the precursors arise from scattering off lateral heterogeneities and therefore are not gross Earth data, we have assumed that the PKP curve is of the Jeffreys type and have computed cell means only for the combinations P'(AB)-P'(DF) and P'(BC)-P'(DF).

The distribution of residuals for these two phase combinations are given in Tables 4.10 and 4.12. Residuals for P'(BC)-P'(DF) were

Table 4.11

Observed deep-focus P'(AB)-P'(DF) times

Distance (deg.)	Mean res. (sec.)	S.E.M. (sec.)	J.B.time (sec.)	Obs.time (sec.)
147.5	-2.3	0.24	10.0	7.7
152.5	-2.9	0.28	23.5	20.6
157.5	-3.2	0.19	38.3	35.1
165.0	-2.2	0.31	63.0	60.8
175.0	-1.5	0.31	101.6	100.1

Table 4.12

Distribution of P'(BC)-P'(DF) residuals (deep focus)

Cell	Interval (sec)					
	0	+1	+2	+3	+4	
146.25°	1	6	0	1	0	0
148.75°	1	0	15	6	0	0
151.25°	0	0	5	10	3	2
153.75°	0	0	8	3	4	1
156.25°	0	1	5	1	3	0

computed by extending the BC branch in the Jeffreys model with a ray parameter of 2.2 sec/deg. In computing the cell means listed in Tables 4.11 and 4.13 all observations were given equal weight.

From Figure 4.11, which displays the observations of P'(AB)-P'(DF), we see that Bolt's [1968] times are in good agreement with the data. Figure 4.12 shows the residuals for P'(BC)-P'(DF). The point C is not well defined by these data but lies somewhere near 155^{o}. The cell means centered at 153.75^{o} and 156.25^{o} may be biased by spurious arrivals.

Table 4.13

Observed deep-focus P'(BC)-P'(DF) times

Distance (deg.)	Mean res. (sec.)	S.E.M. (sec.)	J.B.time (sec.)	Obs.time (sec.)
146.25	+0.7	0.30	1.8	2.5
148.75	+1.7	0.11	3.2	4.9
151.25	+2.8	0.20	4.8	7.6
153.75	+2.2	0.24	6.8	9.0
156.25	+1.8	0.34	9.0	10.8

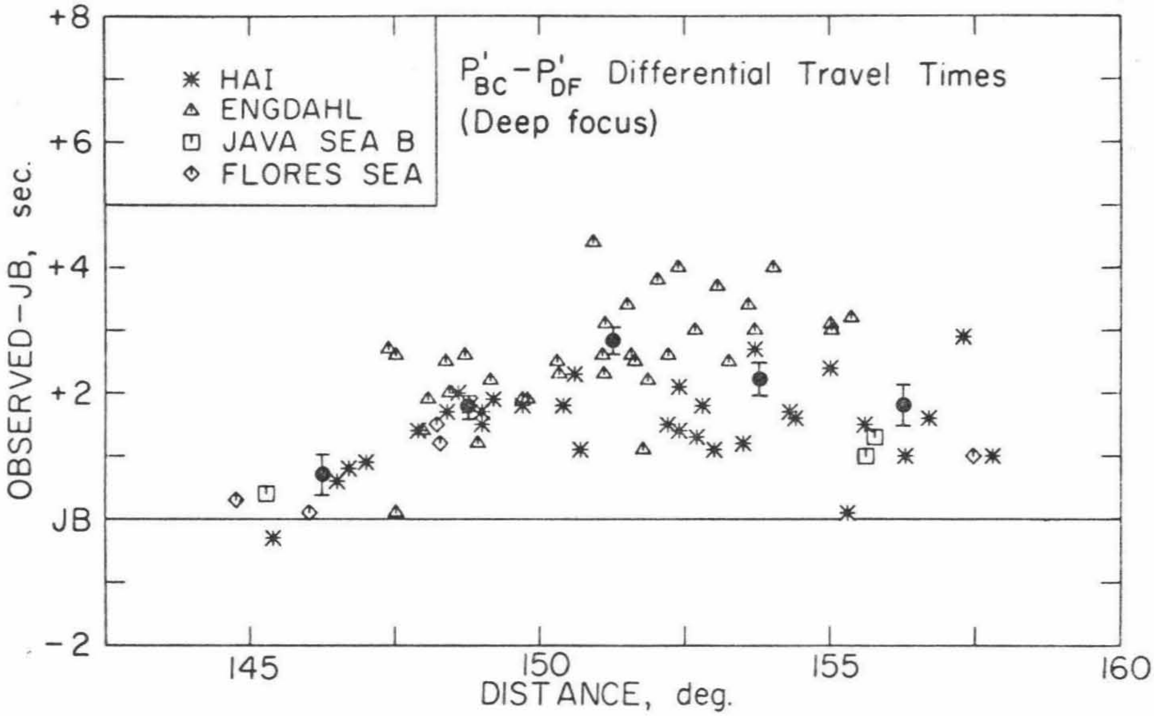

Figure 4.12. P'(BC) - P'(DF) residuals from deep-focus events. Black dots are cell means; error bars represent one standard error in the mean.

Chapter 5

NUMERICAL MODELING OF THE RADIAL VARIATIONS

5.1 Introduction. This chapter is concerned with actual numerical modeling of the radial distributions of velocity and density in the Earth. The data we shall attempt to fit are the Earth's mass and moment of inertia, the observed eigenperiods of oscillation, and the differential travel times presented in Chapter 4. The algorithm that we shall employ was outlined in Chapter 2: a starting model is constructed and tested against the data, a correction is computed by solving the linear perturbation equations, the data functionals are re-evaluated, and the procedure is iterated until the fit is satisfactory.

Because the inverse problem is nonlinear and has no unique solution, interpretation of any numerical results is a tricky business. A common mistake is to infer that because a certain model satisfies the data some feature of that model actually exists in the Earth, when in reality the data do not require this feature. To guard against this kind of breach of scientific method, one must insure that the calculated perturbations are resolvable - are really required by the data. The resolving power of the data in a linear neighborhood of any model can be judged by examining the averaging kernels given in equation (2.8.3). To calculate the perturbations we shall use equation (2.7.12); it provides an approximate solution which has been filtered of any linearly unresolvable components.

As we emphasized in §2.3, the success of an algorithm based on linear estimation depends critically on the model used to "start" the computation. In the design of the starting model we must strike a balance between two opposing considerations. On the one hand, because the eigenperiods and travel times are nonlinear functionals, the starting model should be as linearly close as possible to the sought representation of the Earth. Otherwise, the model that results from successive perturbations may end up in a local minimum far removed from this representation, and resolving power computations may be deceptive. Generally speaking, the starting model should include any major discontinuities that exist in the Earth. A starting model in which the velocities and density are taken to be constants is an example of an inadequate representation. On the other hand, we desire that the starting model be "simple" - devoid of any features that might not exist in the spherically averaged Earth. For this reason published models generally make poor starting models.

The procedure we shall adopt is to construct starting models based on a series of reasonable but "simple" physical assumptions. These will be detailed in section 5.4. Since the inversion algorithm provides the minimum deviations (in a norm sense) from these starting models necessary to fit the data, the resulting models will, in some sense, be as simple as possible.

We discuss in the next section the adaptation of the inversion theory given in Chapter 2. The data sets used in the inversions are presented in §5.3, and §5.4 is devoted to construction of the starting models. In §5.5 models are derived and evaluated. In section 5.6 the resolving kernels are displayed. The last section contains conclusions.

5.2 The inversion algorithm. Estimates of the spherically averaged compressional velocity $v_{p0}(r)$, shear velocity $v_{s0}(r)$, and density $\rho_0(r)$, which constitute a spherically symmetric Earth model $\mathbf{m}_0$, were sought given the observed values of the Earth's mass and moment of inertia and the sample means of available sets of eigenperiod and differential travel-time data. The data values were arranged in a vector $\mathbf{d}_0$. The errors in the data were assumed to be samples of independently distributed, Gaussian random variables with zero means and known variances. The vector $\delta\mathbf{m}_0$ was defined to be equal to the difference between $\mathbf{m}_0$ and some initial guess $\mathbf{m}_s$, and the vector $\delta\mathbf{d}_0$ was defined equal to $\mathbf{d}_0 - \mathbf{d}(\mathbf{m}_s)$. As an approximation, $\delta\mathbf{m}_0$ and $\delta\mathbf{d}_0$ were assumed to be related by equation (2.5.1), where $\mathbf{n}$ is the vector containing the noise components and $\mathbf{A}$ is the linear operator whose ith row is the Fréchet kernel of the ith datum in $\mathbf{d}_0$. Under these assumptions the theory presented in Chapter 2 was applicable.

The inner product between any two vectors $\mathbf{m}$ and $\mathbf{m}'$ in the space of Earth models was defined by the equation

$$(5.2.1)\qquad \mathbf{m}\cdot\mathbf{m}' = \int_0^R [v_p(r)v_p'(r)w_p(r) + v_s(r)v_s'(r)w_s(r) + \rho(r)\rho'(r)w_\rho(r)]\,dr.$$

The measure on the interval [0,R] was chosen to be linear in r, so that the weighting functions w_p, w_s, and w_ρ in the integral (5.2.1) are simply constants. These constants were chosen to render the inner product dimensionless. The velocities were expressed in units km/sec, and the density was expressed in units of gm/cm^3. We write

$$
(5.2.2) \qquad \begin{aligned} [v_p] &= [v_s] = \text{km/sec}, \\ [\rho] &= \text{gm/cm}^3. \end{aligned}
$$

The inner product is dimensionless if

$$
(5.2.3) \qquad \begin{aligned} [w_p] &= [w_s] = \text{sec}^2/\text{km}^3, \\ [w_\rho] &= \text{cm}^6/\text{gm}^2\ \text{km}, \end{aligned}
$$

where the units of radius are taken to be kilometers. We specified the weighting functions to be numerically equal to R^{-1}. This specification implies that unit perturbations of both velocities and density are of equal weight. Although arbitrary, this decision was motivated by the near numerical equality of v_{p0}, v_{s0}, and ρ_0 when expressed in the units given in (5.2.2).

The four types of data functionals which compose a data vector $\mathbf{d}$ are the mass of the model, denoted M; its moment of intertia I; spheroidal and toroidal eigenperiods of radial order n and angular order ℓ, denoted ${}_n t_\ell^\sigma$ and ${}_n t_\ell^\tau$ respectively; and the ray-theoretical travel times $T_x(\Delta,h)$ of a phase x at angular distance Δ from a source with focal depth h. The functionals M and I were normalized by their observed values (given in §5.3) and thus are dimensionless. The eigenperiods and travel times were expressed in seconds. The scale factors for these functionals appearing in the inner product on the data space were set equal to 1 sec^{-2}.

With these conventions, a computer program was written to calculate the best linear estimate $\overline{\delta \mathbf{m}}$ given by equation (2.7.12) and the averaging kernels appearing in equation (2.8.3). Rewriting (2.7.12) and

(2.8.3) in terms of the inner product (5.2.1), we find that

$$\overline{\delta \mathbf{m}} = C_{ss} \cdot A^{*}(A \cdot C_{ss} \cdot A^{*} + \tan\theta \; C_{nn})^{-1} \delta d_0, \tag{5.2.4}$$

and that

$$\mathscr{A} = C_{ss} \cdot A^{*}(A \cdot C_{ss} \cdot A^{*} + \tan\theta \; C_{nn})^{-1} A \quad , \tag{5.2.5}$$

the angle θ being the parameter of the tradeoff curve.

The foward calculation of the eigenperiods and the calculation of their Fréchet kernels was performed in subroutines written by Mr. Martin Smith. The travel-time routines were kindly provided by Dr. Bruce Julian.

Since the error components are assumed to be uncorrelated, the form of the noise autocorrelation operator C_{nn} is given by equation (2.5.12). This form was used with the variances along the diagonal set equal to the squares of the standard errors in the means estimated from the scatter in the data.

Specification of the operator C_{ss} requires some discussion. We saw in §2.6 that the meaning attached to C_{ss} in the stochastic formulation, where it plays the role of an autocorrelation operator, makes sense only if we impose on the model space an a priori probability distribution. This is because sample ensembles for the solution process are unavailable, and probabilities cannot be interpreted as the limits of sample frequencies. In §2.6 we also saw that, if quadratic convergence is sufficient to identify vectors, then choosing C_{ss} is equivalent to specifying the norm on the space of models. With this realization we chose $\mathbf{C}_{ss}$ in the following manner: for each of the model functions $v_p(r)$, $v_s(r)$, and $\rho(r)$, the interval $[0,R]$ was partitioned into several sub-intervals, each bounded by radii at which discontinuities are known or thought to exist. Considering only one model function for a moment, let us label these radii a_p, where $p = 1,2,\dots,P$. We define $a_0 = 0$ and assume that $a_P \equiv R$, so that on the pth interval the radius varies between a_{p-1} and a_p, $p = 1,2,\dots,P$. On each of these sub-intervals we defined a smoothing operator $C_p(r,r')$ by the equation

$$(5.2.6) \qquad C_p(r,r') = k_p/2 \left\{ e^{-k_p|r-r'|} + D^{-1}[A\, e^{-k_p(a_p-a_{p-1})} \times \cosh k_p(r-r') + B \cosh k_p(a_p+a_{p-1}-r-r') + C \sinh k_p(a_p+a_{p-1}-r-r')] \right\},$$

where
$$A = [1 - a_{p-1}(k_p+\alpha_p)][1 + a_p(k_p-\beta_p)],$$
$$B = \alpha_p a_{p-1} + \beta_p a_p - [k_p^2 - k_p(\alpha_p+\beta_p) + \alpha_p\beta_p]a_{p-1}a_p - 1,$$
$$C = k_p(a_p-a_{p-1}),$$
$$D = [1 - \alpha_p a_{p-1} - \beta_p a_p + (\alpha_p\beta_p-k_p^2)a_{p-1}a_p]\sinh k_p(a_{p-1}-a_p) - k_p[a_p - a_{p-1} + (\beta_p-\alpha_p)a_p a_{p-1}] \cosh k_p(a_{p-1}-a_p).$$

Equation (5.2.6) is similar to equation (2.6.16); in fact, $C_p(r,r')$ satisfies the system (2.6.15) with $w(r) = p(r) = 1$, $a = a_{p-1}$, $b = a_p$, $\alpha = \alpha_p$, and $\beta = \beta_p$. Having done this for each of the three model functions, we specify $\mathbf{C}_{ss}$ to be a block-diagonal operator as in equation (2.6.10) with each of the three blocks in the form

$$
(5.2.7) \qquad
\begin{array}{c|c|c|c|c|c}
 & 0 \text{ --- } a_1 & a_1 \text{ --- } a_2 & \cdots & a_{P-1} \text{ --- } R \\
\hline
0 \text{ --- } a_1 & C_1 & 0 & \cdots & 0 \\
\hline
a_1 \text{ --- } a_2 & 0 & C_2 & \cdots & 0 \\
\hline
\vdots & \vdots & \vdots & \ddots & \vdots \\
\hline
a_{P-1} \text{ --- } R & 0 & 0 & \cdots & C_P \\
\end{array}
$$

This block-diagonal form of the operator $\mathbf{C}_{ss}$ expresses the conviction that between the radii of discontinuities the solution $\delta\mathbf{m}_0$ behaves smoothly. The estimation is therefore weighted in favor of this behavior. The parameter k_p is simply the mean wavenumber of the smoothing operator C_p. In the minimization to obtain the best linear estimate $\overline{\delta\mathbf{m}}$, components with unit amplitude and wavenumber k_p measure twice as much as components with unit amplitudes and wavenumbers near zero. Since the minimization seeks out the "smallest" solution that satisfies the data, low-wavenumber components; i.e., smoother components, are preferred.

The parameters α_p and β_p specify the boundary conditions applied at the radii a_{p-1} and a_p. If they are set equal to zero, the derivatives of the solution will vanish at these radii (inside the interval); whereas if they are set equal to infinity, the values of the solution itself will vanish.

This form of the solution autocorrelation operator is quite versatile. By its manipulation, one can introduce information about the solution not contained in the data or search for solutions with specified constraints. Often this is a convenient way to test hypotheses; e.g., does a solution to the inverse normal mode problem exist with a density at the top of the mantle equal to 3.33 gm/cm^3?

We return now to a discussion of the numerical algorithm. Because the computer available to us was fairly small (an IBM 370/155 with 320 kilobytes = 80 K words of core), it was not feasible to invert all three functions, v_p, v_s, and ρ, simultaneously. Instead, a FORTRAN program was written to invert either compressional velocity and density or shear velocity and density simultaneously. The iteration scheme employing the estimate given in (5.2.4) was designed to alternate between these two possiblities. At each step, up to eighty data could be inverted. Convergence was always rapid as long as tan θ was kept at a value greater than 5; no model presented in this chapter required more than eight iterations. Typically, a run involving one iteration on a data set consisting of 50 normal modes and 30 travel times required about twenty minutes on the 370/155 and cost about fifty dollars. Over eighty per cent of this time was devoted to calculating the mode periods and Fréchet kernels. Calculation of the operator $\mathscr{A}$ took an additional five minutes.

5.3 The data set. The basic data set comprised a total of 219 data. Of these, 178 were normal mode periods, 39 were differential travel times, and the remaining two were mass and moment of inertia. We devote this section to a discussion of each of these three subsets.

The normal mode data. Gilbert [1972] observed that the average period of singlets in a mode multiplet split by disturbing influences such as rotation, ellipticity of figure, and the presence of lateral heterogeneities equals, to a first-order approximation, the degenerate eigenperiod of a spherically averaged Earth model.[1] Unfortunately, resolution of the multiplet structure of an eigenperiod is, with the exceptions of only the very gravest modes, impossible at the present time. Instead, we must rely on averages of many observations to give periods that can be interpreted in terms of an average Earth structure.

Averages of observed free oscillation periods were given by Pekeris in 1966. However, the wide variations in the quality of the early recordings (mainly from the Chilian earthquake of 1960) and the procedure used to reduce the data largely negated the advantage of using these averages; much of the early inversion work was done with values obtained from single records. Anderson [1967], who also presented averages, picked "best values" to evaluate various Earth models. As investigators have set themselves to the task of gleaning from existing records information about the mode spectrum, the situation

---

[1] This will be true as long as the disturbing influences leave the linear system describing small oscillations Hermitian.

has improved considerably. Derr [1969] averaged the observations available through 1968 using a complex, somewhat arbitrary system of weights to enhance the importance of high-resolution recordings. Although the great majority of the more than 1500 data he used were of the fundamental mode, he attempted to obtain averages of some of the higher modes as well. Backus and Gilbert [1968] had shown inclusion of higher modes greatly improves the resolving power of the normal mode data set.

Recently, a major contribution to the study of the normal mode spectrum has been made by Dziewonski and Gilbert [1972]. Using a comprehensive series of criteria to identify modes, they have analyzed 84 long-period seismograms of the great Alaskan earthquake of 1964 and tentatively identified all but 30 of the 136 theoretically predicted multiplets in the normal mode spectrum with periods greater than 300 seconds, as well as a number of modes in the period range 200 - 300 seconds. Besides their extensive listing of higher-mode periods, they also give cumulative averages of fundamental mode data for periods greater than 176 seconds (${}_0S_3$ - ${}_0S_{50}$, ${}_0T_3$ - ${}_0T_{46}$).

Their averages, listed with standard errors in the means in Tables 2-5 of their paper, formed the basis of our normal mode data set. They did not list averages of the modes ${}_0S_2$ and ${}_0T_2$, and the period they give for ${}_0S_3$ (2140.57 sec, at the limit of their resolution) is evidently too large; for these modes we have used the periods given by Derr [1969]. In addition, we included in our data set the average periods of the modes ${}_0S_{51}$ to ${}_0S_{63}$ given in Table 2 of Dziewonski and

Landisman [1970]. These data are listed with fits to the models derived in §5.5 in Table A3.1. The consistency of this data set is indicated by the precision with which these models satisfy the data. One model, model B1, has eigenperiods which differ from the observed values by no more than 0.4% in the extreme; generally, the fit is much better. This strongly suggests (but, of course, does not prove) that these data are representative of the averaged Earth.

The travel-time data. Because of the problem of baseline errors, we used only differential travel times in the inversion. Included in the data set were the 39 differential travel-time averages listed in Tables 4.5, 4.7, 4.9, 4.11, and 4.13 for the phase combinations PcP-P (surface focus), PcP-P (deep focus), ScS-S (deep focus), P'(AB)-P'(DF) (deep focus), and P'(BC)-P'(DF) (deep focus). These data along with the fits to the models are summarized in Table A3.2.

The mass and moment of inertia. The mass M and normalized moment of inertia I/MR^2 used in the inversion are given by Jeffreys [1970]. These are

$$(5.3.1)\qquad \begin{aligned} M &= 5.977 \pm 0.0006 \times 10^{27}\ \mathrm{gm}, \\ I/MR^2 &= 0.330841 \pm 0.00018 \end{aligned}$$

Partitioning of the data sets. Two subsets of the basic data set were formed. These were designated data set I and data set II. Data set I, used in the inversion of compressional velocity and density, consisted of the eigenperiods of the following modes and the differential travel times of the following phase combinations: ${}_{0-4}S_0$, ${}_0S_2$, ${}_0S_3$, ${}_0S_5$, ${}_0S_7$, ${}_0S_9$, ${}_0S_{12}$, ${}_0S_{15}$, ${}_1S_2$, ${}_1S_{7-10}$, ${}_2S_{1-4}$, ${}_2S_6$, ${}_2S_{15}$, ${}_3S_{2-9}$, ${}_3S_{11}$,

${}_4S_{1-10}$, ${}_5S_2$, ${}_5S_3$, ${}_6S_1$, ${}_6S_4$, ${}_6S_5$, ${}_7S_2$, ${}_7S_3$, ${}_7S_5$, ${}_8S_1$, ${}_8S_2$, PcP-P [Tables 4.5 and 4.7], P'(AB)-P'(DF) [Table 4.11], P'(BC)-P'(DF) [Table 4.13]. Data set I included all modes observed by Dziewonski and Gilbert [1972] with greater than 25% compressional energy or greater than 5% compressional energy in the outer core (as given in their Table B2).

Data set II, used in the inversion of shear velocity and density, consisted of the following modes and travel times: ${}_0S_2$, ${}_0S_3$, ${}_0S_{5-9}$, ${}_0S_{12}$, ${}_0S_{15}$, ${}_0S_{18}$, ${}_0S_{21}$, ${}_0S_{25}$, ${}_0S_{30}$, ${}_0S_{37}$, ${}_0S_{45}$, ${}_0S_{54}$, ${}_0S_{63}$, ${}_1S_2$, ${}_1S_4$, ${}_1S_5$, ${}_1S_{7-10}$, ${}_1S_{14-17}$, ${}_2S_2$, ${}_2S_{8-14}$, ${}_3S_{4-11}$, ${}_4S_{1-3}$, ${}_4S_{10}$, ${}_5S_2$, ${}_8S_2$, ${}_0T_{3-6}$, ${}_0T_8$, ${}_0T_{10}$, ${}_0T_{11}$, ${}_0T_{13}$, ${}_0T_{16}$, ${}_0T_{21}$, ${}_0T_{23}$, ${}_0T_{25}$, ${}_0T_{29}$, ${}_0T_{35}$, ${}_0T_{41}$, ${}_0T_{46}$, ScS-S [Table 4.9]. This data set provided good coverage of the fundamental mode as well as the higher modes sensitive to variations in shear velocity and density.

5.4 Construction of the starting models. Two starting models, designated model A and model B, were constructed. In this section we describe their derivation.

The central idea behind the construction was the assumption that discontinuities in density and shear velocity are associated with discontinuities in compressional velocity. For density, this assumption is well-motivated; available laboratory data on the behavior of mantle-type materials indicates that the compressional velocity - density systematics are very regular over wide ranges of temperature and pressure. Birch [1961] proposed that, for materials of constant mean atomic weight, v_p and ρ are related by a linear law. The invariance of this relationship to temperature and pressure variations has been discussed by Anderson et.al.[1971]. Such a linear relationship was used to construct the upper mantle density profiles in the starting models. Densities in the lower mantle and core were derived using the Adams-Williamson integration procedure [Williamson and Adams, 1923]. By fixing the density at the base of the crust and fitting the mass and moment of inertia, construction of the density profile was made deterministic once the velocities were chosen. This was exactly the procedure used by Birch [1964] to construct his model II.

We review the construction of the velocity models region by region:

The crust (Bullen's region A). The crust was modeled as a layer 21 km thick with $v_p = 6.2$ km/sec and $v_s = 3.4$ km/sec. This roughly corresponds to an areal average of the six crustal types listed by

Brune [1969] (oceanic, shield, ridge, alpine, basin and range, and island arc) taken in proportion to their surface areas.

The upper mantle and the transition zone (regions B and C). The presence of large velocity gradients and the existence of strong lateral heterogeneity complicate the interpretation of seismic data sensitive to the upper mantle and transition zone. Evidence from surface waves has confirmed Gutenberg's hypothesis that a low-velocity channel exists for shear waves 100 km or so below the base of the crust [Anderson, 1967]. Structure in the transition zone between 400 km and 700 km has been illuminated by $dT/d\Delta$ studies using large seismic arrays [Niazi and Anderson, 1965; Johnson, 1967]. These have confirmed the presence of at least two major discontinuities at depths near 400 and 650 kilometers (corresponding to breaks in $dT/d\Delta$ at distances of about 20 and 25 degrees). However, lateral variation of these structures is great, and currently available data sample only a small fraction of the Earth's surface.

Because the average structure of these regions is in doubt, we have used simple representations as starting models. The compressional velocity below the crust was fixed at 8.0 km/sec and increased linearly with depth to a value of 8.8 km/sec at 420 km. The shear velocity in the upper mantle was taken to be a constant 4.55 km/sec. Thus, the starting models have no low-velocity zone in this region.

The transition region was modeled by two discontinuities at depths of 420 km and 671 km with the velocities varying linearly in between. Only in this region do the starting models A and B differ. Model A is characterized by discontinuities of second-order. In this model, the compressional velocity rises from 8.80 km/sec at 420 km to a value of 10.86 km/sec at 671 km. In the same region shear velocity varies linearly between values of 4.55 km/sec and 6.13 km/sec.

In model B the discontinuities were chosen to be of first-order. At 420 km the compressional velocity jumps from 8.80 km/sec to 9.5 km/sec, and the shear velocity jumps from 4.55 km/sec to 5.33 km/sec. Between this depth and the discontinuity at 671 km, the compressional velocity increases at a rate of 0.27 km/sec per 100 km, and the shear velocity is constant.

Although the variation of velocities in these regions is somewhat *ad hoc*, the values chosen were designed to give the same baseline for teleseismic P as the 1968 Tables and the same baseline for teleseismic S as Hales and Roberts [1970 a].

The lower mantle (region D). The Earth's lower mantle is a region characterized by relatively uniform increases in the velocities with depth. The models of lower mantle velocities derived from travel-time studies have changed very little since the early work of Jeffreys and Gutenberg. The travel times through this region show very little azimuthal dependence [Jeffreys, 1962], and it may be inferred that the lateral heterogeneity is small, at least in comparison with the upper mantle.[2]

The velocities in the lower mantle we have used in our starting models were taken from the studies of Herrin *et.al*. [1968] (compres-

[2] A recent study of ISS P times by Sengupta and Julian [in preparation] indicates, however, some lateral variation in the lowermost 600 km.

Table 5.1

Positions of the major discontinuities

Region		Radius (km)
------		6371
A	Crust	
------		6350
B	Upper mantle	
------		5951
C	Transition zone	
------		5700
D	Lower mantle	
------		3485
E,F	Outer core	
------		1215
G	Inner core	
------		0

sional velocity) and Randall [1971] (shear velocity). Both of these studies used ISS times from the same set of sources.

The radius of the core-mantle boundary. Since the radius of this discontinuity was fixed during the inversion, its accurate determination for the starting models was critical. The procedure we followed was to fit the differential travel times of PcP-P given in Tables 4.5 and 4.7 by varying this radius. The times were calculated for both depths of focus using the mantle and crustal velocities for model A described above. The differences between the observed times (5° cell means) and the computed times were minimized with an RMS of 0.4 seconds for the radius 3485 km. Since differential times were used, this determination is essentially independent of the upper mantle model we assumed. The radius we obtained is 12 km greater than Jeffrey's value and 7 km greater than the value obtained by Taggart and Engdahl [1968].

Table 5.2

The starting models

Radius (km)	Model A v_p (km/sec)	Model A v_s (km/sec)	Model A ρ (gm/cm^3)	Model B v_p (km/sec)	Model B v_s (km/sec)	Model B ρ (gm/cm^3)
0	11.20	3.50	12.57		same as model A	
600	11.20	3.50	12.50		.	
1215	11.20	3.50	12.28		.	
1215	10.12	0.00	12.28		.	
1600	10.07	0.00	12.05		.	
2000	9.85	0.00	11.76		.	
2400	9.50	0.00	11.40		.	
2800	9.06	0.00	10.95		.	
3200	8.51	0.00	10.42		.	
3485	8.10	0.00	9.98		.	
3485	13.67	7.30	5.51		.	
3700	13.57	7.23	5.41		.	
4000	13.22	7.11	5.26		.	
4300	12.87	6.97	5.11		.	
4600	12.51	6.81	4.95		.	
4900	12.15	6.66	4.79		.	
5200	11.71	6.48	4.63		.	
5500	11.22	6.29	4.45		.	
5700	10.86	6.13	4.33		.	
5700	10.86	6.13	4.33	10.71	5.33	4.09
5951	8.80	4.55	3.61	9.50	5.33	3.85
5951	8.80	4.55	3.61		same as model A	
6350	8.00	4.55	3.33		.	
6350	6.20	3.40	2.79		.	
6371	6.20	3.40	2.79		.	

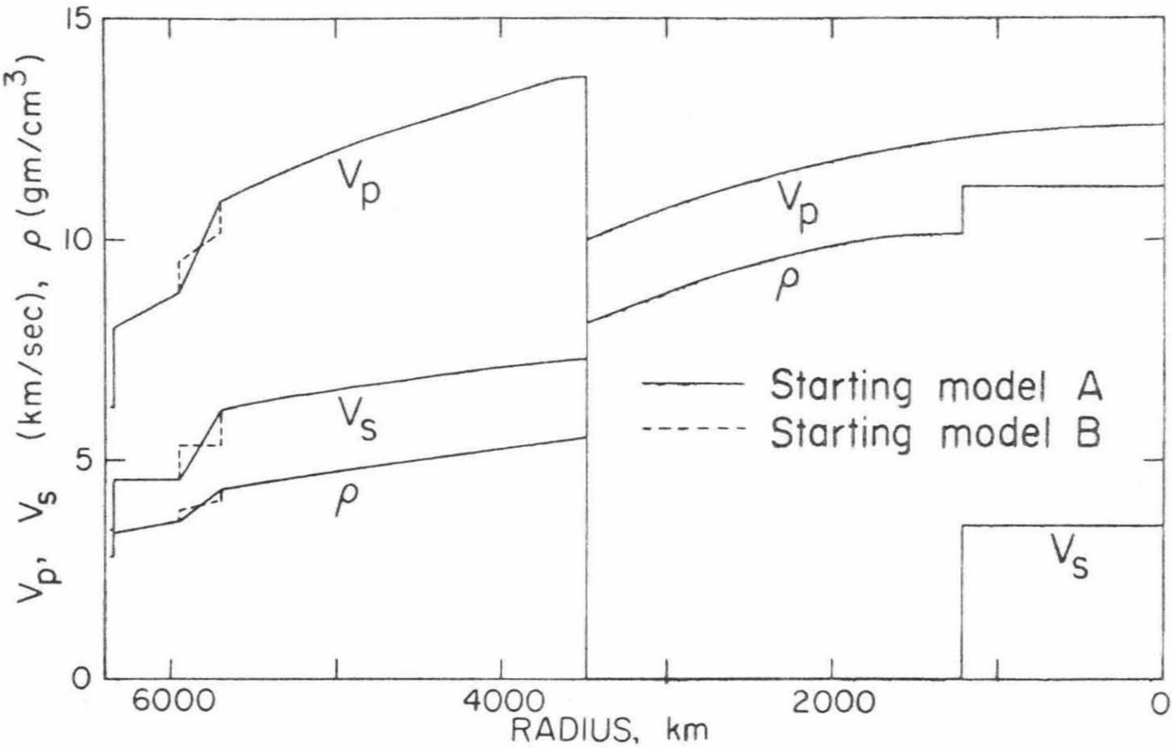

Figure 5.1. The starting models A and B.

<u>The core (regions E, F, and G)</u>. A simple model of compressional velocity in the core was designed which fits most of the well-observed features of the PKP travel-time curve. It consists of an inner core and outer core separated by a discontinuity located at 1215 km. The velocity at the core-mantle boundary was taken to equal Jeffrey's value of 8.10 km/sec. The velocities in the outer core varied smoothly from this value to a value of 10.12 km/sec at the inner core - outer core boundary. Below this discontinuity, a constant velocity of 11.20 km/sec was assumed. For this model, the point A of the PKP travel-time curve occurred at a distance of 176°, the point B at 145°, the point C at 158°, and the point D at 111°. It fits Bolt's [1968] absolute times for the AB and DF branches within 2 seconds.

The shear velocity in the outer core was assumed to be zero. The shear velocity in the inner core was taken to equal to 3.5 km/sec, the value determined by Dziewonski and Gilbert [1972].

Once the velocity models had been constructed, it was possible to determine a unique density distribution from the observed values of the Earth's mass and moment of inertia using the method of Birch [1964]. The density in the crust was assumed to equal 2.79 gm/cm^3. In the upper mantle and in the transition zone the density was assumed to obey the Birch law $\rho = a\,v_p + b$. The density at the top of the mantle was fixed at 3.33 gm/cm^3, yielding a value of 1.54 gm/cm^3 for the constant b. Below the discontinuity at 671 km, density was determined by integrating the Adams-Williamson equations [Bullen, 1963, p.229]. At the top of the core these equations were re-initiated with a new value of the density (call it ρ_c), and the solution was continued to the center. The values of the free parameters a and ρ_c were determined by fitting the mass and moment of inertia. For both models, the values obtained were 0.349 and 9.98, respectively. These can be compared with Birch's values of 0.379 and 9.96 for his solution II.

The starting models are listed in Table 5.2 and plotted in Figure 5.1.

5.5 Inversion results. We have used the inversion algorithm described in §5.2, the data sets presented in §5.3, and the starting models constructed in §5.4 to derive three estimates of the radial distributions of compressional velocity, shear velocity, and density in the Earth. These results are presented in this section.

Model A1. In this first experiment we were concerned with obtaining a model with a very simple structure in the upper mantle. Model A was used as the starting model. Initially, the fit to the eigenperiod data in data sets I and II was 0.3%, RMS relative deviation. The computed differential travel times deviated from the observed by at most 3 seconds (for ScS-S at 30^{o}). The autocorrelation operators for the functions v_p, v_s, and ρ were partitioned, or "decorrelated", at the radii of the discontinuities separating the inner and outer cores (1215 km), the outer core and mantle (3485 km), and the crust and mantle (6350 km). In each of these regions a correlation operator of the form given in equation (5.2.6) was used, and in all cases we assumed that $\alpha_p = \beta_p = 0$. For this experiment, the correlation wavelengths $\lambda_p = 2/k_p$ were set

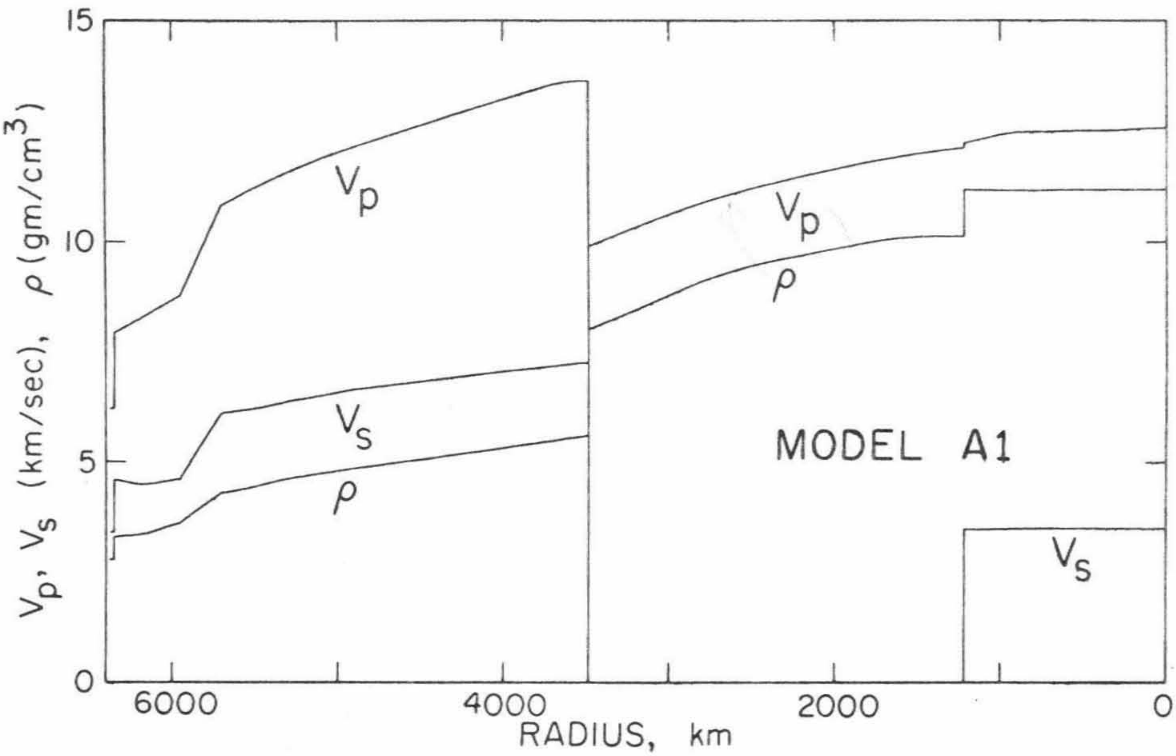

Figure 5.2. Model A1.

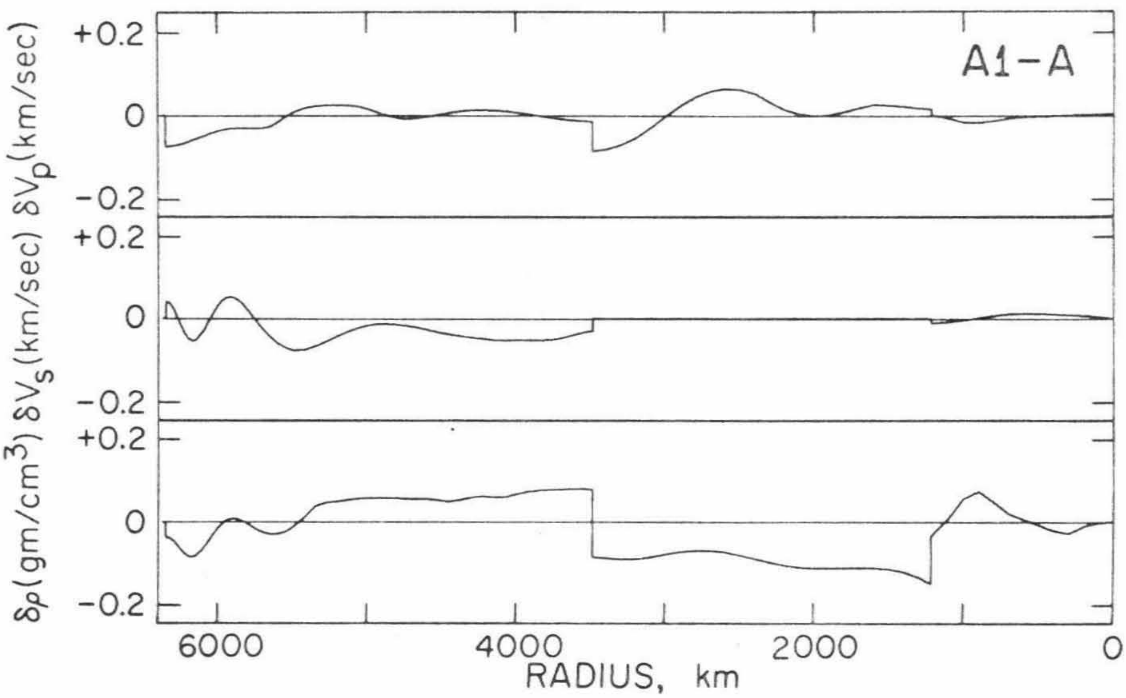

Figure 5.3. Cumulative perturbation for model A1.

equal to 1000 km. The diagonal components of the noise autocorrelation operator (the only nonzero components in the form we have assumed) were taken to equal the squares of the standard errors in the means of the data. In the algorithm we alternated between an inversion of v_p and ρ using data set I and an inversion of v_s and ρ using data set II. At each step the perturbation was computed from equation (5.2.4.). The perturbation was "overdamped" by setting $\tan\theta$ in this equation equal to 10. Although this value is ten times the "optimal" value of 1, doing this insured more rapid convergence.

For this model, convergence was achieved in six iterations. The final model is plotted in Figure 5.2, and the cumulative perturbation is plotted in Figure 5.3. A listing of the model and its fit to all of the data are given in Appendix 3.

As can be seen from Figure 5.3, the compressional velocity in model A1 differs from the starting model by less than 0.05 km/sec everywhere except in the upper mantle and outer core. The value of the velocity at the top of the core is 8.01 km/sec, which is in agreement with Hales' and Roberts' [1971] conclusion that the velocities in this region are less than the values given by the Jeffreys model. Their study was based on the differential travel times of SKKS-SKS. The computed times of SKKS-SKS for model A1 are listed along with times computed for equation 3 of their paper in Appendix 3. The agreement is excellent .

The times of P'(DF) are almost 0.3 seconds less than those given by Cleary and Hales [1971] and roughly one second greater than the times of Bolt [1968]. The times of P'(AB) computed for A1 are a few tenths of a second greater than Bolt's.

The decrease of the compressional velocity in the upper mantle introduced in the inversion shifts the baseline of teleseismic P by about one second. If this amount is added to the P times given in the 1968 tables, then they agree with the times computed from model A1 to within 0.2 seconds at distances greater than 30°.

The perturbation in the shear velocity distribution in going from model A to model A1 is most dramatic in the lower mantle. In this region the perturbation is negative and averages about 0.03 km/sec in magnitude. The effect on the S times is to introduce a "drift" of nearly 5 seconds in the distance range 30° to 80°. Most responsible for this net decrease in shear velocity are the eigenperiods of the fundamental mode torsional oscillations of low angular order. The incompatibility of torsional oscillation eigenperiods with travel-time data has been evident since the early work of MacDonald and Ness [1961]. However, there seems to be no significant incompatibility between the oscillation data and the ScS-S travel-time data; for model A1 all of this data (except for $T_{ScS-S}(40^{\circ})$ which, due to interference with sS and SS, is poorly determined) is fit to within their 95% confidence intervals.

Because the solution was tightly correlated throughout the upper mantle, model A1 has almost no low-velocity zone for shear waves. The need for this feature is evident from the fit of this model to the fundamental torsional mode data. At periods near 200 seconds, the periods computed from the model deviate from the observations by as much as 0.5%, beyond the limits of probable error.

The perturbations to shear velocity in the inner core are very small, confirming the correctness of Dziewonski's and Gilbert's [1972] determination of 3.5 km/sec as the mean velocity of this region. The high phase velocity arrival seen at LASA by Julian, Davies, and Sheppard [1972] and identified by them as PKJKP implies, with this identification, a shear velocity in the inner core of about 2.8 km/sec. This value is incompatible with the mode data.

The cumulative perturbations to the density in the upper mantle are negative. In the resulting model the average density in the upper two hundred kilometers of the mantle is only about 3.33 gm/cm^3. In the lower mantle the perturbations are positive, and in the outer core they are again negative. The inversion introduces a small jump in the density at the boundary between the inner and outer cores, but the significance of this feature is very doubtful.

Model B1. In this second experiment, model B was used as the starting model. The inversion procedure was essentially the same as we used to derive model A1, the principal difference being a different specification of the solution autocorrelation operator. For this inversion, the distributions in the inner core, the outer core, and the lower mantle were decorrelated and assigned correlation wavelengths of 1000 km, as before. In addition, the transition region and the upper mantle were decorrelated. For the former, the correlation wavelengths for each of the three distributions were chosen to be 200 km. For the latter, the

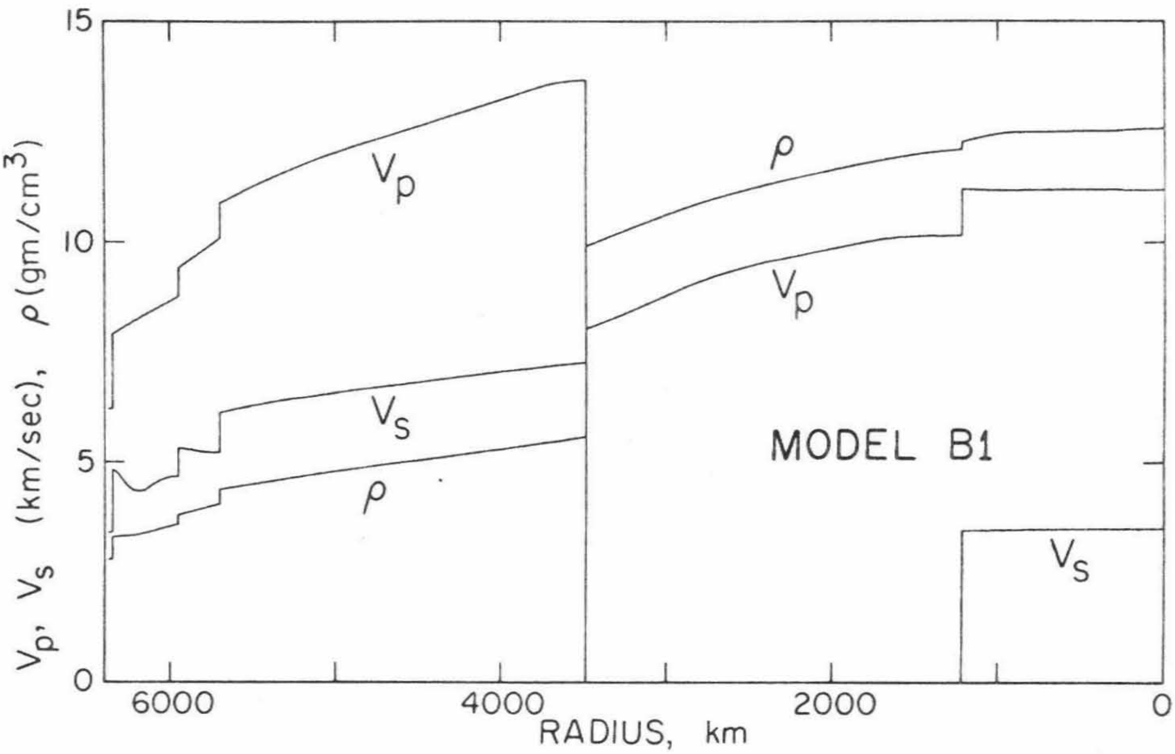

Figure 5.4. Model B1.

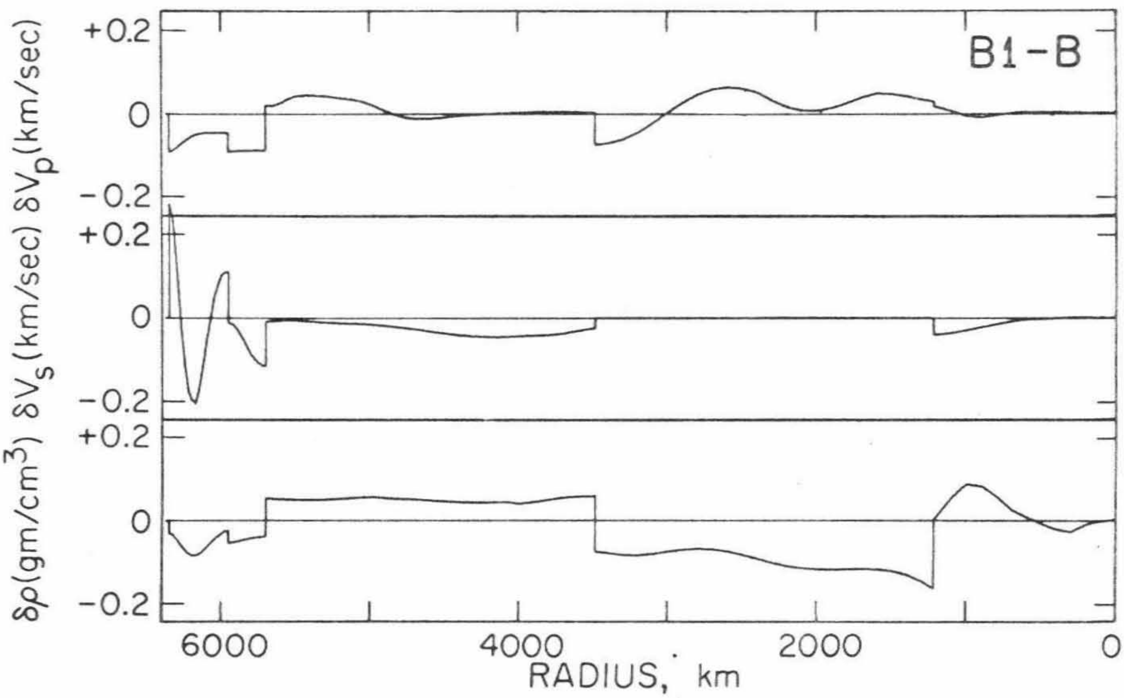

Figure 5.5. Cumulative perturbation for model B1.

correlation wavelengths for the velocities were chosen to be 100 km, and the correlation wavelength for the density was chosen to be 300 km. As before, the distributions in the crust were not inverted.

Convergence was achieved in eight iterations. The final iterate, designated model B1, is listed in Appendix 3 and is plotted in Fig. 5.4. The cumulative perturbations are pictured in Figure 5.5.

The fit of this model to the fundamental spheroidal and torsional mode data sets (given in Table A3.1) is considerably improved over model A1. This improvement results from the introduction of a more profound shear wave low-velocity zone in the upper mantle, made possible by relaxing the smoothing in the upper mantle.

A second feature which distinguishes this model from model A1 is that the strong negative perturbation, centered at about 5600 km radius and broadly spread over the upper part of the lower mantle in model A1, is localized in the transition zone in model B1. Examination of the averaging kernels for this perturbation confirms that this difference is indeed due to localization of the averaging. As a result, the transition zone of model B1 is characterized by a decrease in shear velocity with depth. A similar localization can be observed in the density in this region.

Other than these features, the models A1 and B1 are essentially the same.

Model B2. A second experiment using model B as the starting model was attempted. The purpose of the experiment was to see if modifications in the velocities at the very base of the mantle had any significant

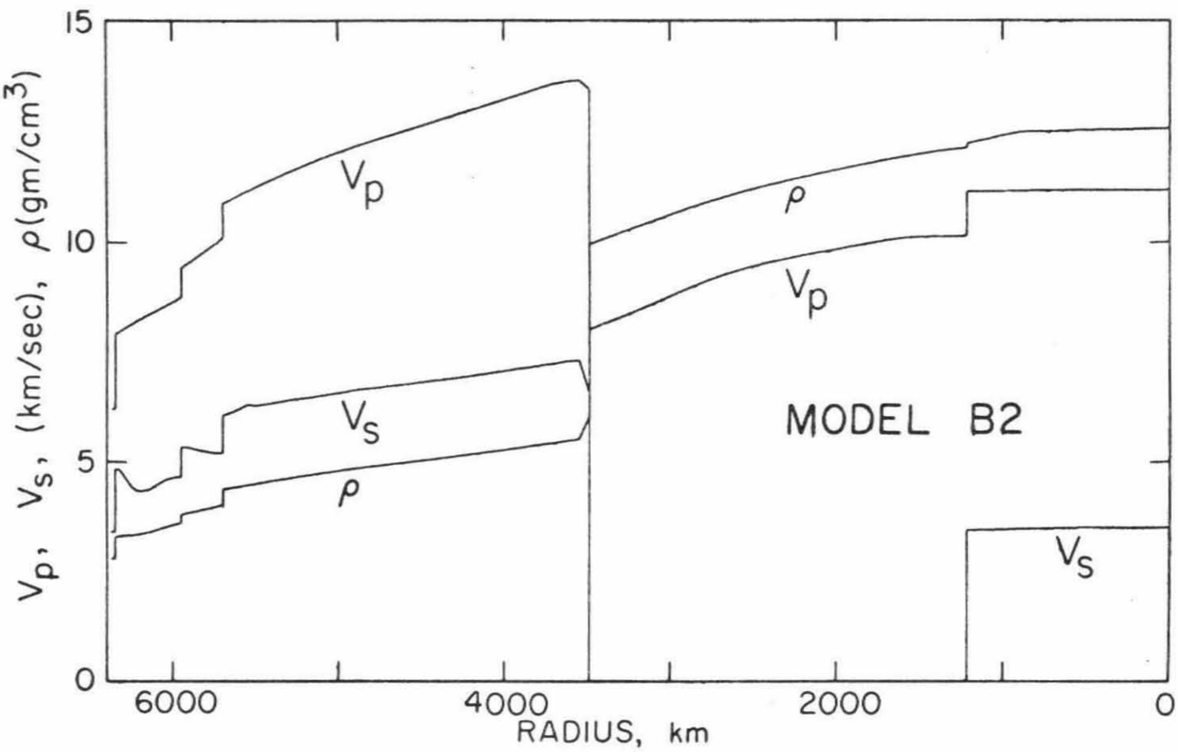

Figure 5.6. Model B2.

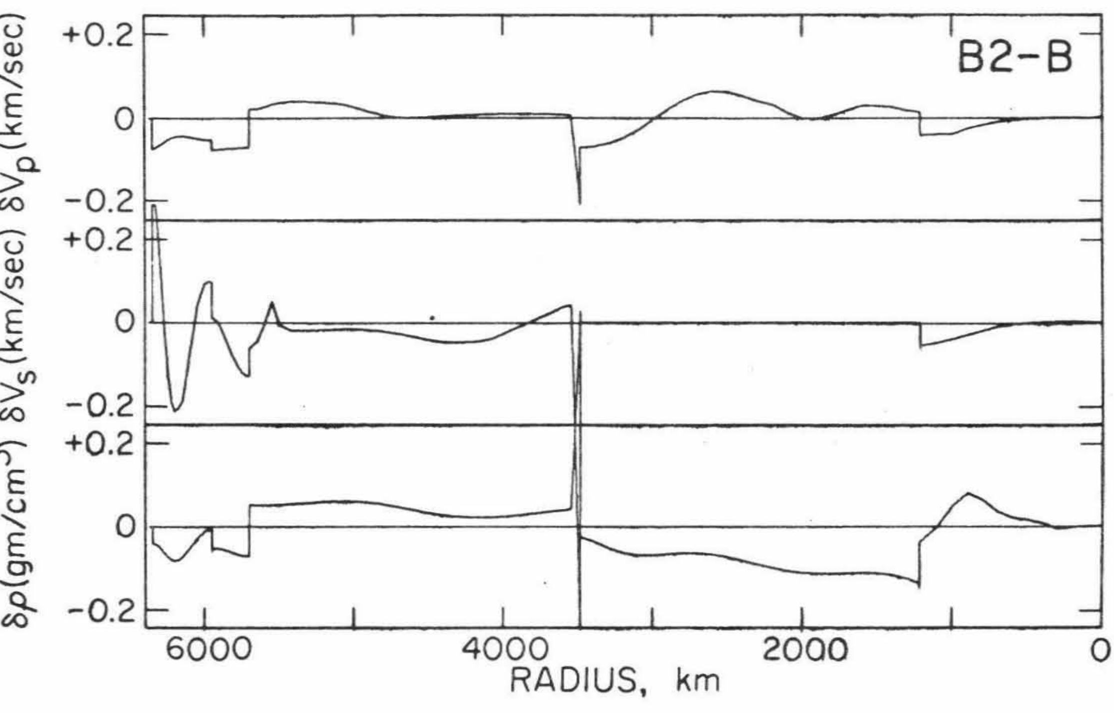

Figure 5.7. Cumulative perturbation for model B2.

effect on the inversion results and to attempt to further localize the averages of shear velocity at the top of the lower mantle by decorrelating at a radius of 5500 km. The existence of a transition zone at the base of the mantle has been the subject of some debate among seismologists since the paper of Dahm in 1936, and the recent observations by Cleary [1966] of so-called diffracted S which indicate a significant decrease in the velocity of S waves in this region, have heightened the speculation. This motivated us to modify the model B in the following way: The compressional velocity at the base of the mantle was decreased to 13.40, the shear velocity was decreased to 6.50, and the density was increased to 6.0. Linear gradients were used to connect these values to the unmodified values for model B at a radius of 3510 km.

The resulting model was inverted as before, except that the shear velocity was decorrelated at a radius of 5500 km. This was done to localize the averages of shear velocity in this region and to test the hypothesis that a discontinuity in shear velocity exists at this radius. This has been suggested by Hales and Roberts [1970a], among others, on the basis of a discontinuity in the $dT/d\Delta$ of shear waves at 42°. The correlation wavelength assumed in the region from 5500 km to 5700 km was 100 km.

The results of this inversion, which took eight iterations, was the model B2 plotted in Figure 5.6. Like the other models, it is listed in Appendix 3 along with the fits to the data. The cumulative perturbation for this model sequence is plotted in Figure 5.7.

The inversion was successful; out of the 166 modes listed in Table A3.1, this model fit 114 of them with a relative error of less than 0.1%. The inversion introduced a region of negative velocity gradient between the depths of 821 and 851 kilometers and a corresponding break in the travel-time curve of S near 42°. However, the somewhat simpler model B1 fit the data better; it had 121 of the 166 modes fit with relative errors less than 0.1%. It cannot be argued on the basis of this experiment that the additional features appearing in model B2, in particular the negative gradients in shear velocity in the mantle, are warranted by the data used in the inversion.

5.6 Averaging kernels. We present in this section the averaging kernels, rows of the operator $\mathscr{A}$ given by equation (5.2.5), for various data sets and choices of the solution autocorrelation operator C_{ss}. Six figures are presented. In each, the kernels of $\mathscr{A}$ corresponding to several radii for a given function, v_p, v_s, or ρ, are plotted. The radii are indicated by the numbers in the corners of the plot; the function to which the kernel corresponds is indicated by whether the radius is plotted on the left or the right hand side of the graph: the left hand side indicates velocity, and the right hand indicates density.

Figure 5.8. This plot shows the results of an experiment to compare the resolving power of absolute versus differential travel times. Two data sets were used. Panel (a) of this figure shows several kernels computed from a data set consisting of 32 ScS-S differential travel times in the distance range 30° to 94°. Panel (b) shows kernels centered at the same radii for a data set consisting of 64 S and ScS absolute times. All data were assumed to have errors of 1 second.

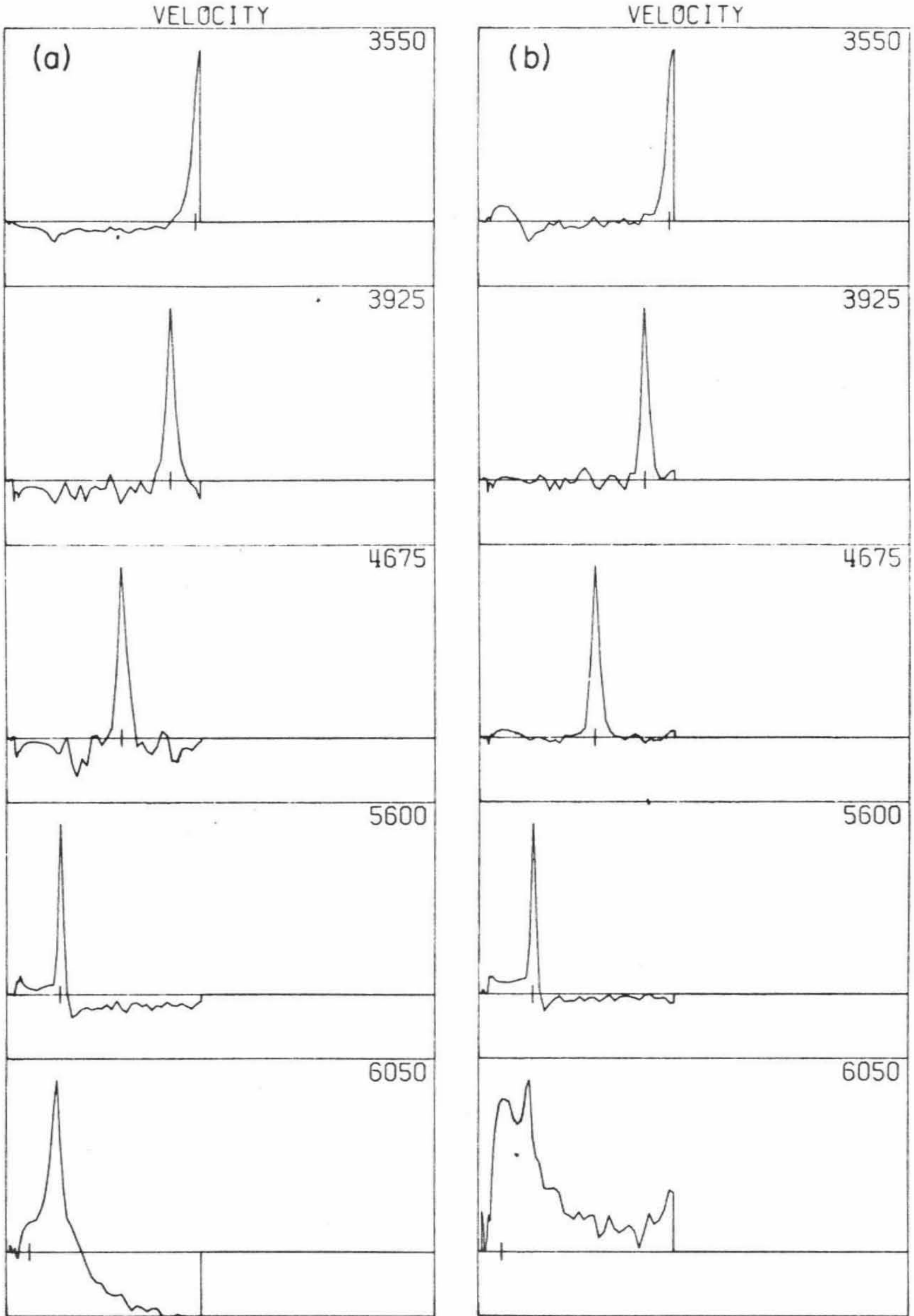

Figure 5.8. Averaging kernels for travel times.

a) ScS-S differential times, 30°(2°)94°.

b) S and ScS absolute times, 30°(2°)94°.

The model used is A1, and the solution autocorrelation is 100 km. For all radii in the lower mantle, both sets of data yield highly peaked kernels with half-widths of about 75 km, roughly the spacing between the bottoming depths of the S rays. The absolute travel times give somewhat more localized averaging kernels, but the difference is not appreciable. We conclude that not much resolution is lost by using the more precisely observed differential travel times. Of course, since neither data set contains rays which have turning points in the upper mantle, neither yields localized kernels in this region, as can be seen from examination of the kernels centered at 6050 km.

Figure 5.9. Shown in this figure are averaging kernels computed from model A1 for compressional velocity using the Fréchet kernels of data set I. The averaging is reasonably localized, although some tradeoff exists between perturbations in compressional velocity and density in the outer core beyond the radii at which P'(AB) rays bottom. Note the localization in the vicinity of the inner core - outer core boundary. This results from using the differential travel times of P'(BC)-P'(DF) The correlation operator used in this computation was the same as was used in the derivation of model A1.

Figure 5.10. This figure displays the averaging kernels for density using the same model, data set, and correlation operator as for Figure 5.9. The averaging in the inner core is extremely poor and unlocalized. We infer that our estimates of density in this region are correspondingly poor. In particular, we doubt that the jump in the density at the inner core - outer core boundary, present in all three models, is significant.

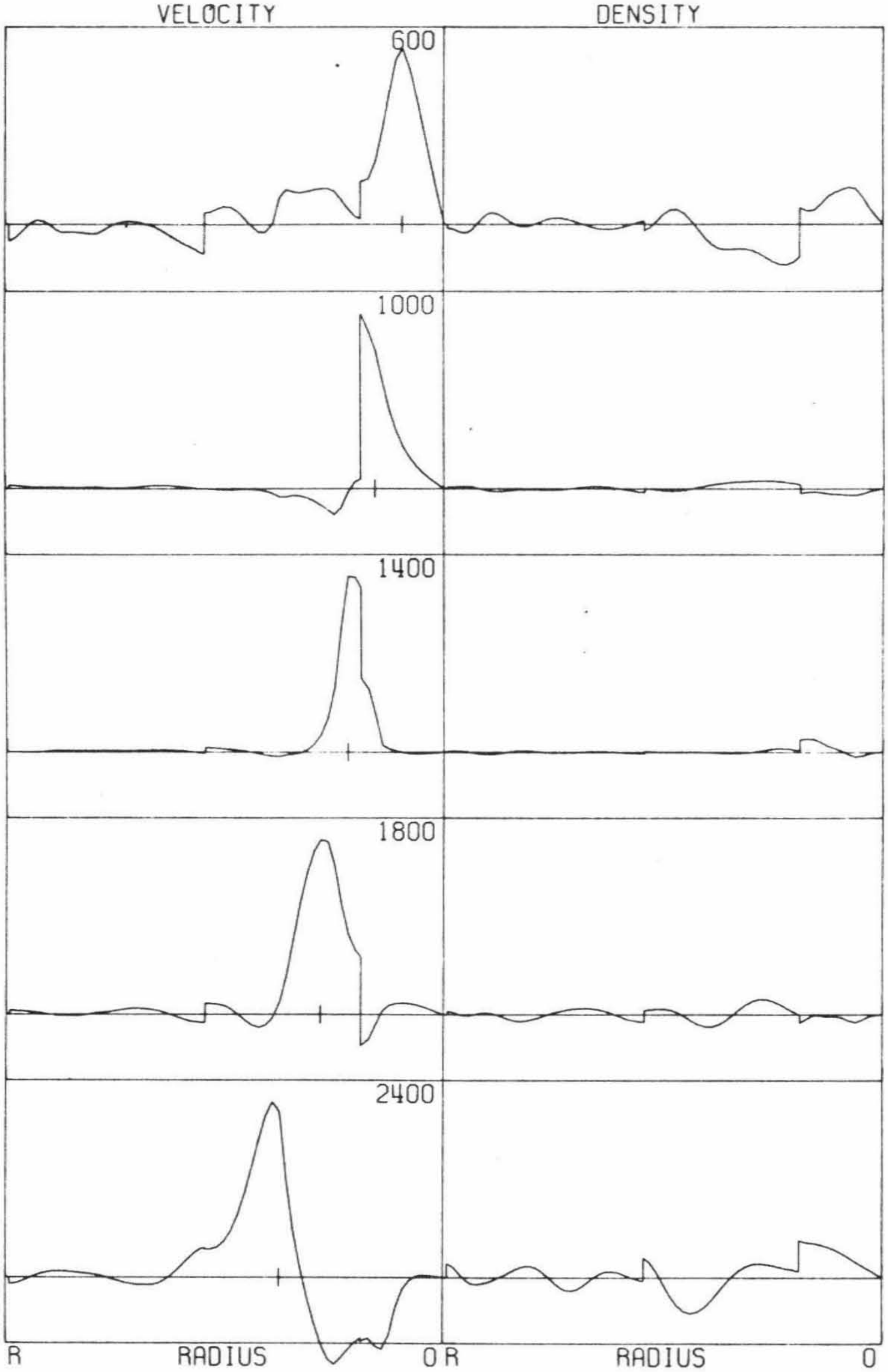

Figure 5.9. Averaging kernels for compressional velocity computed using data set I and the correlation operator for model A1. Functions inverted are compressional velocity and density.

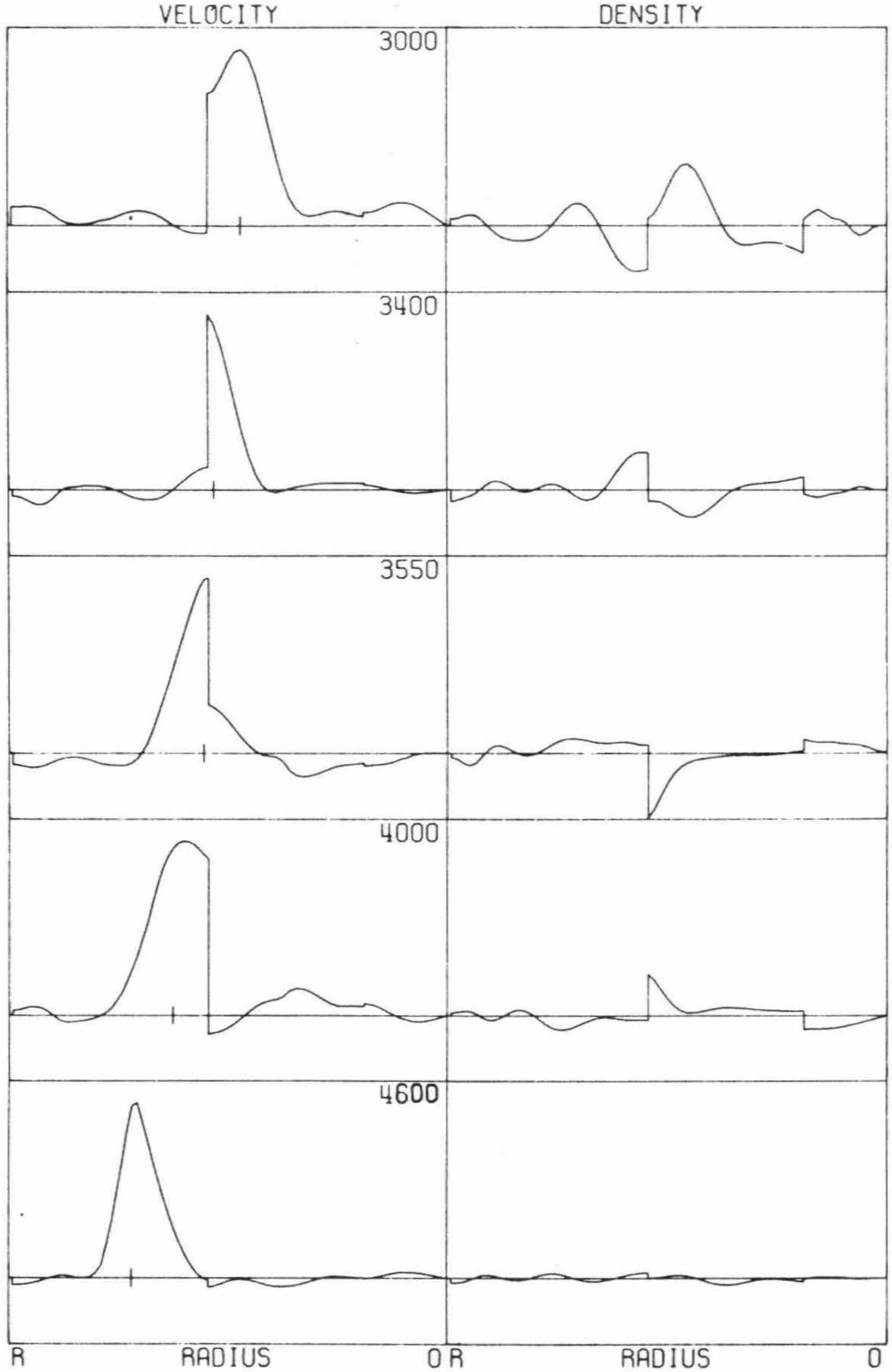

Figure 5.9. (cont.)

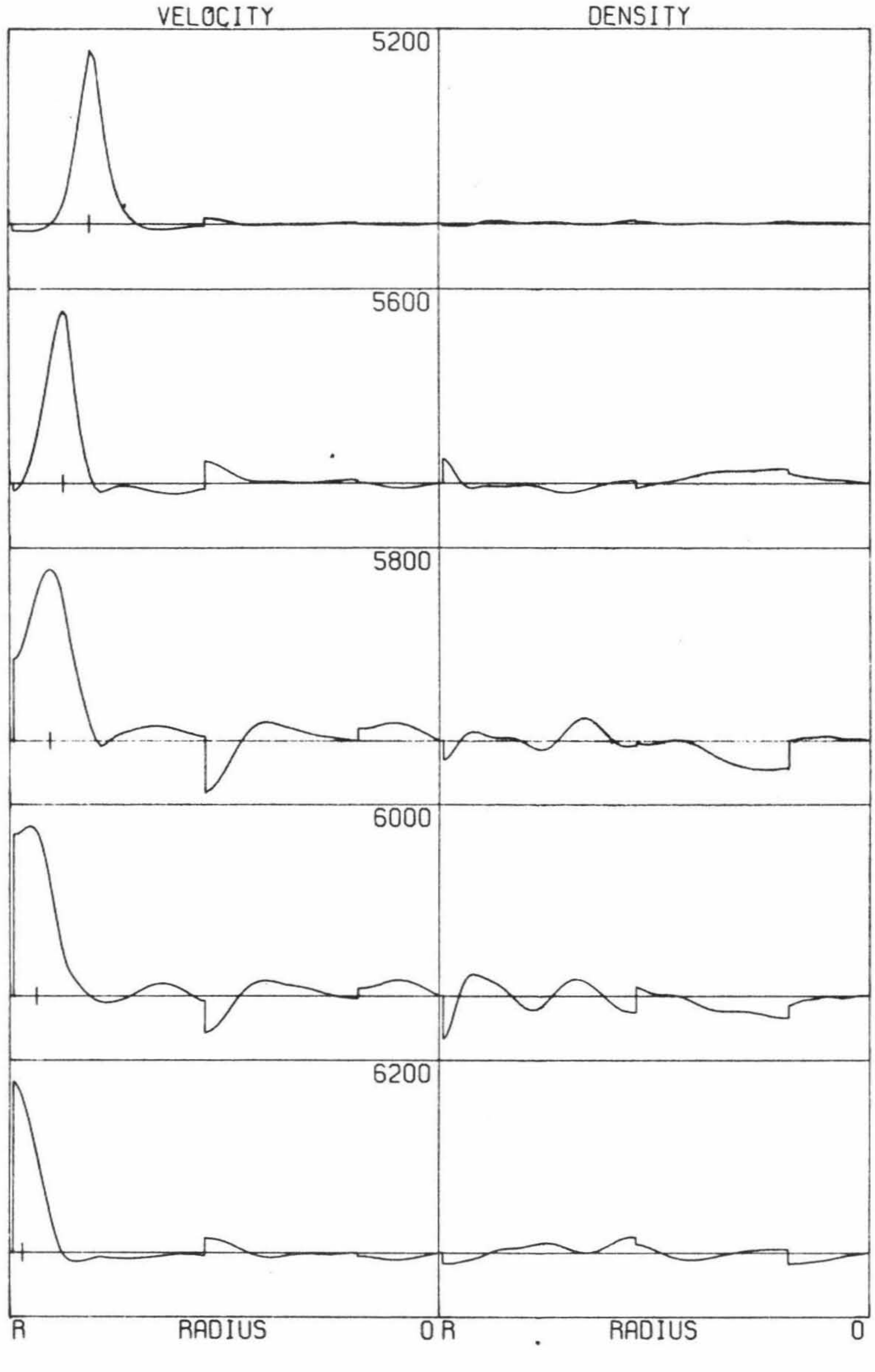

Figure 5.9. (cont.)

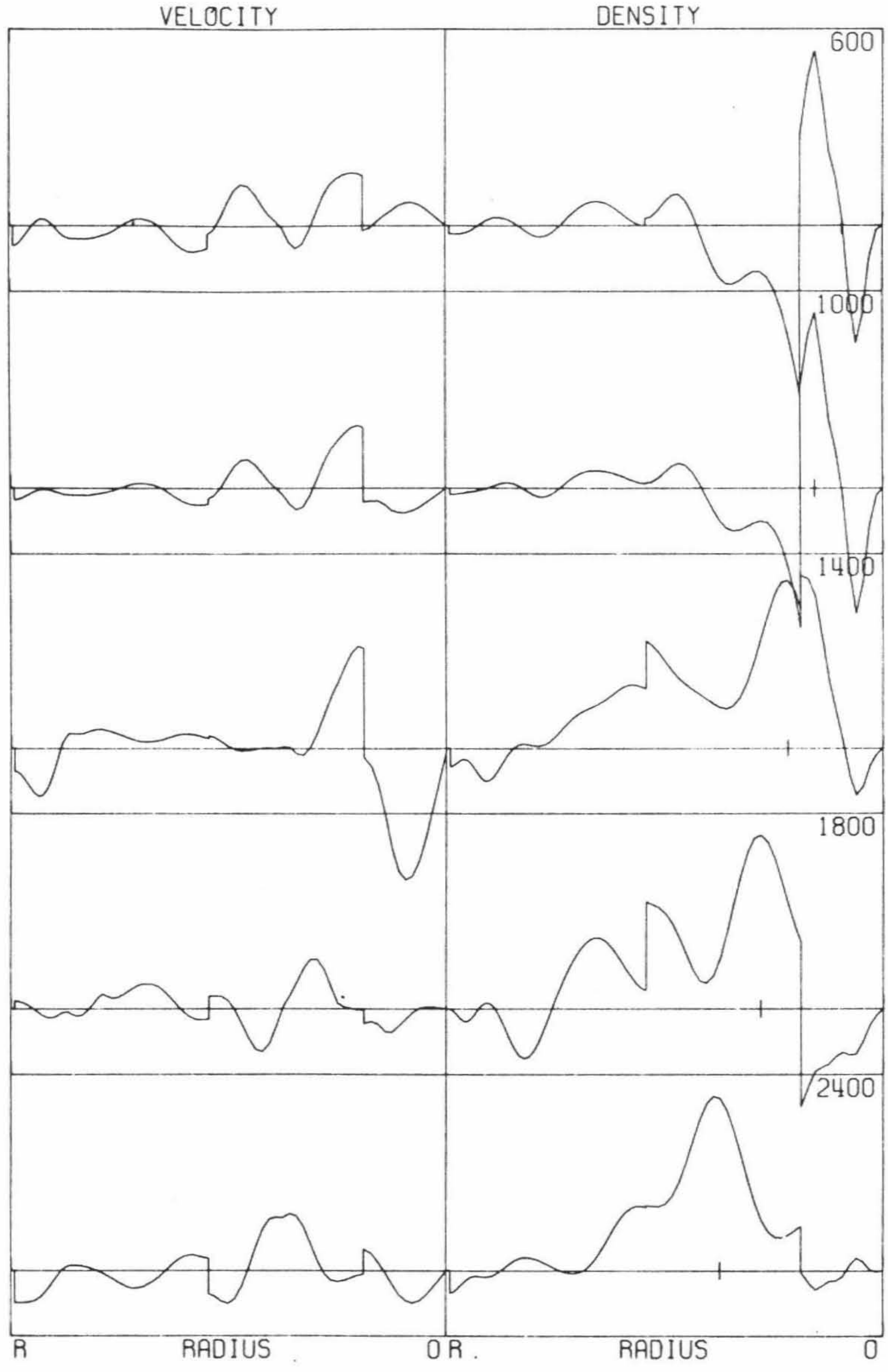

Figure 5.10. Averaging kernels for density computed using data set I and the correlation operator for model A1. Functions inverted are compressional velocity and density.

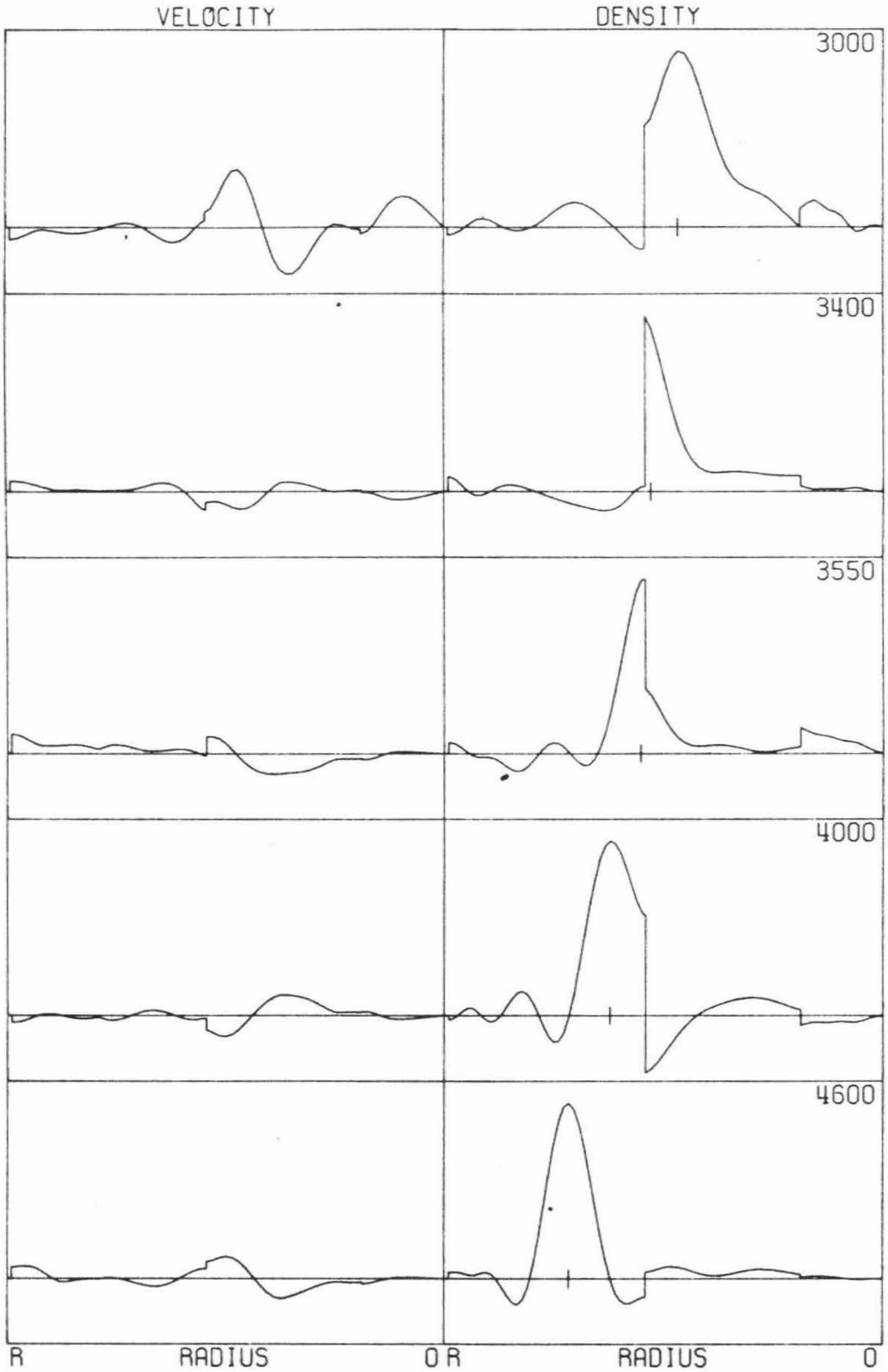

Figure 5.10. (cont.)

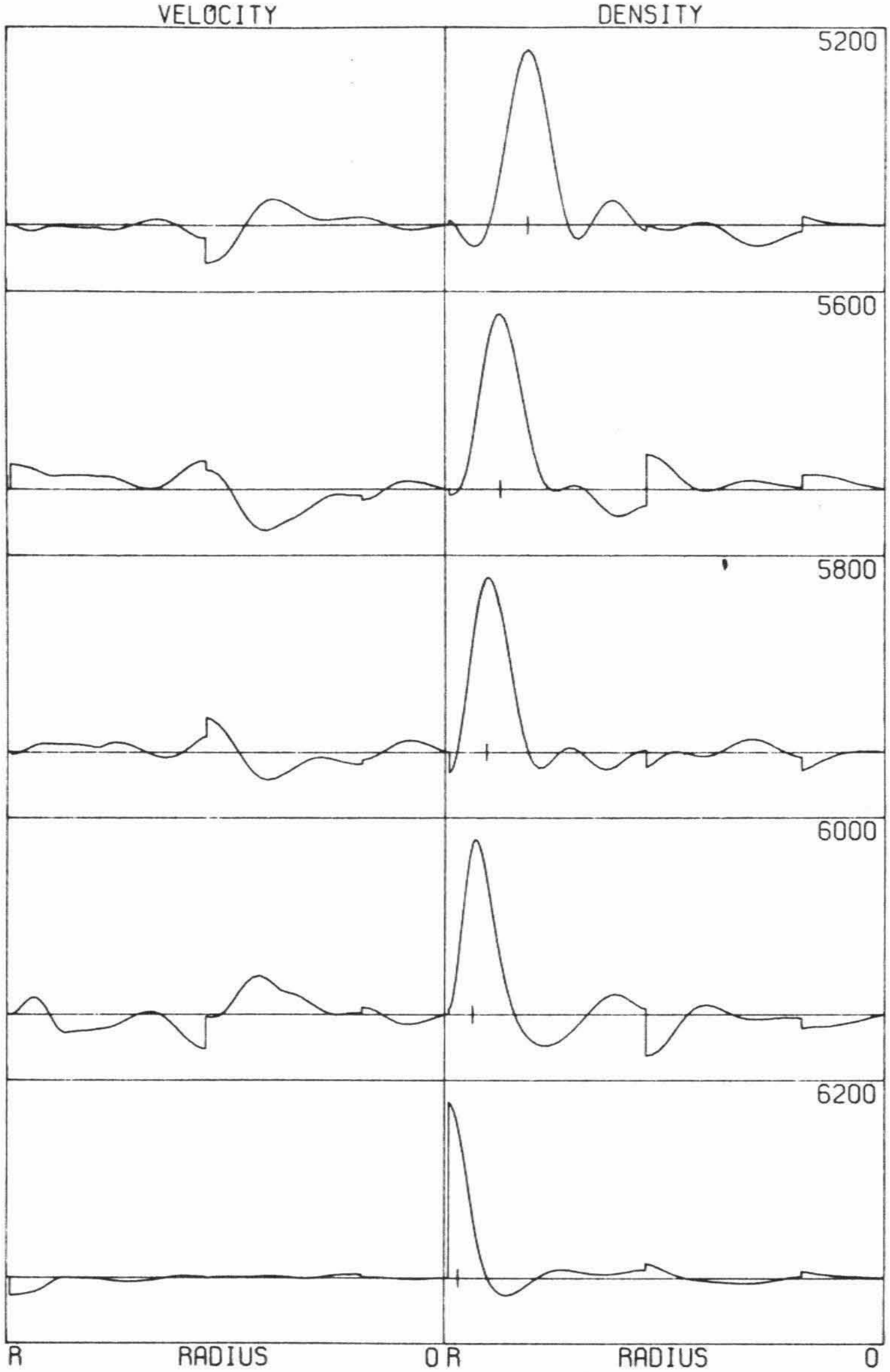

Figure 5.10. (cont.)

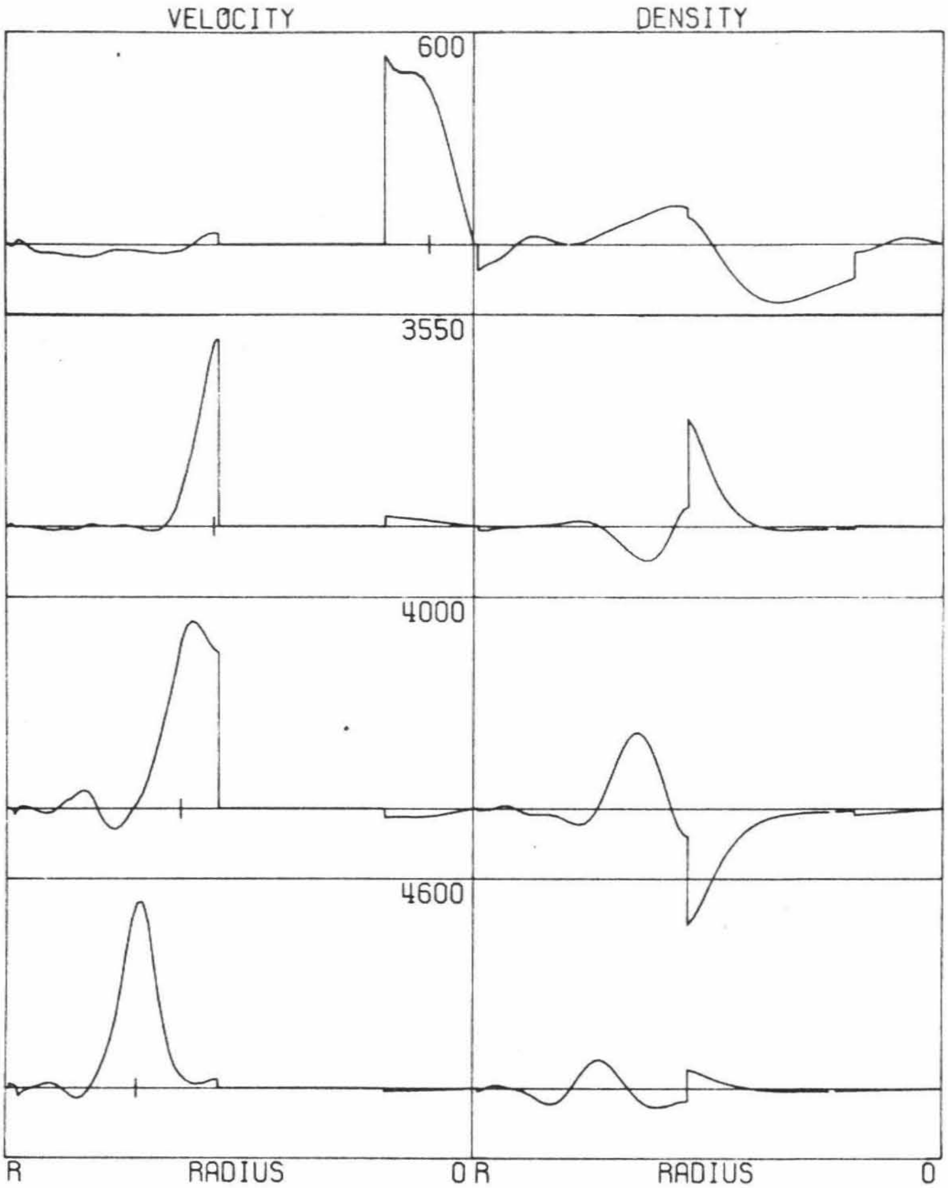

Figure 5.11. Averaging kernels for shear velocity computed using data set II and the correlation operator for model A1. Functions inverted are shear velocity and density.

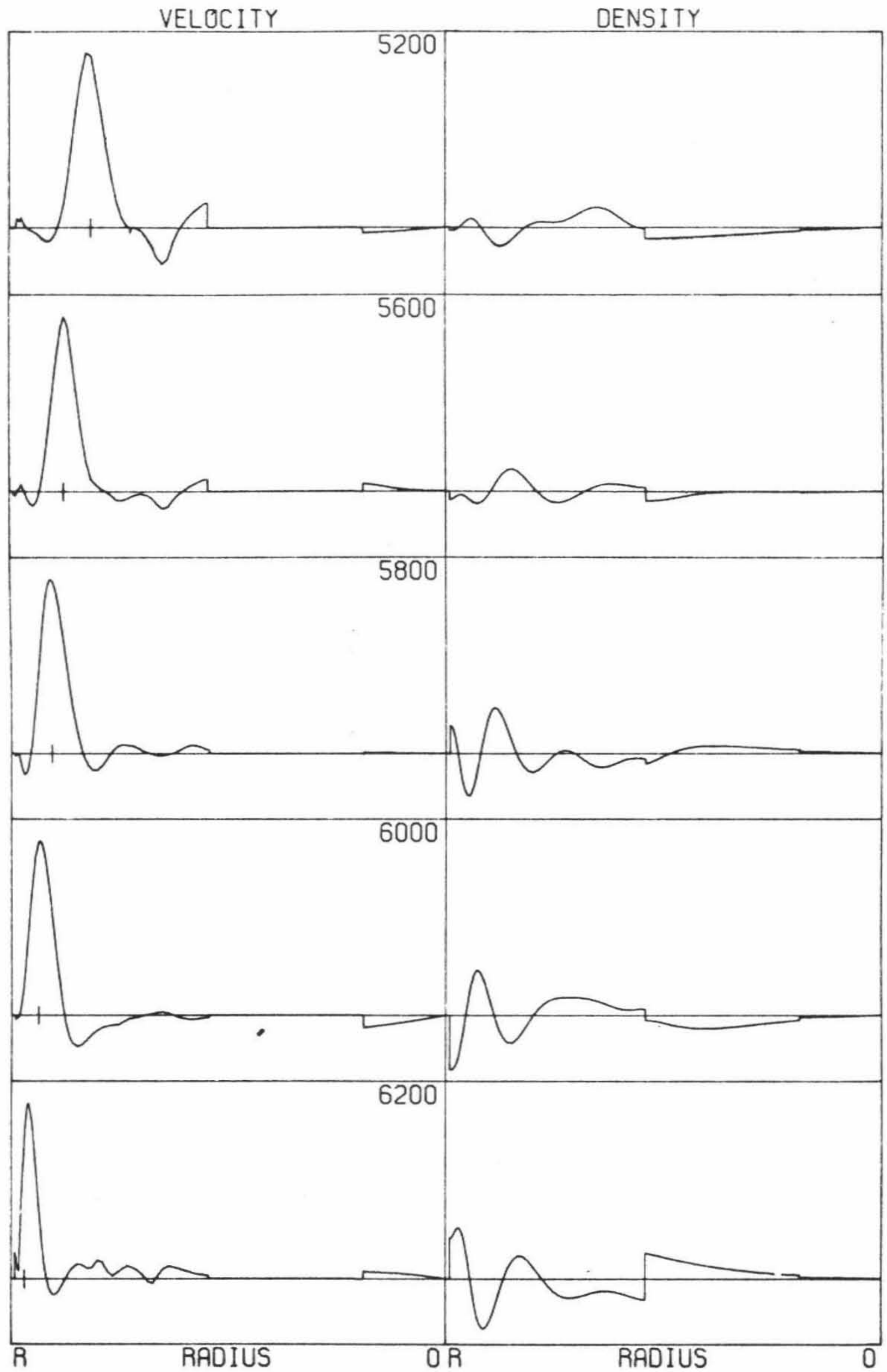

Figure 5.11. (cont.)

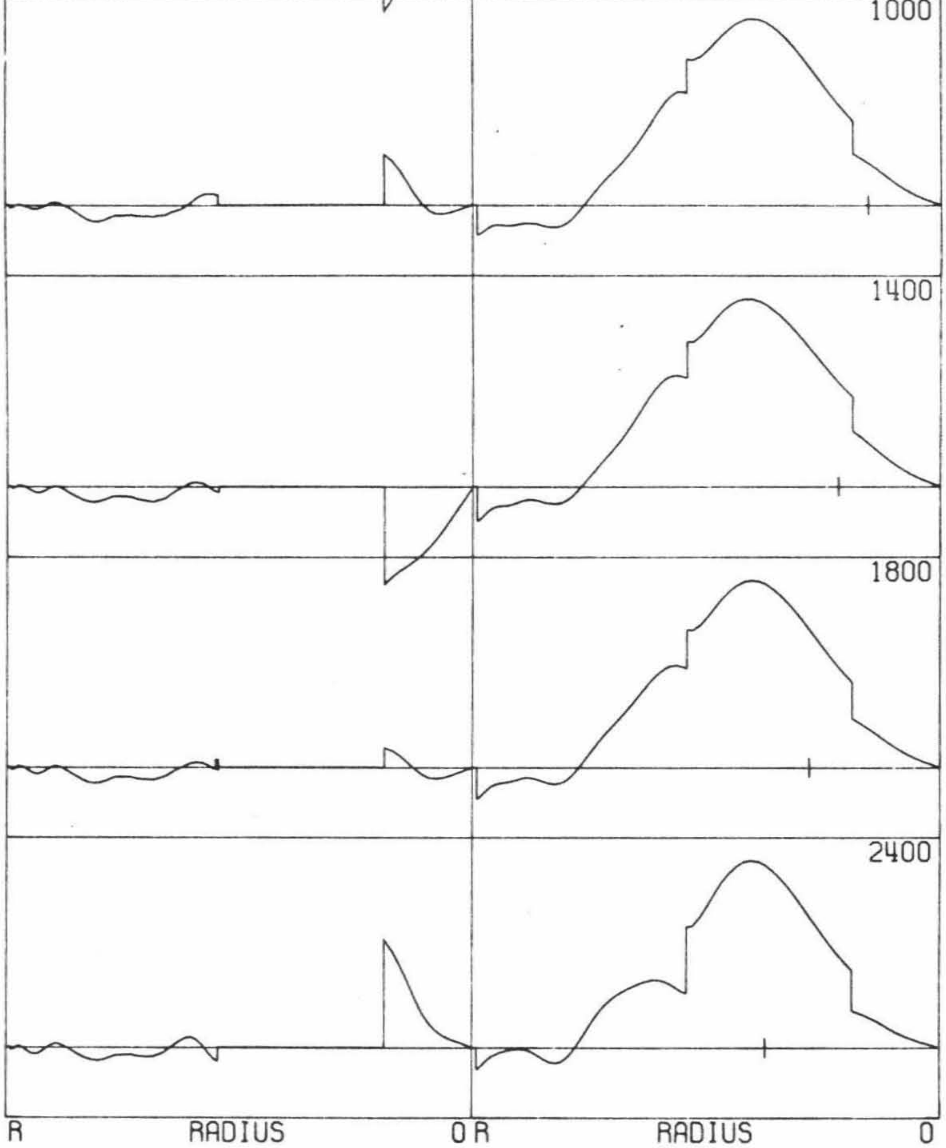

Figure 5.12. Averaging kernels for density computed using data set II and the correlation operator for model A1. Functions inverted are shear velocity and density.

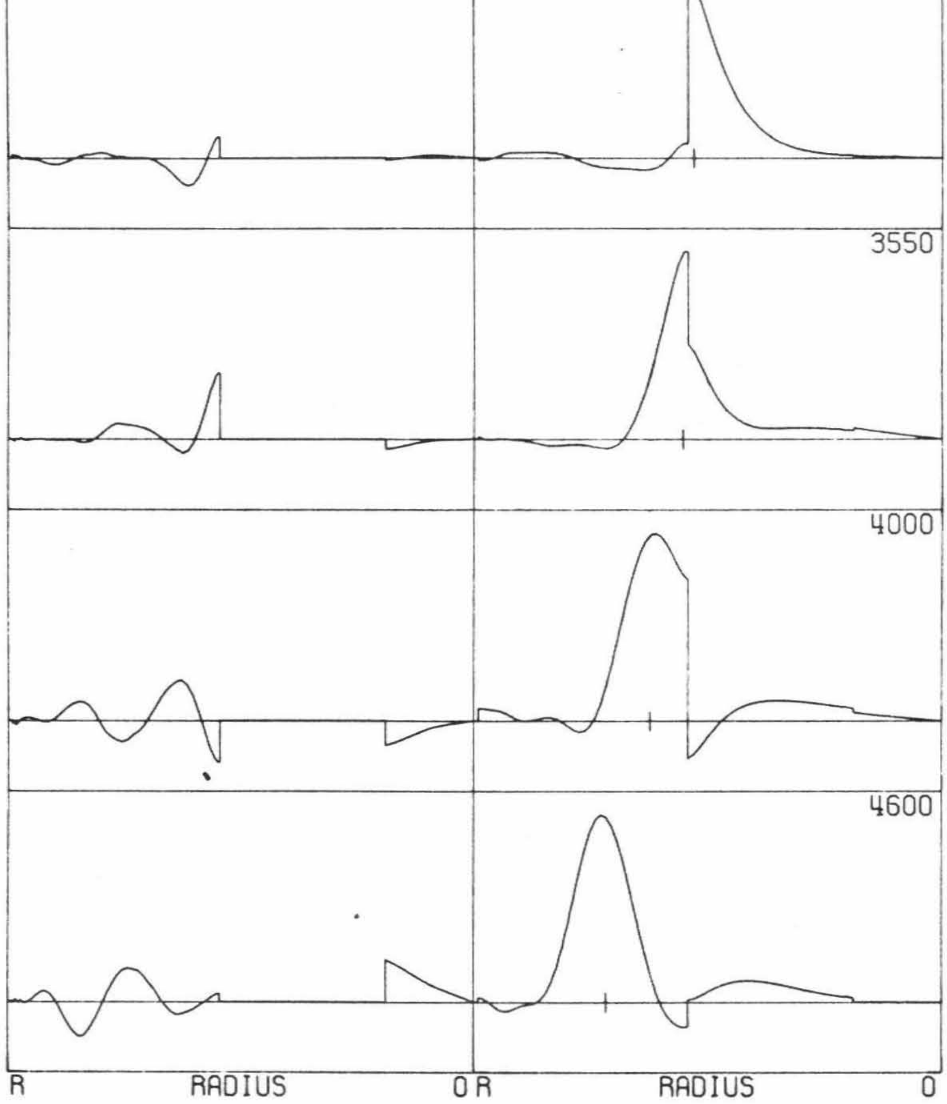

Figure 5.12. (cont.)

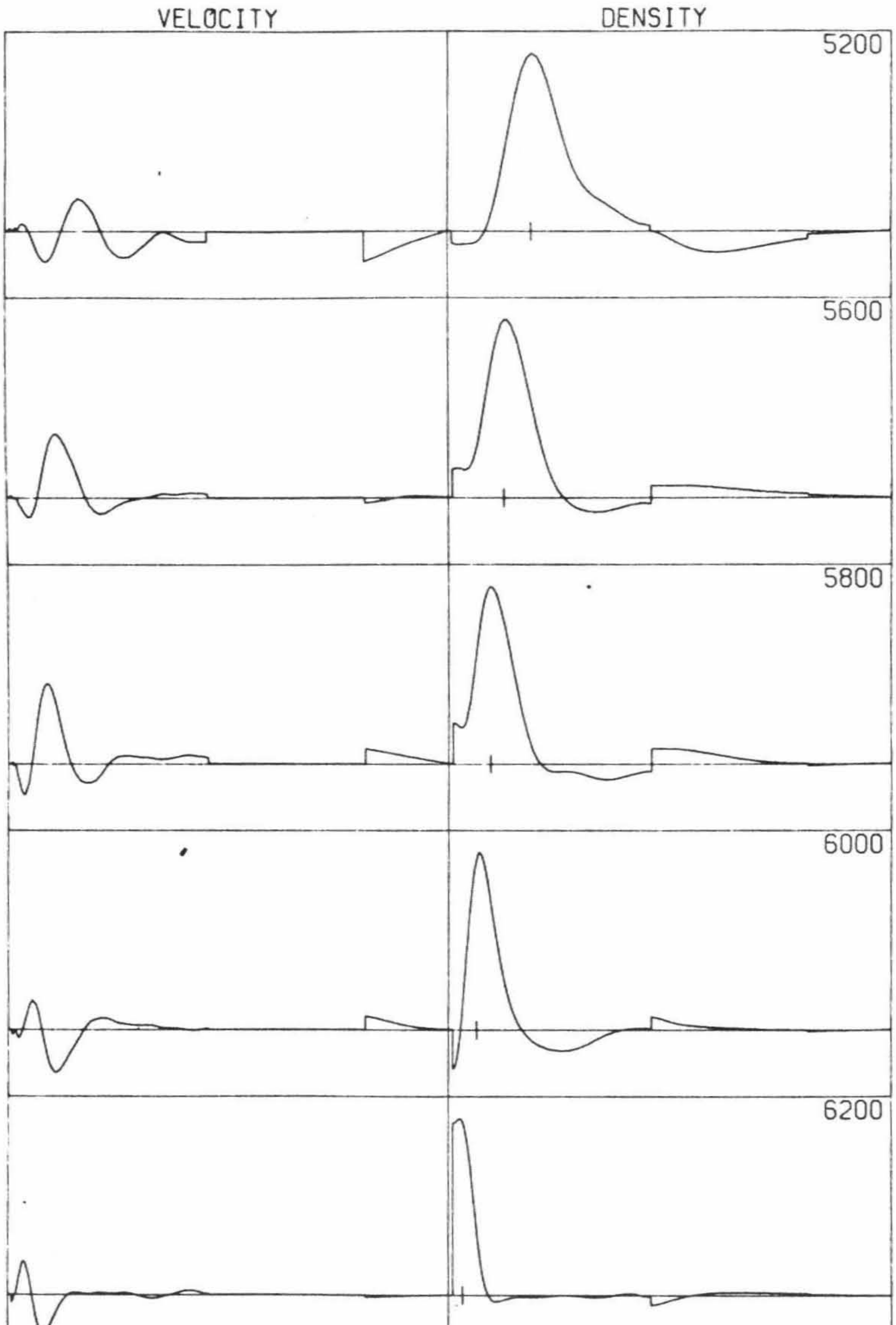

Figure 5.12. (cont.)

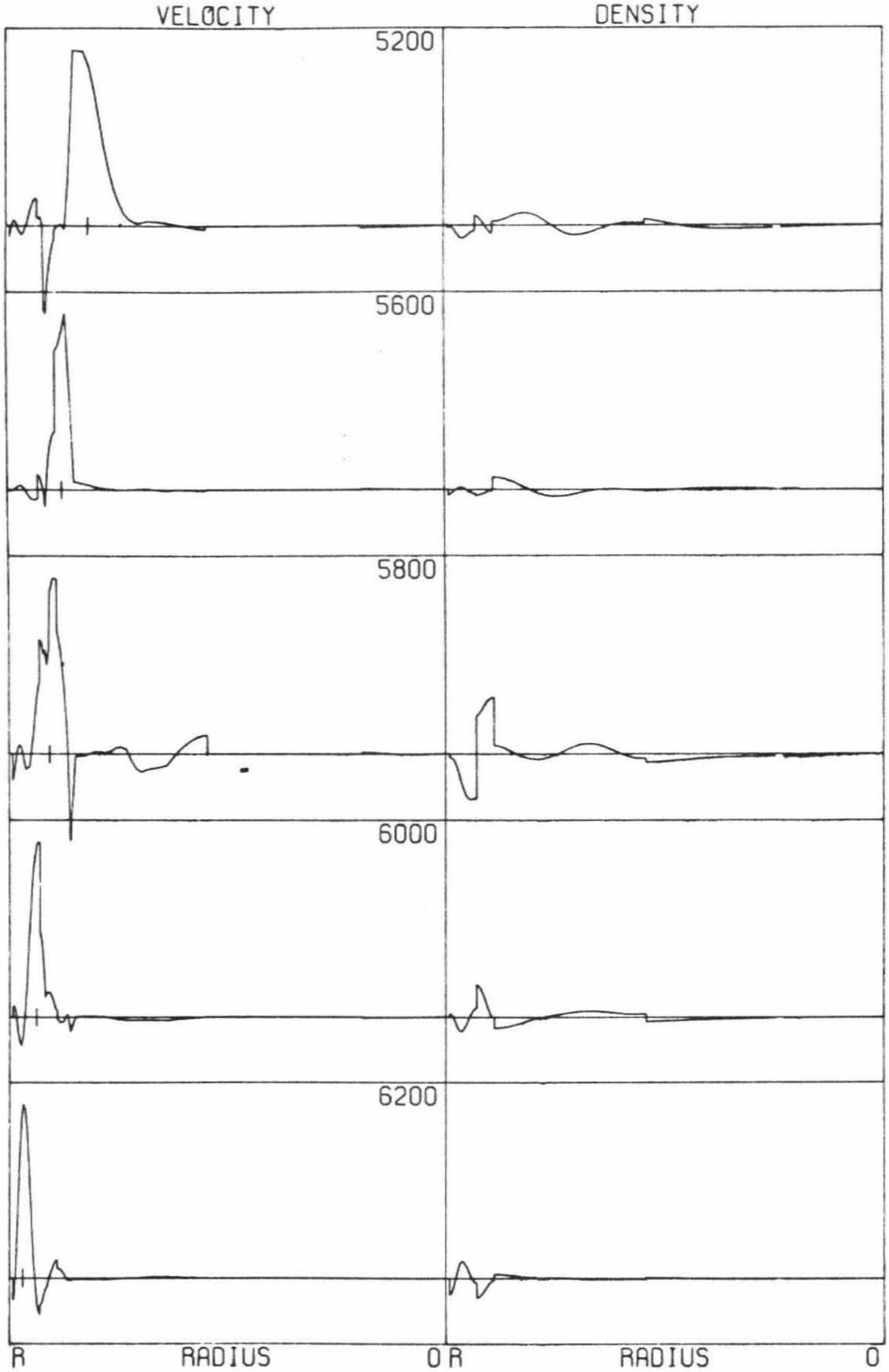

Figure 5.13. Averaging kernels for shear velocity computed using data set II and the correlation operator for model B2. Functions inverted are shear velocity and density.

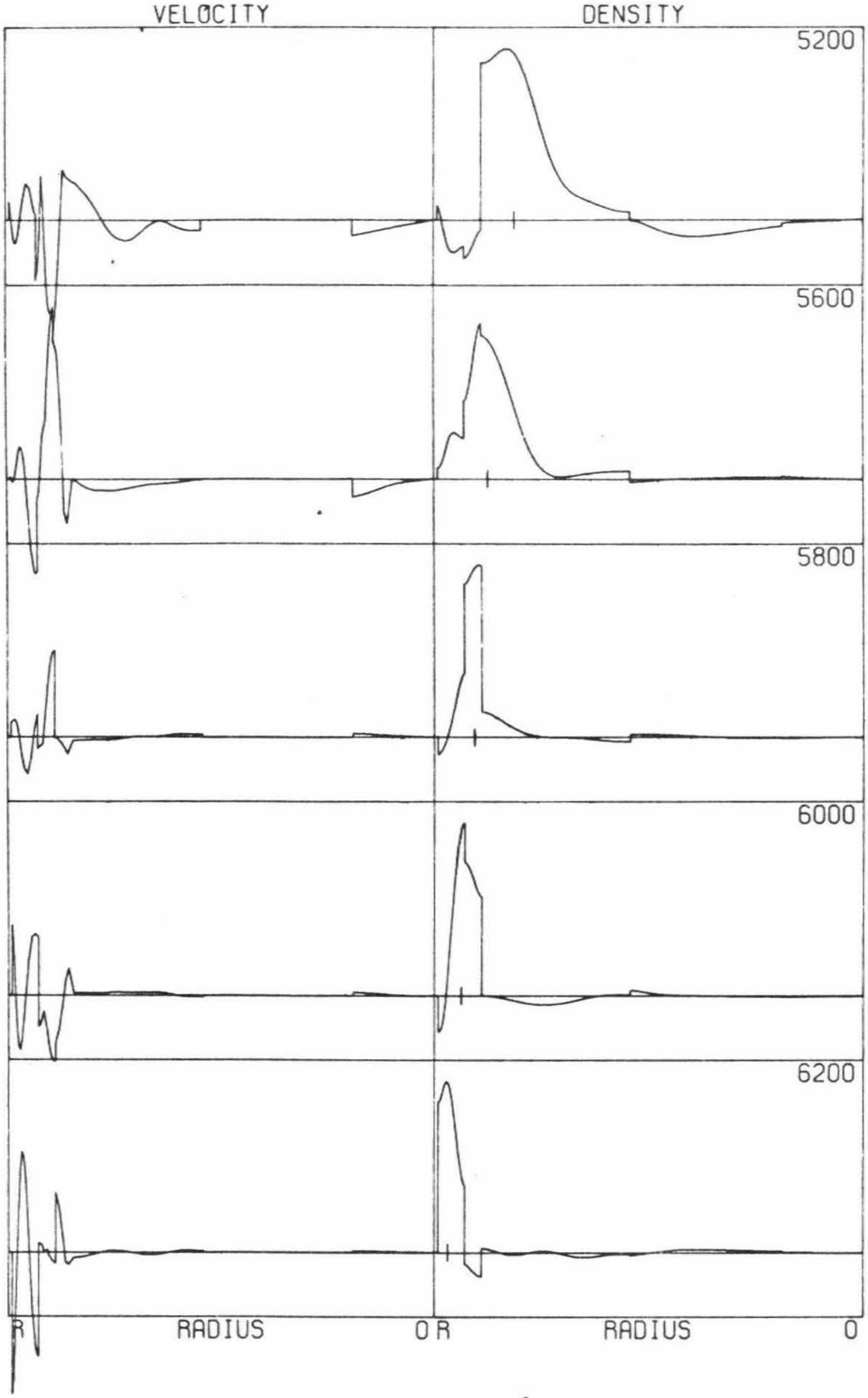

Figure 5.14. Averaging kernels for density computed using data set II and the correlation operator for model B2. Functions inverted are shear velocity and density.

Figure 5.11. We show in this figure the averaging kernels for shear velocity computed from model A1 using data set II. The correlation operator is the same as before, although naturally shear velocity in the outer core has been fixed. Most interestingly, we see that the averages of shear velocity in the inner core are reasonably localized, resulting from the inclusion of modes such as $_0S_2$, $_2S_2$, $_5S_2$, and $_8S_2$ in the data set. It can be inferred that the average shear velocity in the inner core is near the value 3.5 km/sec given by Dziewonski and Gilbert [1972]. As the radius is increased, the averaging kernels become progessively more peaked. However, for kernels centered in the upper mantle and transition zone the tradeoff between shear velocity and density is considerable.

Figure 5.12. This figure corresponds to Figure 5.11, except here the kernels for density are displayed. As we might expect, the averages of density in the core given by this data set are very broad. In fact they are not even localized for radii below about 2400 km. However, at the very top of the core the averaging kernels narrow considerably. The kernels centered in the mantle are similar to those for shear velocity.

Figures 5.13 and 5.14. The averaging kernels shown in these figures correspond to some of the averaging kernels given in Figures 5.11 and 5.12, except that here we use model B2 and its corresponding correlation operator. By comparison of the kernels used in the derivations of these two models, the effect of changing the autocorrelation operator can be seen. Comparison of the kernels for shear velocity centered at 6200 km radius in Figure 5.11 and 5.13, for example, illustrates how manipulation of the solution autocorrelation operator can be used to localize the averaging.

5.8 Summary. In this section we summarize our conclusions.

An inversion procedure has been developed to estimate the radial variation of compressional velocity, shear velocity, and density in the Earth. The radial distributions are defined as spherically symmetric averages of the actual distributions in the laterally heterogeneous Earth, and the nature of this averaging implied by averaging certain sets of eigenperiod and travel-time data has been examined. For travel-time data, the spherical averaging is simple if the data sample a distribution which results from a uniform distribution of sources and receivers. Since this is difficult to obtain for absolute times, we have used differential travel times to derive our estimates. It has been shown that the inherent bias in available sets of differential travel-time data is considerably less than for equivalent sets of absolute travel-time data. Observations have been presented for the phase combinations PcP-P, ScS-S, P'(AB)-P'(DF), and P'(BC)-P'(DF).

The inversion algorithm developed, based on a linear approximation to the perturbation equations, has been shown to provide a stable method for estimating the radial variations from a finite set of gross Earth data. One advantage of this approach is that it allows one to estimate the resolving power of the data and the resolvability of specified features in the Earth.

Three estimates of the radial distributions have been derived using an extensive set of eigenperiod and differential travel-time data, each representing a different level of complexity. Besides satisfying the data used in the inversion, these models also satisfy extensive sets of auxillary data.

The resolving power of the various data sets used in the inversions has been examined by computing their corresponding averaging kernels. It has been shown from this analysis that little resolving power is lost by using differential times in place of absolute times. It has demonstrated that the nature of the averaging for given sets of gross Earth data can be manipulated and improved by a judicious specification of the norm on the space of models.

BIBLIOGRAPHY

Adams, R. D. and M. J. Randall. The fine structure of the Earth's core, B.S.S.A., 54, 1299, 1964.

Anderson, D. L. The latest information from seismic observations, in The Earth's Mantle, edited by T. F. Gaskell, Academic Press, N. Y., 1967.

Anderson, D. L. and T. Jordan. The composition of the lower mantle, in Phys. Earth Planet. Interiors, 3, 23, 1970.

Anderson, D. L. and B. Julian. Shear velocities and elastic parameters of the mantle, J.G.R., 74, 3281, 1969.

Anderson, D.L. and C. Sammis. Partial melting in the upper mantle, Phys. Earth Planet. Interiors, 3, 41, 1970.

Anderson, D. L. and C. Sammis and T. Jordan. Composition and evolution of the mantle and the core, Science, 171, 1103, 1970.

Anderson, D. L. and M. N. Toksoz. Surface waves on a spherical earth, 1, upper mantle structure from Love waves, J.G.R., 68, 3483, 1963.

Archambeau, C. B., E. A. Flinn and D. G. Lambert. Fine structure of the upper mantle, J.G.R., 74, 1969.

Archambeau, C. B. Perturbation theory for the inversion of body wave and travel-time data, Tech. Rept., Earth Sciences Division, Teledyne Industries, Inc., 1966.

Arnold, E. P. Smoothing travel-time tables, B.S.S.A., 58, 1345, 1968.

Backus, G. Inference from inadequate and inaccurate data, Proc. N.A.S., 65, 1, 1970a; 65, 281, 1970b; 67, 282, 1970c.

Backus, G. F. Gilbert. Numerical applications of a formalism for geophysical inverse problems, Geophys. J. R. ast. Soc., 13, 247, 1967.

Backus, G. and F. Gilbert. The resolving power of gross Earth data, Geophys. J.R. ast. Soc., 16, 1968.

Backus, G. and F. Gilbert. Constructing P-velocity models to fit restricted sets of travel-time data, B.S.S.A., 59, 1407, 1969.

Backus, G. and F. Gilbert. Uniqueness in the inversion of inaccurate gross Earth data, Phil. Trans. Roy. Soc. (London), Ser. A, 266, 123, 1970.

Birch, F. The variation of seismic velocities within a simplified Earth model in accordance with the theory of finite strain, B.S.S.A., 29, 463, 1939.

Birch, F. Elasticity and constitution of the earth's interior, J.G.R., 57, 227, 1952.

Birch, F. The velocity of compressional waves in rocks to 10 kilobars, 1, J.G.R., 65, 1083, 1960.

Birch, F. The velocity of compressional waves in rocks to 10 kilobars, 2, J.G.R., 66, 2199, 1961.

Birch, F. Density and composition of mantle and core, J.G.R., 69, 4377, 1964.

Bjerhammar, A. Rectangular reciprocal matrices with special reference to geodetic calculations, Bull. Geodesique, 188, 1951.

Block, B. and R. D. Moore. Tidal to seismic frequency investigations with a quartz accelerometer of new geometry, J.G.R., 75, 1493, 1970.

Bolt, B. A. Travel times of PKP up to 145°, Geophys, J. R. astr. Soc., 2, 190, 1959.

Bolt, B.A. Estimation of PKP travel times, B.S.S.A., 58, 1305, 1968.

Brune, J. N. Surface waves and crustal structure, The Earth's Crust and Upper Mantle, Geophy. Monogr. 13, edited by P. J. Hart, American Geophysical Union, Washington, D. C., 1969.

Buchbinder, G. G. R. Properties of the core- mantle boundary and PcP, B.S.S.A., 55, 441, 1965.

Buchbinder, G. G. R. A velocity structure of the Earth's core, B.S.S.A., 61, 429, 1971.

Bullen, K. E. The variation of density and the ellipticities of strata of equal density within the earth, Mon. Not. R. Astr. Soc., Geophys. Suppl., 3, 395, 1936.

Bullen K. E. The ellipticity correction to travel times of P and S earthquake waves, Mon. Not. R. Astr. Soc., Geophys. Suppl., 4, 143, 1937.

Bullen, K. E. Introduction to the Theory of Seismology, 3rd ed., University Press, Cambridge, 1963.

Cleary, J. R. The S velocity at the core- mantle boundrary from observations of diffracted S, B.S.S.A., 59, 1399, 1969.

Cleary, J. R. and A. L. Hales. PKIKP and S station anomalies, J.G.R., 76, 7249, 1971.

Courant, R. and D. Hilbert. Methods of Mathematical Physics, I, Interscience, New york, 1937.

Dahlen, F. A. The normal modes of a rotating, elliptical Earth, Geophys. J. R. astr. Soc., 16, 329, 1968.

Dahm, C. G. Velocity of P waves in the earth calculated from the Macelwane P curve, 1933, B.S.S.A., 26, 1, 1936.

Davenport, W. B. and W.L. Root. Random Signals and Noise, McGraw-Hill, N.Y., 1958.

Derr, J. S. Free oscillation observations through 1968, B.S.S.A., 59, 2079, 1969.

Dziewonski, A.M. and F. Gilbert. Observations of normal modes from 84 recordings of the Alaskan earthquake of 28 March 1964, Geophys. J. R. Astr. Soc., (in press), 1972.

Dziewonski, A. M. and M. Landisman. Great circle Rayleigh and Love wave dispersion from 100 to 900 seconds, Geophys. J. R. Astr. Soc., 19, 37, 1970.

Doob, J. L. Stochastic Processes, John iley and Sons, New york, 1953.

Dunford, N. and J. schwartz. Linear Operators, Vol. I, Interscience, New York, 1958.

Engdahl, E. R. Core phases and the Earth's core, PhD thesis, Geophysics Dept., St. Louis University, 1968.

Engdahl, E. R. and E. A. Flinn and C. T. Romney, Seismic waves reflected from the Earth's inner core, Nature, 228, 852, 1970.

Franklin, J. N. Well-posed stochastic extensions of the ill-posed linear problems, J. Math. Anal. Appl., 31, 682, 1970.

Freedman, Helen W. Seismological measurements and measurement error, B.S.S.A., 58, 2161, 1968.

Freeman, H. Introduction to Statistical Inference, Addison-Wesley, Reading, 1963.

Gerver, M. L. and V. M. Markushevich. On the characteristic properties of travel-time curves, Geophys. J. R. astr. Soc., 13, 241, 1967.

Gilbert, F. Inverse problems for the Earth's normal modes, in The Nature of the Solid Earth, edited by Eugene C. Robertson, McGraw-Hill, New York, 1972.

Gilbert, F. The diagonal sum rule and average eigenfrequencies, Geophys. J. R. astr. Soc., (in press), 1972.

Gradshteyn, I. and I. Ryzhik. Table of integrals, sums, series and and products, Academic Press, New York and London, 1965.

Gutenberg, B. The boundary of the Earth's inner core, Trans. Am. Geophys. Un., 38, 750, 1957.

Gutenberg, B. and C. F. Richter. On seismic waves, G. Beitr., 43, 56, 1934; 45, 280, 1935; 47, 73, 1936; 54, 94, 1939.

Haddon, R. A. W. Corrugations on the mantle-core boundary or transition layers between inner and outer cores?, Trans. Amer. Geophys. Un., 53, 600, 1972.

Hai, Nguyen. Propogation des ondes longitudinales dans le noyau terrstre, Tome 19, Fascicule 4, 1963.

Hales, A. L. and J. L. Roberts. The travel times of S and SKS, B.S.S.A., 60, 461, 1970a.

Hales, A. L. and J. L. Roberts. Shear velocities in the lower mantle and the radius of the core, B.S.S.A., 60, 1427, 1970b.

Hales, A. L. and J. L. Roberts. The velocities in the outer core, B.S.S.A., 61, 1051, 1971.

Herglotz, G. Phys. Z., 8, 145, 1907.

Herrin, E. (chairman) 1968 Seismological tables for P phases, B.S.S.A., 58, 1193, 1968.

Herrin, E. and J. Taggart. Regional variations in P travel times, B.S.S.A., 58, 1325, 1968.

Hide, R. Free hydromagnetic oscillations of the Earth's core and the theory of the geomagnetic secular variation, Phil. Trans.Roy. Soc. (London), Ser. A259, 615, 1966.

Hide, R. and K. Horai. On the topography of the core-mantle interface, Phys. Earth Planet. Interiors, 1, 305.

Jackson, D. Inversion of inaccurate and insufficient data, Geophys. J. R. astr. Soc., (in press), 1972.

Jacob, K. H. Global tectonic implications of anomalous seismic P travel times from the nuclear explosion Longshot, J.G.R., 77, 2556, 1972.

Jeffreys, H. Travel times for Pacific explosions, Geophys. J. R. astr. Soc., 7, 212, 1962.

Jeffreys, Sir Harold, The Earth, 5th edition, Cambridge University Press, Cambridge, 1970.

Johnson, L. R. Array measurements of P velocities in the upper mantle, J. G. R., 72, 6309, 1967.

Johnson, L. R. Array measurements of P velocities in the lower mantle, J. G. R., 59, 973, 1969.

Johnson, L. E. Inversion and inference for teleseismic ray data, PhD thesis, U. C. S. D., 1971.

Jordan, T. H. and J. N. Franklin. Optimal solutions to a linear inverse problem in Geophysics, Proc. Nat. Acad. Sci., 68, 291, 1971.

Jordan T. H. and J. B. Minster. Applications of a stochastic inverse to the geophysical inverse problem, in The Mathematics of Profile Inversion, edited by Lawrence Colin, Marcell Dekker Inc., New York, (in press), 1972.

Julian, B. R. and D. L. Anderson. Travel times, apparent velocities, and amplitudes of body waves, B. S. S. A., 58, 339, 1968.

Julian, B. R. and R. M. Sheppard. PKJKP, Nature (in press), 1972.

Kanamori, H. Spectrum of P and PcP in relation to the mantle-core boundary and attenuation in the mantle, J.G.R., 72, 559, 1967.

Kanamori, H. Travel times to Japanese stations from Longshot, Bull. Earth. Res. Inst., 46, 811, 1968.

Kogan, S. D. Travel times of longitudinal and transverse waves calculated from data on nuclear explosions made in the region of the Marshall Islands, Izv. Geophys. Ser., 371, 1960.

Keilis-Borok, V.I. and T. B. Yanovskaya. Inverse problems of seismology, Geophys. J. R. astr. Soc., 13, 223, 1967.

Lambert, D.G., D.H. von Seggen, S.S. Alexander, and G.A. Galat shot Experiment, Vol. 1, Seismic Data Laboratory Rept.No.234, Alexandria, Va., 1968.

Lanczos, C. Linear differential operators, D. Van Nostrand, London, 1961.

Loeve, M. Probability Theory, D. Van Nostrand, Princeton, 1955.

McGinley, John, PhD thesis, California Institute of Technology, 1968.

Mitronovas and Isacks. Seismic velocity anomalies in the upper mantle beneath the Tonga-Kermadec island arc, J. G. R., 76, 7154,1971.

Moore, E. H. Bull. Amer. Math. Soc., 26, 394, 1920.

Morse, P.M. and H. Feshback. Methods Of Theoretical Physics, vol. I, McGraw-Hill, N.Y., 1953.

Niazi, M. and D.L. Anderson. Upper mantle structure of western North America from apparent velocities of P waves, J.G.R., 70, 4633,1965.

Nuttli, O. Seismological evidence pertaining to the structure of the Earth's upper mantle, Rev. of Geophys., 1, 351, 19 3.

Pekeris, C. L. The internal constitution of the Earth, Geophy. J. R. astr. Soc., 11, 85, 1966.

Penrose, R. A generalized inverse for matrices, Proc. Camb. Phil. Soc., 51, 406, 1955.

Phinney, R. A. and S.S. Alexander. P wave diffraction theory and the structure of the core-mantle boundary, J. G. R., 71, 5959, 1966.

Press, F. Earth models obtained by Monte Carlo inversion, J.G.R., 73, 5223, 1968.

Press, F. Earth models consistent with geophysical data, Phys. Earth Planet. Interiors, 3, 3, 1970.

Press, F. The Earth's interior as inferred from a family of models, in The Nature of the Solid Earth, edited by Eugene C. Robertson, McGraw-Hill, New York, 1972.

Slichter, L. B. The theory of the interpretation of seismic travel-times curve in horizontal structures, Physics, 3, 273, 1932.

Sorrells, G. G. and J. B. Crowley and K. F. Veith. Methods for computing ray paths in complex geological structures, B.S.S.A., 61, 27, 1971.

Strand, O. N. and E. R. Westwater, Statistical estimation of the numerical solution of the Fredholm integral equation of the first kind, J. Assoc. Comp. Mach., 15, 100, 1968.

Subiza, . and M. Båth. Geophys. J. R. astr. Soc., 8, 496, 1964.

Tseng, Ya. Yu. Generalized inverses of unbounded operators between two unitary spaces, Doklady Akad. Nank S.S.S.R., 67, 431, 1949.

Twomey, S. On the numerical solution of Fredholm integral equations of the first kind by the inversion of the linear system produced by quadrature, J. Assoc. Comp. Mach., 10, 79, 1963.

Witcomb, J. H. and D. L. Anderson. Reflection of P'P' seismic waves from dicontinuities in the mantle, J.G.R,,75, S713, 1970.

Wiechert, E. Phys. Z., 11, 294, 1910.

Wiener, N. Time Series, M.I.T., Cambridge, 1949.

Wiggins, R. The general linear inverse problem: implications of surface waves and free oscillations for the earth's structure, Rev. of Geophys. and Space Phys., 10, p.251, 1972.

Williamson, E. D. and L. H. Adams. Density distribution in the Earth, J. Washington Acad. Science, 13, 413, 1923.

APPENDICES

Appendix 1

A1.1 Ray-theoretical travel times in a spherically symmetric body.

Suppose that in a sphere $S(R)$ of radius R a signal propogates along a ray with parameter p at a velocity $v_0(r)$ that varies with radius only. Let $P_0 = (r_0, \Omega_0)$ be the position of the source and $P_s = (r_s, \Omega_s)$ be the position of the station, where $r_0, r_s \in [0,R]$ and $\Omega_0, \Omega_s \in \partial S(1)$, the surface of $S(1)$. The ray-theoretical travel time of this signal is

$$T_0 = \int_{P_0}^{P_s} \frac{ds}{v_0}, \tag{A1.1.1}$$

where ds is a differential element of arc length along the ray path between P_0 and P_s. Fermat's principle states that the permissible paths are those for which T_0 is stationary with respect to path variations.

The travel time T_0 depends on v_0, P_0, and P_s. We assume that the station is located on $\partial S(R)$, the surface of $S(R)$, so that $r_s = R$. Then, because the velocities are spherically symmetric, T_0 depends only on v_0, Δ, and h, where Δ is the angular distance between the source and receiver, and h is the focal depth. Δ and h are assumed to be fixed, and dependence of T_0 on these quantities will usually be suppressed.

Spherical symmetry implies there exists a function $K(r)$, $r \in [0,R]$, such that

$$T_0 = \int_0^R \frac{K(r)}{v_0(r)}\, dr. \tag{A1.1.2}$$

Because s(r) is a multi-valued function, the kernel K(r) is the sum of n+1 terms, n being the number of turning points of the ray generalized to include reflections from and transmissions through discontinuities:

$$\text{(A1.1.3)} \qquad K(r) = \sum_{i=1}^{n+1} \left| \frac{ds_i}{dr}(r) \right| .$$

The function $s_i(r)$ represents arc length along the ith ray segment and is single-valued. From Bullen [1963],

$$\text{(A1.1.4)} \qquad \left| \frac{ds_i}{dr}(r) \right| = \frac{\eta(r)}{(\eta^2(r)-p^2)^{1/2}} \; H[\varepsilon_i(r-\rho_{i-1})] \; H[\varepsilon_i(\rho_i - r)] .$$

Here $\eta(r) = r/v_0(r)$, ρ_i is the ith turning radius ($\rho_0 \equiv r_0 = R-h$, $\rho_{n+1} \equiv r_s = R$), $H[\sim]$ is the Heaviside function, and ε_i equals either +1 or -1 depending on whether the direction of propogation is upward or downward.

The path of the ray can be traced in the following manner. Let $\Pi_{i-1} \equiv (\rho_{i-1}, \Omega_{i-1})$ be the position vector of the (i-1)th turning point. Then the position vector along the ith ray segment, $P_i(r) \equiv (r, \Omega_i(r))$, satisfies the following vector and scalar relationships:

$$\text{(A1.1.5)} \qquad \begin{aligned} P_i(r) \cdot P_0 \times P_s &= 0, \\ P_i(r) \cdot \Pi_{i-1} &= r\, \rho_{i-1} \cos \gamma_i(r), \\ \gamma_i(r) &= \int_{\rho_{i-1}}^{r} \frac{\varepsilon_i\, p}{r'(\eta^2(r')-p^2)^{1/2}}\, dr', \\ \varepsilon_i\, \rho_{i-1} \le \varepsilon_i\, &r \le \varepsilon_i\, \rho_i . \end{aligned}$$

The first equation states that the ray path lies in the plane defined by the source, the station, and the origin of coordinates; the second defines $\gamma_i(r)$, and the third is from Bullen [1963].

A1.2 <u>The Fréchet kernel for travel times</u>. If the velocity distribution in S(R) is varied from $v_0(r)$ by an amount $\delta v(r,\Omega)$, then Fermat's principle implies that the perturbation in the travel time, to first order in δv, is equal to an integral of the velocity perturbation along the ray path [Archambeau and Flinn, 1966; Backus and Gilbert, 1969]:

$$\delta T = \int_{P_0}^{P_s} \frac{-\delta v}{v_0^2}\, ds. \tag{A1.2.1}$$

This expression can be written as an integral over (r,Ω):

$$\delta T(P_0,P_s) = \int_0^R \int_{\partial S(1)} a(P_0,P_s;r,\Omega)\, \delta v(r,\Omega)\, d\Omega\, dr. \tag{A1.2.2}$$

The function $a(P_0,P_s;r,\Omega)$ is the Fréchet kernel for the three-dimensional perturbation problem and is given by

$$a(P_0,P_s;r,\Omega) = \sum_{i=1}^{n+1} -v_0^{-2}(r) \left|\frac{ds_i}{dr}(r)\right| \delta[\Omega - \Omega_i(r)]. \tag{A1.2.3}$$

Here $\delta[\sim]$ is the Dirac delta distribution on $\partial S(1)$, and $\Omega_i(r)$ is determined by (A1.1.5). If the velocity perturbations are spherically symmetric, the equation (A1.2.2) can be written

$$\delta T = \int_0^R a(r)\, \delta v(r)\, dr , \tag{A1.2.4}$$

where

$$a(r) = \int_{\partial S(1)} a(P_0,P_s;r,\Omega)\, d\Omega \tag{A1.2.5}$$

is the spherically symmetric Fréchet kernel for travel times.

A1.3 <u>Proof of the averaging theorem for travel times</u>. In §3.4 we stated a simple averaging theorem for travel times. Its proof is a simple matter. Without loss of generality assume that all sources and receivers are located on the surface $\partial S(R)$. To first order, the travel time $T(P_0,P_s)$ between a source located at P_0 and a station located at P_s can be written as the sum of two terms:

$$T = T_0 + \delta T. \tag{A1.3.1}$$

The first term on the right-hand side of this expression is the travel time through the spherically symmetric Terrestrial Monopole, defined by equation (3.2.1). The second term is the first-order perturbation in the travel time due to an aspherical perturbation δv in the velocity. The first term depends only on the angular distance Δ separating the source and receiver, while the second term depends only on P_0, Δ, and the azimuth ζ from P_0 to P_s.

The hypothesis of the existence of uniform distributions of sources and receivers implies that the probability that a source lies in the region $d\Omega_0$ about the point P_0 and that, for a fixed Δ, a receiver lies between the azimuths ζ and $\zeta + d\zeta$ is constant. The averaging theorem is proved if we can show that the mean fluctuation $\overline{\delta T}$ is zero. Because the distributions are uniform, we have

$$\overline{\delta T} \propto \int_{S(1)} \int_0^{2\pi} \delta T(\Omega_0,\zeta)\, d\zeta\, d\Omega_0 , \tag{A1.3.2}$$

where $\delta T(\Omega_0,\zeta)$ is given by equation (A1.2.2). Equation (A1.2.2) can be integrated immediately with respect to Ω. This yields

(A1.3.3) $$\delta T(\Omega_0,\zeta) = \int_0^R \sum_{i=1}^{n+1} a_i(r)\ \delta v(r,\Omega_i)\ dr,$$

where $a_i(r) \equiv -v_0^{-2}(r)\ |ds_i(r)/dr|$. In equation (A1.3.3) Ω_i will depend on r, Ω_0, and ζ through the relations (A1.1.5).

Now, we substitute (A1.3.3) into (A1.3.2) and interchange the order of integration. We obtain that $\overline{\delta T}$ is proportional to

(A1.3.4) $$\int_0^R \sum_{i=1}^{n+1} a_i(r) \int_{S(1)} \int_0^{2\pi} \delta v(r,\Omega_i)\ d\zeta\ d\Omega_0\ dr.$$

At any specified radius r, the locus of the intersection of S(r) and the ith ray segment describes, for fixed Ω_0 as ζ is varied, a circle on S(r). These circles cover S(r) uniformly, and, therefore,

(A1.3.5) $$\int_{S(1)} \int_0^{2\pi} \delta v(r,\Omega_i)\ d\zeta\ d\Omega_0 \propto \int_{S(1)} \delta v(r,\Omega)\ d\Omega.$$

By definition, however, aspherical perturbations average to zero when integrated over the sphere. Thus, the integral on the right-hand side of (A1.3.5) is zero, implying that $\overline{\delta T}$ is zero. This proves the averaging theorem.

Appendix 2

A2.1 PcP-P differential travel-time data [nuclear explosions].

EVENT	STATION	Δ (deg.)	TIME (sec.)	OBS-JB (sec.)
KOGAN (S. PACIFIC)				
(h = 0 km)	UGL	42.05	114.7	-0.8
	TEM	46.68	92.8	-1.3
	TEM	46.72	93.4	-0.5
	TEM	46.90	89.7	-3.5
	KAB	61.75	40.7	+0.4
	COL	62.10	40.0	+0.2
	IRK	63.20	37.2	+0.1
	SEM	77.88	10.5	-0.5
BUCHBINDER (BILBY)				
(h = 0 km)	AAM	25.36	213.3	-0.3
	ATL	26.06	207.5	-1.0
	LND	27.19	200.8	+0.0
	BL-	27.48	198.6	-0.3
	BLA	28.28	192.6	-1.0
	CSC	28.57	191.4	-0.4
	BR-	29.11	188.0	-0.2
	SCP	29.75	184.3	+0.3
	OTT	31.17	175.5	+0.3
	DH-	31.86	171.0	+0.1
	COL	33.61	159.8	-0.8
	HN-	36.56	143.3	-0.6
	HW-	38.48	133.5	-0.2
	RES	39.03	130.9	+0.2
	MBC	39.30	128.1	-1.3
	NP-	39.32	128.0	-1.3
	BHP	43.24	107.9	-1.9
	SJG	47.36	90.4	-0.9
	ALE	48.90	84.3	-0.6
	CAR	51.40	73.7	-1.2
	TRN	55.56	62.0	+2.2
	KON	73.71	17.1	+1.0
KANAMORI (LONGSHOT)				
(h = 0 km)	TSK	31.61	171.3	-1.1
	MAT	32.56	165.5	-1.1
	MYK	35.27	149.3	-1.4
	SHK	37.28	138.8	-1.1
	SEO	38.91	129.8	-1.5

EVENT	STATION	Δ (deg.)	TIME (sec.)	OBS-JB (sec.)
LAMBERT ET.AL.(LONGSHOT)				
(h = 0 km)	WH-	26.60	204.0	-0.8
	WL-	29.80	181.9	-4.6
	MTJ	31.60	171.5	-1.1
	SI-	31.80	168.7	-0.6
	MAT	32.60	165.7	-1.2
	PHC	32.90	151.9	-2.6
	FL-	33.00	163.9	-0.1
	MBC	34.00	155.6	-2.5
	NP-	34.00	156.1	-2.0
	PG-	34.50	156.2	+1.0
	KIP	34.80	152.2	-1.8
	HON	34.90	151.0	-2.5
	CMC	35.00	150.8	-1.8
	YKA	36.10	145.9	-0.8
	VIC	36.20	144.7	-1.3
	YKC	36.20	145.3	-1.2
	KV-	36.40	145.0	-0.2
	TUM	37.20	140.5	-0.2
	SHK	37.30	139.2	-1.5
	JP-	37.40	138.8	-0.3
	HIL	37.60	137.5	-1.9
	PAH	37.80	136.2	-1.6
	LON	38.00	135.7	-0.7
	PNT	38.10	135.2	-0.8
	COR	38.20	134.4	-1.1
	SEO	38.90	129.5	-2.4
	RM6	39.40	132.1	+2.2
	EDM	39.90	127.4	+0.9
	LD6	39.90	129.0	+2.5
	YR-	40.10	123.2	-1.7
	BMO	41.70	116.5	-0.4
	HHM	41.80	116.6	+0.2
	ORV	42.10	113.8	-0.9
	BA6	42.50	112.1	-1.3
	BKS	42.70	111.5	-0.9
	BRK	42.70	112.5	-0.3
	SW-	42.70	112.3	-0.4
	ALE	42.80	109.7	-2.4
	PCC	42.80	111.1	-0.1
	NRR	43.10	109.2	-1.2
	BLC	43.40	111.1	+1.8
	GCC	43.40	108.5	-1.1
	MHC	43.40	108.3	-0.6
	UNN	43.70	106.6	-1.1

EVENT	STATION	Δ (deg.)	TIME (sec.)	OBS-JB (sec.)
LAMBERT ET.AL.(LONGSHOT, CONT.)				
	JAS	43.80	106.3	-0.9
	HL2	44.10	105.7	+0.7
	HV-	44.20	106.8	+1.6
	PRS	44.20	104.4	-1.1
	SH6	44.20	104.8	-1.0
	LLA	44.30	103.8	-1.4
	BOZ	44.60	103.6	+0.3
	PRI	44.80	102.0	-1.1
	MN-	44.90	99.7	-2.7
	CH6	45.20	100.3	-0.9
	FFC	45.20	101.7	+0.1
	EUR	45.60	97.8	-1.2
	TIN	45.70	97.4	-1.2
	TNP	45.70	97.5	-1.1
	TF-	45.80	97.0	-1.0
	KRC	45.90	96.7	-1.4
	WU6	46.00	96.8	+0.1
	ISA	46.40	94.6	-0.7
	SBC	46.40	93.9	-1.4
	PI6	46.60	97.0	+2.1
	FTC	46.70	93.9	-0.7
	CLC	46.90	92.8	-1.0
	LAO	47.10	92.2	-0.2
	MWC	47.60	90.3	+0.3
	PAS	47.60	89.0	-1.3
	GSC	47.70	89.6	-0.2
	RVR	48.20	88.6	+0.8
	BCN	48.60	85.9	-1.2
	IRF	48.60	84.8	-1.6
	FGU	48.70	86.0	+0.4
	PLM	48.90	84.0	-0.6
	UBO	49.00	84.0	-0.8
	KN-	49.10	83.4	-1.0
	BAR	49.50	82.2	-0.1
	HAY	49.50	83.3	+0.7
	RG-	49.60	83.6	+1.6
	CP-	49.70	81.7	+0.1
	GCA	49.80	81.0	+0.5
	RCD	50.40	79.2	+1.0
	RK-	51.50	75.9	+1.0
	LAR	50.70	77.9	-2.8
	PA6	51.80	73.3	-0.3
	TA6	51.80	73.2	-0.1
	TFO	51.80	72.8	-0.6

EVENT	STATION	Δ (deg.)	TIME (sec.)	OBS-JB (sec.)
LAMBERT ET.AL.(LONGSHOT, CONT.)				
	GOL	51.90	72.8	-0.4
	SA6	51.90	72.8	-0.7
	WN-	52.60	70.6	+0.7
	TUC	53.40	67.7	+0.9
	TRG	53.90	66.1	+0.5
	ALQ	54.30	64.5	+0.9
	GWC	56.00	57.8	-0.4
	LC-	56.00	56.9	-1.8
	MHT	57.30	55.2	+1.0
	HKC	57.40	54.0	-0.5
	WW6	57.40	54.6	+0.9
	BAG	57.90	52.5	-0.3
	LUB	58.00	53.1	+0.7
	MAN	58.90	48.2	-3.6
	WMO	59.20	48.8	+0.2
	SV3	60.80	44.6	+0.4
	ROL	60.90	47.0	+2.2
	GV-	61.40	42.2	+0.0
	JCT	61.40	41.3	-0.9
	DAL	61.60	41.8	-0.2
	AAM	62.30	42.3	+2.4
	DAV	62.30	40.3	+0.3
	EN-	62.30	42.3	+2.7
	KJN	62.70	40.2	+1.2
	LRA	62.80	38.0	-0.6
	LND	63.00	37.4	-0.6
	MLF	64.20	32.9	-2.0
	SJ-	64.40	33.3	-1.3
	CPO	66.10	27.4	-3.1
	SCP	66.40	30.8	+0.8
	PMG	66.60	28.6	-0.8
	DH-	66.70	32.3	+3.6
	HN-	66.90	30.0	+1.6
	FN-	67.20	29.3	+1.4
	BLA	67.70	28.2	+1.5
	SFO	67.80	27.1	+0.8
	NHA	68.10	26.9	-4.4
	PAL	68.20	28.7	+2.6
	ATL	68.40	29.3	+3.5
	UDD	68.40	24.5	-2.4
	STJ	71.80	15.5	-3.7
	BE-	73.10	15.5	-2.4
	RAR	74.70	14.0	-1.0
	DOU	78.70	4.4	-4.8

A2.2 PcP-P differential travel-time data [deep-focus events].

EVENT	STATION	Δ (deg.)	TIME (sec.)	OBS-JB (sec.)	QUAL.
MINDINAO					
(h = 605 km)	CHG	26.51	181.9	-2.2	1
PERU-BRAZIL A					
(h = 587 km)	BEC	41.67	102.9	-0.1	4
	SOM	43.64	92.0	-2.3	4
	ATL	44.01	92.4	-0.3	5
	BLA	46.79	80.6	-0.7	4
	GEO	47.99	76.9	+0.3	4
	DAL	48.20	75.2	-0.2	5
	OGD	49.94	96.4	0.0	4
	SCP	49.96	69.4	+0.1	4
	WES	51.17	65.0	0.0	4
	LUB	51.37	64.6	+0.2	5
	AAM	52.32	61.2	+0.1	4
	ALQ	54.93	53.2	+0.4	5
	GOL	57.85	44.2	-0.1	4
	RCD	60.24	36.5	-1.6	4
	GSC	61.53	34.1	-0.8	4
	DUG	62.20	32.5	-0.8	4
	BOZ	65.31	25.2	-1.3	3
	BKS	66.58	23.1	-1.0	4
	COR	71.00	15.4	-1.1	2
FIJI B					
(h = 627 km)	CTA	32.37	147.2	-1.3	3
	RAB	32.49	147.5	-0.3	5
	PGM	34.42	136.8	-0.6	4
	GUA	49.24	70.2	-0.8	3
	MUN	58.14	41.5	-1.4	2
	DAV	61.01	35.9	+0.4	4
	MAN	68.55	19.8	-0.3	3
	BAG	69.84	14.1	-3.8	1
ARGENTINA					
(h = 571 km)	BOG	32.33	150.4	-0.6	3
	SJG	44.01	93.7	+0.5	3
	LPS	47.50	77.1	-1.8	2
	ATL	62.54	31.8	-1.0	1
	SPA	64.09	63.0	+0.3	4
	BLA	65.03	24.4	-2.9	2
	SOB	71.22	15.7	-0.5	4
	WIN	71.97	15.3	+0.2	3
	SBA	72.30	14.4	-0.2	1

EVENT	STATION	Δ (deg.)	TIME (sec.)	OBS-JB (sec.)	QUAL.
PERU-BRAZIL B					
(h = 598 km)	SJG	27.47	173.9	-4.6	1
	BEC	41.68	101.8	-0.8	2
	SHA	42.68	98.3	+0.1	4
	SOM	43.63	93.1	-0.9	3
	ATL	44.01	91.9	-0.5	4
	BLA	46.79	80.2	-0.8	4
	JCT	47.87	76.4	-0.4	4
	GEO	48.00	76.5	+0.2	4
	OGD	49.95	69.1	0.0	5
	WES	51.18	64.7	-0.1	5
	LUB	51.37	64.1	0.0	5
	AAM	52.32	61.0	+0.1	5
	ALQ	54.92	53.1	+0.5	5
	TUC	55.75	50.1	0.0	5
	GOL	57.85	43.6	-0.6	5
	GSC	61.53	33.6	-1.1	5
	DUG	62.19	31.4	-1.8	3
	BOZ	65.31	24.8	-1.6	4
	COR	71.00	15.0	-1.4	3
JAVA SEA A					
(h = 606 km)	CHG	27.94	174.8	-0.4	1
	ANP	32.26	146.0	-4.0	1
	CTA	35.79	131.2	+0.2	2
	GUA	37.73	117.5	-3.6	2
	RIV	45.36	85.9	-0.6	2
	TAU	47.99	76.0	-0.2	2
	MAT	48.78	72.7	-0.5	3
	WEL	65.47	24.7	-1.3	3
FIJI C					
(h = 643 km)	TAU	35.44	129.0	-2.4	2
	GUA	49.15	70.8	-0.1	1
	MUN	58.04	43.2	+0.3	4
CHINA					
(h = 555 km)	CHG	35.63	130.2	-3.4	4
MARIANAS					
(h = 602 km)	HKC	29.28	166.3	-1.0	4
	SNG	44.79	87.2	-1.8	2
	SHL	49.62	70.1	-0.1	2
	COL	63.59	30.2	+0.2	2
	NIL	65.17	24.5	-2.2	4

EVENT	STATION	Δ (deg.)	TIME (sec.)	OBS-JB (sec.)	QUAL.
SEA OF OKHOTSK					
	ANP	35.21	130.9	-4.1	4
	BAG	43.23	92.6	-3.7	3
	NOR	46.30	83.6	+0.2	2
	KBS	46.95	80.2	-0.7	3
	KEV	51.85	62.3	-0.6	3
	CHG	52.56	59.9	-0.6	3
	RAB	56.18	47.9	-1.3	1
	KTG	57.61	44.6	-0.5	3
	UME	58.23	42.1	-1.2	5
	NDI	58.43	42.6	-0.3	5
	BKS	59.17	34.4	-4.5	3
	NUR	59.83	38.1	-1.1	4
	SNG	61.06	34.1	-2.3	4
	PMG	61.47	34.1	-1.0	3
	AKU	62.18	32.3	-0.2	2
	DUG	62.67	32.7	+0.4	2
	QUE	63.52	28.8	-1.6	2
	GOL	66.88	23.2	-0.4	2
	POO	67.98	20.7	-0.9	3
	TUC	69.62	18.3	-0.4	2

A2.3 ScS-S differential travel-times [deep-focus events].

EVENT	STATION	Δ (deg.)	TIME (sec.)	OBS-JB (sec.)	QUAL.
FIJI A					
(h = 535 km)	RIV	31.30	307.0	+9.0	4
	CTA	33.18	287.2	+8.2	3
	ADE	41.44	211.0	+6.6	3
	KIP	43.57	182.8	-4.6	2
	GUA	47.55	161.3	+3.4	4
	MUN	59.91	89.1	+5.8	5
	DAV	60.33	89.0	+7.8	3
	BAG	68.80	50.3	+5.3	2
	LEM	72.44	32.3	-0.7	3
	SEO	75.14	30.2	+4.8	4
	BKS	76.69	19.5	-2.0	2
NEW HEBRIDES					
(h = 641 km)	RIV	26.72	345.6	+7.3	5
	TAU	35.42	257.3	+7.5	4
	ADE	35.66	251.7	+4.2	3
	GUA	36.76	236.7	-0.9	2
	MUN	52.65	120.5	+1.1	4
	BAG	57.40	95.5	+3.0	3
	LEM	61.92	75.0	+4.8	4
	SEO	65.03	61.8	+5.0	1
	HKC	65.48	55.9	+0.9	2
	CHG	77.22	13.9	-4.7	4
MINDINAO					
(h = 605 km)	SEO	29.93	310.5	+3.6	4
	SHL	35.22	254.0	-0.3	3
	CTA	35.34	258.4	+5.2	3
PERU-BRAZIL A					
(h = 587 km)	SJG	27.45	342.6	+7.6	2
	LPS	29.16	321.8	+5.3	3
	SOM	43.64	182.4	-1.7	4
	ATL	44.01	183.2	+2.0	5
	DAL	48.20	150.7	-0.1	3
	OGD	49.94	132.6	-6.5	5
	SCP	49.96	132.5	-6.5	2
	WES	51.17	133.9	+2.8	3
	LUB	51.37	130.2	+0.4	3
	AAM	52.32	125.8	+1.9	4
	ALQ	54.93	108.7	+0.4	4
	GOL	57.85	90.9	-1.3	4
	RCD	60.24	36.5	-2.0	3

EVENT	STATION	Δ (deg.)	TIME (sec.)	OBS-JB (sec.)	QUAL.
PERU-BRAZIL A (CONT.)					
	GSC	61.53	71.1	+2.7	4
	COR	71.00	37.3	+0.8	4
	PTO	76.13	20.4	-1.6	3
	TOL	78.81	16.6	+0.6	3
	SDB	82.82	12.5	+3.6	1
FIJI B					
(h = 627 km)	RIV	29.18	319.1	+7.2	3
	CTA	32.37	285.0	+4.9	4
	RAB	32.47	285.0	+5.9	4
	ADE	39.44	219.0	+3.7	3
	KIP	46.57	164.2	+4.0	4
	GUA	49.24	137.5	+4.3	3
	MUN	58.14	90.5	+1.4	5
	MAN	68.55	47.3	+3.5	4
	BAG	69.84	38.4	-1.0	1
	ANP	73.68	34.6	+6.9	2
	COR	82.78	9.9	+1.1	3
	TUC	84.13	14.6	+7.6	1
	LON	84.94	14.1	+8.0	1
ARGENTINA					
(h = 571 km)	SOM	27.09	342.0	+1.7	3
	BOG	32.33	287.7	+2.8	5
	GIE	36.40	246.5	+0.7	5
	BHP	38.35	231.5	+3.2	4
	LPS	47.50	156.7	+0.2	3
	BEC	58.13	94.6	+3.3	3
	ATL	62.54	72.8	+3.2	5
	SPA	64.09	63.0	+0.3	4
	BLA	65.03	59.1	+0.3	5
	OXF	65.23	60.7	+2.8	5
	GEO	65.94	55.3	+0.3	5
	JCT	66.33	56.7	+3.2	5
	OGD	67.64	48.0	-0.5	4
	SCP	67.94	45.8	-1.5	4
	WES	68.53	46.0	+0.8	3
	FLO	69.41	46.1	+4.0	5
	LUB	69.87	44.3	+3.8	5
	AAM	70.64	39.7	+1.7	5
	SDB	71.22	36.5	+0.4	3
	SBA	72.30	33.4	+0.7	2
	TUC	73.77	30.6	+2.1	4
	GOL	76.42	22.5	+0.9	5
	GSC	79.44	14.7	-0.3	4

EVENT	STATION	Δ (deg.)	TIME (sec.)	OBS-JB (sec.)	QUAL.
PERU-BRAZIL B					
(h = 598 km)	STG	27.47	343.1	-3.5	3
	BEC	41.68	202.2	+3.4	1
	SHA	42.68	191.6	+0.7	2
	SOM	43.63	181.8	-1.7	5
	ATL	44.01	182.6	+2.0	4
	BLA	46.79	161.0	+0.8	5
	JCT	47.87	152.7	+0.1	4
	GEO	48.00	146.1	-5.6	2
	OGD	49.95	131.8	-6.7	4
	WES	51.18	133.8	+3.3	4
	AAM	52.32	123.3	+2.9	4
	ALQ	54.92	109.1	+1.2	2
	TUC	55.75	107.8	+4.6	3
	GOL	57.85	90.4	-1.3	4
	GSC	61.53	73.0	-0.4	2
	DUG	62.19	72.7	+2.3	3
	BOZ	65.31	60.4	+3.5	2
	BKS	66.58	54.3	+2.5	1
	COR	71.00	36.4	+0.1	3
	LON	71.40	34.4	-0.6	1
	PTO	76.15	21.2	-0.6	2
	TOL	78.83	14.9	-0.9	3
	VAL	80.04	10.5	-3.0	1
JAVA SEA A					
(h = 606 km)	CHG	27.94	330.3	+2.3	3
	ANP	32.26	282.1	-0.8	2
	PMG	34.66	264.4	+4.9	4
	CTA	35.79	250.6	+1.7	5
	SHL	37.14	234.8	+1.0	3
	GUA	37.73	235.0	+3.5	3
	SHK	44.66	175.5	+0.2	3
	RIV	45.36	169.9	-0.2	3
	TAU	47.99	152.0	+0.7	3
	NDI	48.31	153.4	+4.3	4
	MSH	64.82	63.7	+5.0	4
	WEL	65.47	56.9	+0.9	2
	AAE	74.83	26.6	+1.6	3
	AFI	74.92	33.3	+9.5	2
	NAI	75.47	25.0	+1.6	5
	SBA	77.05	17.8	-1.8	3

EVENT	STATION	Δ (deg.)	TIME (sec.)	OBS-JB (sec.)	QUAL.
FIJI C					
(h = 643 km)	TAU	35.44	253.3	+3.9	5
	KIP	46.62	163.9	+5.0	5
	GUA	49.15	144.6	+3.1	4
	MUN	58.04	90.4	+1.4	5
	SHK	71.66	33.9	+0.6	4
	LEM	71.84	33.0	+0.3	2
	ANP	73.59	26.2	-1.5	4
	COR	82.85	8.9	+0.2	2
CHINA					
(h = 555 km)	BAG	27.00	343.7	+1.1	4
	DAV	35.09	260.0	+0.9	4
	COL	49.38	143.9	-0.4	1
	LEM	53.05	119.5	-1.3	1
	PMG	53.29	121.5	+2.2	3
	MSH	54.13	114.4	+0.2	4
	TAB	62.29	72.4	+1.2	3
	SHI	62.72	69.4	+0.1	5
	IST	71.36	36.6	+0.6	1
	HLW	77.14	16.2	-4.0	4
MARIANAS					
(h = 602 km)	CHG	43.69	185.2	+2.2	5
	SNG	44.79	175.5	+1.0	3
	SHL	49.62	141.0	+0.5	5
	KIP	52.37	120.7	-2.2	2
	COL	63.59	64.8	+0.8	3
	NIL	65.17	54.3	-3.0	3
	KOD	65.82	57.4	+2.7	5
	MSH	75.79	27.2	+4.6	2
	COR	78.23	17.9	+0.9	4
	LON	78.69	15.2	-0.9	2
	BKS	80.78	9.3	-2.8	1
	SHI	83.28	6.6	-1.6	4
SEA OF OKHOTSK					
(h = 580 km)	COL	32.77	280.1	+0.3	4
	ANP	35.21	256.6	+0.4	3
	HKC	41.30	204.4	+1.4	3
	MAN	44.56	177.7	+0.2	5
	NOR	46.30	167.3	+2.7	4
	KBS	46.95	162.1	+2.1	5
	KIP	48.92	148.6	+2.3	3
	DAV	49.73	140.7	-0.1	4

EVENT	STATION	Δ (deg.)	TIME (sec.)	OBS-JB (sec.)	QUAL.
SEA OF OKHOTSK (CONT.)					
	KEV	51.85	128.2	+1.1	5
	CHG	52.56	121.0	-1.7	3
	LON	53.42	118.1	+0.7	4
	COR	54.03	119.3	+5.5	3
	RAB	56.18	99.2	-2.3	3
	NIL	57.31	94.0	-1.3	4
	GDH	57.49	97.3	+3.0	5
	KTG	57.61	94.6	+0.9	4
	UME	58.23	90.2	-0.2	5
	NDI	58.43	89.8	+0.4	5
	BKS	59.17	85.9	+0.3	3
	NUR	59.83	32.0	-0.2	4
	SNG	61.06	73.9	-2.3	4
	PMG	61.47	73.4	-0.9	2
	HNR	61.82	74.5	+1.8	4
	AKU	62.18	72.3	+1.3	3
	DUG	62.67	70.8	+2.1	2
	QUE	63.52	67.5	+2.5	4
	GSC	64.05	64.7	+2.0	3
	KON	64.32	60.1	-1.4	5
	GOL	66.88	55.6	+4.5	2
	TAB	69.05	42.4	-0.7	4
	TUC	69.62	45.0	+3.8	2
	SHI	72.26	31.3	-1.4	3
	AFI	73.13	31.3	+1.2	3
	STU	74.36	26.8	+0.1	4
	VAL	74.40	24.5	-2.1	2
	AAM	74.52	27.9	+1.6	4
	IST	74.57	26.9	+0.8	5
	FLO	74.67	29.2	+3.4	3
	TRI	75.97	23.7	+1.2	5
	SCP	77.98	20.1	+2.2	3
	OXF	78.66	18.4	+2.0	5
	OGD	78.90	16.0	-0.5	1
	ATU	79.31	16.0	+0.9	3
	BLA	80.17	12.8	-0.6	4
	ATL	81.81	13.5	+3.0	3
	SHA	82.44	9.4	-0.1	2

A2.4 P'(AB)-P'(DF) differential travel-time data [deep-focus events].

EVENT	STATION	Δ (deg.)	TIME (sec.)	OBS-JB (sec.)
HAI				
(h = 600 km)	CLL	145.40	3.2	-1.7
	JEN	146.00	3.4	-2.9
	LWI	146.30	3.9	-3.2
	BNS	146.70	6.1	-1.9
	DUR	147.00	7.1	-1.7
	CCP	147.90	8.7	-2.3
	STU	148.60	11.2	-1.7
	TUB	148.80	10.9	-2.5
	STR	149.00	11.4	-2.5
	HLE	149.00	11.2	-2.7
	PAR	149.20	11.4	-3.0
	PRU	149.70	14.1	-1.7
	BNS	150.40	15.3	-2.4
	VIE	150.60	16.0	-2.2
	DUR	150.60	15.1	-3.1
	GAR	150.70	15.3	-3.2
	CFF	152.20	19.5	-3.2
	STU	152.20	20.5	-2.2
	TUB	152.40	20.7	-2.6
	JEN	152.40	20.0	-3.3
	MSS	152.80	22.1	-2.3
	PAR	153.00	21.6	-3.4
	BNS	153.50	24.0	-2.4
	MCN	153.70	24.0	-3.0
	NEU	154.30	26.4	-2.3
	GAR	154.40	26.1	-3.9
	STU	155.00	28.9	-1.9
	PTO	155.30	28.0	-3.7
	MSS	155.60	31.4	-1.2
	STR	155.60	30.1	-2.5
	PAR	156.30	32.5	-2.2
	CHU	156.70	33.4	-2.5
	MCN	157.30	35.5	-2.2
	TCL	157.60	35.4	-3.2
	GAR	157.80	36.4	-2.8
	MON	160.10	45.3	-1.1
	MBO	161.90	48.9	-3.4
	ALG	164.90	60.4	-2.2
	SET	165.00	61.6	-1.4
	REL	166.10	64.4	-2.6
	BAB	171.40	86.0	-1.1
	TAM	173.70	94.4	-1.9
	TAM	175.20	100.9	-1.5

EVENT	STATION	Δ (deg.)	TIME (sec.)	OBS-JB (sec.)
ENGDAHL (PERU-BRAZIL A)				
(h = 590 km)	LEM	164.19	59.4	-0.7
	HKC	165.80	63.0	-2.5
	BAG	166.27	64.5	-3.1
	CHG	166.51	68.2	-0.2
ENGDAHL (FIJI B)				
(h = 639 km)	KSA	146.53	6.3	-1.3
	CHZ	147.52	10.3	+0.2
	RAC	147.98	8.3	-3.0
	VAL	148.07	7.4	-4.1
	BNS	149.79	11.9	-4.1
	TNS	150.33	14.6	-2.9
	WRM	151.11	16.2	-3.4
	KRL	151.51	15.4	-5.4
	PRK	151.64	18.9	-2.2
	TUB	151.86	18.8	-2.5
	STR	152.03	19.5	-2.7
	MSS	152.21	19.3	-3.4
	ZAG	152.39	21.2	-2.0
	FEL	152.67	20.1	-3.9
	LJU	152.70	16.2	-7.9
	ZUR	153.06	22.4	-2.8
	TRI	153.25	23.3	-2.4
	BES	153.59	25.5	-1.2
	NEU	153.70	23.9	-3.1
	ATH	154.02	24.3	-3.6
	VAM	155.01	29.5	-1.3
	RSL	155.03	25.8	-5.1
	LNS	155.37	28.8	-3.1
	MNY	155.88	29.4	-4.0
	BNG	155.99	30.8	-2.9
	ISO	156.41	32.5	-2.5
	RCM	157.03	32.4	-4.5
	BDB	158.11	36.0	-4.2
	PTO	158.52	38.3	-3.1
	LIS	160.52	44.5	-3.3
	TOL	160.85	44.6	-4.3
	MBO	161.85	50.5	-1.7
	ALI	162.79	53.4	-1.9
	MAL	163.81	55.7	-3.1
	SET	164.44	63.4	+2.4
	RBA	165.51	60.4	-4.4
	AVE	165.86	61.3	-4.8
	TAM	175.28	101.5	-1.3

EVENT	STATION	Δ (deg.)	TIME (sec.)	OBS-JB (sec.)	QUAL.
JAVA SEA A					
(h = 606 km)	BEC	153.61	23.4	-3.3	2
	GIE	156.44	32.7	-2.4	2
	ARE	157.37	33.9	-4.0	4
	LPB	157.61	33.9	-4.7	5
	NNA	159.94	42.2	-3.7	4
	BHP	167.85	72.4	-1.0	3
	SJG	167.87	70.3	-3.2	2
	TRN	172.27	89.3	-1.2	2
	BOG	173.49	95.6	+0.2	2
	CAR	175.46	101.4	-2.1	5
JAVA SEA B					
(h = 599 km)	ARE	157.08	34.2	-2.8	5
	LPB	157.47	34.7	-3.5	4
	NNA	159.37	41.4	-2.7	5
	QUI	166.79	67.1	-2.4	3
	BHP	166.88	69.2	-0.6	5
	SJG	168.05	73.0	-1.2	2
	BOG	172.46	92.1	-0.8	4
	TRN	173.12	92.4	-1.5	5
	CAR	175.61	102.6	-1.5	5
FLORES SEA					
(h = 618 km)	SHA	145.28	2.8	-1.8	3
	NNA	155.62	28.7	-3.9	4
	LPB	155.77	29.2	-3.9	4
	BHP	161.62	49.6	-1.8	5
	ARE	166.06	62.6	-4.2	2
	SJG	167.78	70.7	-2.4	4
	TRN	176.21	102.5	-4.2	5

A2.5 P'(BC)-P'(DF) differential travel-time data [deep-focus events].

EVENT	STATION	Δ (deg.)	TIME (sec.)	OBS-JB (sec.)
HAI				
(h = 600 km)	CLL	145.40	1.0	-0.3
	KEW	146.50	2.5	+0.6
	BNS	146.70	2.8	+0.8
	DUR	147.00	3.1	+0.9
	COP	147.90	4.0	+1.4
	KRL	148.40	4.6	+1.7
	STU	148.60	5.1	+2.0
	TUB	148.80	5.0	+1.8
	STR	149.00	4.8	+1.5
	HLE	149.00	5.0	+1.7
	CLL	149.00	5.0	+1.7
	PAR	149.20	5.3	+1.9
	PRU	149.70	5.5	+1.8
	BNS	150.40	6.0	+1.8
	VIE	150.60	6.6	+2.3
	GAR	150.70	5.5	+1.1
	CFF	152.20	7.0	+1.5
	STU	152.70	7.2	+1.3
	TUB	152.40	7.7	+2.1
	JEN	152.40	7.0	+1.4
	MSS	152.80	7.7	+1.8
	PAR	153.00	7.2	+1.1
	BNS	153.50	7.7	+1.2
	MON	153.70	9.4	+2.7
	NEU	154.30	9.0	+1.7
	GAR	154.40	9.0	+1.6
	STU	155.00	10.3	+2.4
	PTO	155.30	8.3	+0.1
	MSS	155.60	9.9	+1.5
	PAR	156.30	10.0	+1.0
	CHU	156.70	11.0	+1.6
	MON	157.30	12.8	+2.9
	GAR	157.80	11.3	+1.0
ENGDAHL (FIJI B)				
(h = 639 km)	KRA	147.39	5.1	+2.7
	JER	147.52	2.6	+0.1
	CHZ	147.52	5.1	+2.6
	RAC	147.98	4.1	+1.4
	VAL	148.07	4.6	+1.9
	CLL	148.38	5.4	+2.5
	HLE	148.44	5.0	+2.0
	CMP	148.71	5.7	+2.6
	IST	148.93	4.5	+1.2

EVENT	STATION	Δ (deg.)	TIME (sec.)	OBS-JB (sec.)	QUAL.
ENGDAHL (FIJI B, CONT.)					
	PRA	149.15	5.6	+2.2	
	KEW	149.70	5.6	+1.9	
	BNS	149.79	5.7	+1.9	
	GG-	150.30	6.6	+2.5	
	TNS	150.33	6.4	+2.3	
	DOU	150.93	9.0	+4.4	
	HEI	151.08	7.3	+2.6	
	WRM	151.11	7.0	+2.3	
	HLW	151.13	7.8	+3.1	
	KRL	151.51	8.4	+3.4	
	STU	151.58	7.6	+2.6	
	PRK	151.64	7.5	+2.5	
	PDA	151.78	6.2	+1.1	
	TUB	151.86	7.4	+2.2	
	STR	152.03	9.1	+3.8	
	MSS	152.21	8.1	+2.6	
	ZAG	152.39	9.6	+4.0	
	FEL	152.67	8.8	+3.0	
	ZUR	153.06	9.9	+3.7	
	TRI	153.25	8.8	+2.5	
	BES	153.59	10.0	+3.4	
	NEU	153.70	9.7	+3.0	
	ATH	154.02	11.0	+4.0	
	VAM	155.01	11.0	+3.1	
	RSL	155.03	10.9	+3.0	
	LNS	155.37	11.4	+3.2	
JAVA SEA B					
(h = 599 km)	SHA	145.28	1.6	+0.4	3
	NNA	155.62	9.5	+1.0	3
	LPB	155.77	9.9	+1.3	2
FLORES SEA					
(h = 618 km)	OXF	144.76	1.1	+0.3	5
	GEO	146.02	1.8	+0.1	1
	ATL	148.22	4.3	+1.5	5
	SHA	148.28	4.1	+1.2	4
	LPB	157.47	11.0	+1.0	2

Appendix 3

Tables A3.1 - A3.3 display the three final inversion models (A1, B1, and B2) derived in section 5.5. Besides listing the defining parameters v_p, v_s, and ρ, we have also listed the values of the seismic parameter $\Phi = v_p^2 - \frac{4}{3} v_s^2$, the bulk modulus K, the shear modulus μ, the modulus λ, the Poisson ratio σ, pressure, and gravity.

Tables A3.4 and A3.5 show the fit of the models to the basic data set described in section 5.3 of the text. The relative errors are computed as (computed - observed)/observed. For comparison we list the standard errors in the mean of the data and the associated symmetric 95% confidence intervals computed from critical t values of the student's t-distribution [Freeman, 1963]. This allows for the fact that the sample variances are only estimates of the true variances.

Of the 177 eigenperiods listed in Table A3.4, model A1 fits 86 within their 95% confidence intervals, model B1 fits 127, and model B2 fits 115. We conclude that B1 is the most satisfactory model from this point of view.

Table A3.6 gives observed and computed absolute travel times for teleseismic distances useful in evaluating the inversion models. Comparing model B1 with P times from the 1968 Herrin Tables, we observe that the difference in baseline is approximately 0.8 seconds. The same comparison with Hales and Roberts [1970a] S times indicates a baseline shift of approximately 5 seconds.

Table A3.7 lists additional differential travel time data.

Table A3.1

MODEL A1

I	RADIUS (km)	DEPTH (km)	VP (km/sec)	VS (km/sec)	RHO (gm/cm^3)	PHI (km^2/sec^2)	K (kb)	MU (kb)	LAMBDA (kb)	SIGMA	PRESSURE (kb)	GRAV (cm/sec^2)
1	1	6370	11.20	3.50	12.58	109.11	13721	1540	12694	0.4459	3611	0
2	100	6271	11.20	3.50	12.57	109.05	13709	1543	12680	0.4457	3608	52
3	200	6171	11.20	3.51	12.56	108.99	13684	1544	12654	0.4456	3600	78
4	300	6071	11.20	3.51	12.53	108.95	13648	1542	12620	0.4455	3588	110
5	400	5971	11.20	3.51	12.52	108.92	13636	1542	12607	0.4455	3572	144
6	500	5871	11.19	3.51	12.52	108.87	13625	1543	12596	0.4454	3552	178
7	600	5771	11.19	3.51	12.51	108.82	13610	1543	12581	0.4454	3527	212
8	700	5671	11.19	3.51	12.49	108.77	13589	1539	12562	0.4454	3499	247
9	800	5571	11.18	3.51	12.49	108.68	13576	1535	12552	0.4455	3466	281
10	900	5471	11.18	3.50	12.49	108.62	13561	1530	12541	0.4456	3428	316
11	1000	5371	11.16	3.50	12.43	108.71	13510	1518	12498	0.4458	3387	350
12	1100	5271	11.19	3.49	12.34	108.96	13444	1504	12442	0.4461	3341	384
13	1215	5156	11.20	3.49	12.24	109.16	13363	1489	12370	0.4463	3284	422
14	1215	5156	10.13	0.0	12.13	102.58	12438	0	12438	0.5000	3284	422
15	1300	5071	10.13	0.0	12.10	102.62	12414	0	12414	0.5000	3239	450
16	1400	4971	10.13	0.0	12.06	102.62	12371	0	12371	0.5000	3183	482
17	1500	4871	10.12	0.0	12.00	102.37	12287	0	12287	0.5000	3123	514
18	1600	4771	10.09	0.0	11.94	101.89	12168	0	12168	0.5000	3059	546
19	1700	4671	10.05	0.0	11.88	101.03	11997	0	11997	0.5000	2992	578
20	1800	4571	9.59	0.0	11.80	99.72	11770	0	11770	0.5000	2922	609
21	1900	4471	9.92	0.0	11.73	98.38	11536	0	11536	0.5000	2849	640
22	2000	4371	9.85	0.0	11.65	96.95	11291	0	11291	0.5000	2772	671
23	2100	4271	9.77	0.0	11.57	95.46	11040	0	11040	0.5000	2692	701
24	2200	4171	9.69	0.0	11.48	93.93	10784	0	10784	0.5000	2610	731
25	2300	4071	9.62	0.0	11.40	92.54	10545	0	10545	0.5000	2524	761
26	2400	3971	9.55	0.0	11.31	91.22	10312	0	10312	0.5000	2436	790
27	2500	3871	9.46	0.0	11.21	89.50	10034	0	10034	0.5000	2346	819
28	2600	3771	9.35	0.0	11.11	87.46	9717	0	9717	0.5000	2253	847
29	2700	3671	9.24	0.0	11.00	85.30	9384	0	9384	0.5000	2157	874
30	2800	3571	9.10	0.0	10.88	82.84	9014	0	9014	0.5000	2060	902
31	2900	3471	8.95	0.0	10.75	80.10	8614	0	8614	0.5000	1961	928
32	3000	3371	8.78	0.0	10.62	77.16	8192	0	8192	0.5000	1861	954
33	3100	3271	8.62	0.0	10.47	74.24	7776	0	7776	0.5000	1759	979
34	3200	3171	8.45	0.0	10.33	71.44	7377	0	7377	0.5000	1656	1003
35	3300	3071	8.29	0.0	10.18	68.79	7002	0	7002	0.5000	1551	1026
36	3400	2971	8.14	0.0	10.03	66.32	6650	0	6650	0.5000	1447	1049
37	3485	2886	8.01	0.0	9.89	64.16	6347	0	6347	0.5000	1357	1068
38	3485	2886	13.65	7.27	5.60	115.97	6488	2955	4518	0.3023	1357	1068
39	3510	2861	13.65	7.26	5.58	115.94	6472	2943	4510	0.3025	1342	1064
40	3550	2821	13.64	7.25	5.56	115.93	6449	2924	4499	0.3030	1318	1059
41	3625	2746	13.61	7.22	5.52	115.78	6396	2877	4477	0.3044	1275	1050
42	3700	2671	13.56	7.18	5.49	115.07	6312	2827	4427	0.3051	1231	1041
43	3775	2596	13.48	7.15	5.45	113.58	6186	2781	4332	0.3045	1189	1034
44	3850	2521	13.39	7.11	5.41	111.36	6049	2737	4224	0.3034	1147	1028
45	3925	2446	13.31	7.09	5.37	110.13	5911	2694	4115	0.3021	1105	1022
46	4000	2371	13.22	7.06	5.33	108.41	5772	2650	4005	0.3009	1064	1017
47	4075	2296	13.13	7.02	5.28	106.72	5634	2604	3897	0.2997	1024	1013
48	4150	2221	13.05	6.99	5.24	105.09	5509	2559	3802	0.2988	984	1009
49	4225	2146	12.96	6.95	5.21	103.56	5391	2517	3712	0.2980	945	1005
50	4300	2071	12.88	6.92	5.16	101.96	5266	2472	3617	0.2970	906	1003

MODEL A1 (cont.)

I	RADIUS (km)	DEPTH (km)	VP (km/sec)	VS (km/sec)	RHO (gm/cm^3)	PHI (km^2/sec^2)	K (kb)	MU (kb)	LAMBDA (kb)	SIGMA	PRESSURE (kb)	GRAV (cm/sec^2)
51	4375	1996	12.78	6.89	5.12	100.20	5131	2427	3512	0.2957	867	1000
52	4450	1921	12.69	6.85	5.08	98.43	4993	2383	3408	0.2942	829	998
53	4525	1846	12.60	6.81	5.04	96.83	4882	2341	3321	0.2933	791	997
54	4600	1771	12.51	6.78	5.01	95.22	4767	2300	3233	0.2921	753	996
55	4675	1696	12.42	6.75	4.97	93.47	4644	2261	3136	0.2905	716	995
56	4750	1621	12.33	6.71	4.93	91.99	4535	2222	3053	0.2894	679	994
57	4825	1546	12.24	6.68	4.89	90.42	4422	2181	2967	0.2881	642	994
58	4900	1471	12.15	6.65	4.85	88.76	4306	2142	2877	0.2866	606	994
59	4975	1395	12.06	6.59	4.81	87.39	4203	2090	2809	0.2867	570	994
60	5050	1321	11.96	6.54	4.77	85.98	4059	2040	2739	0.2866	534	994
61	5125	1246	11.85	6.49	4.72	84.37	3984	1987	2659	0.2862	499	995
62	5200	1171	11.74	6.44	4.68	82.54	3860	1937	2569	0.2850	464	996
63	5275	1096	11.62	6.39	4.63	80.48	3727	1892	2466	0.2829	429	996
64	5350	1021	11.49	6.33	4.58	78.76	3606	1832	2384	0.2827	395	997
65	5425	946	11.36	6.25	4.51	76.82	3462	1768	2283	0.2817	361	998
66	5500	871	11.23	6.21	4.44	74.57	3309	1712	2168	0.2793	327	999
67	5550	821	11.13	6.18	4.40	72.90	3205	1680	2085	0.2768	305	999
68	5600	771	11.03	6.15	4.36	71.12	3100	1651	2000	0.2739	283	999
69	5650	721	10.92	6.13	4.33	69.26	2997	1624	1914	0.2705	261	1000
70	5700	671	10.83	6.10	4.30	67.54	2905	1602	1836	0.2670	240	1000
71	5700	671	10.83	6.10	4.30	67.54	2905	1602	1836	0.2670	240	1000
72	5725	646	10.62	5.96	4.23	65.49	2772	1502	1771	0.2705	229	1000
73	5750	621	10.42	5.81	4.17	63.47	2644	1407	1706	0.2740	219	1001
74	5775	596	10.21	5.67	4.10	61.47	2521	1316	1643	0.2776	208	1001
75	5800	571	10.01	5.52	4.04	59.50	2401	1229	1581	0.2812	198	1000
76	5825	546	9.80	5.37	3.97	57.57	2284	1146	1520	0.2851	188	1000
77	5850	521	9.60	5.23	3.90	55.68	2172	1065	1462	0.2892	178	1000
78	5875	496	9.39	5.08	3.83	53.84	2063	987	1405	0.2936	169	999
79	5900	471	9.19	4.92	3.76	52.05	1958	912	1350	0.2984	159	999
80	5925	446	8.98	4.77	3.69	50.32	1856	838	1297	0.3037	150	998
81	5951	420	8.76	4.60	3.61	48.58	1754	764	1244	0.3098	140	997
82	5951	420	8.76	4.60	3.61	48.58	1754	764	1244	0.3098	140	997
83	5975	396	8.71	4.59	3.59	47.79	1714	757	1209	0.3075	132	997
84	6000	371	8.66	4.58	3.56	47.01	1673	748	1174	0.3055	123	996
85	6050	321	8.56	4.55	3.50	45.56	1594	725	1110	0.3024	105	994
86	6100	271	8.45	4.52	3.44	44.15	1517	702	1049	0.2996	88	992
87	6150	221	8.34	4.50	3.39	42.63	1442	684	986	0.2952	71	990
88	6175	196	8.29	4.50	3.37	41.76	1405	679	951	0.2917	63	989
89	6200	171	8.24	4.50	3.35	40.81	1367	678	914	0.2871	54	988
90	6225	145	8.18	4.51	3.34	39.79	1328	680	875	0.2813	46	987
91	6250	121	8.13	4.53	3.33	38.71	1289	684	833	0.2746	38	987
92	6271	100	8.09	4.55	3.33	37.77	1256	688	797	0.2683	31	986
93	6271	100	8.09	4.55	3.33	37.77	1256	688	797	0.2683	31	986
94	6290	81	8.05	4.57	3.32	36.94	1227	692	765	0.2625	25	985
95	6310	61	8.01	4.58	3.31	36.11	1196	695	733	0.2566	18	984
96	6330	41	7.96	4.59	3.30	35.34	1168	696	703	0.2514	12	984
97	6350	21	7.92	4.59	3.29	34.66	1141	694	678	0.2471	5	983
98	6350	21	6.20	3.40	2.79	23.03	642	322	427	0.2850	5	983
99	6360	11	6.20	3.40	2.79	23.03	642	322	427	0.2850	3	982
100	6371	0	6.20	3.40	2.79	23.03	642	322	427	0.2850	0	982

Table A3.2

MODEL B1

I	RADIUS (km)	DEPTH (km)	VP (km/sec)	VS (km/sec)	RHO (gm/cm^3)	PHI (km^2/sec^2)	K (kb)	MU (kb)	LAMBDA (kb)	SIGMA	PRESSURE (kb)	GRAV (cm/sec^2)
1	1	6370	11.20	3.50	12.58	109.11	13721	1540	12694	0.4459	3609	0
2	100	6271	11.20	3.50	12.57	109.11	13716	1541	12689	0.4459	3606	52
3	200	6171	11.20	3.50	12.56	109.12	13700	1539	12674	0.4458	3598	78
4	300	6071	11.20	3.50	12.53	109.14	13671	1535	12648	0.4459	3586	110
5	400	5971	11.20	3.50	12.52	109.16	13665	1532	12643	0.4459	3570	144
6	500	5871	11.20	3.50	12.51	109.18	13663	1531	12642	0.4460	3550	178
7	600	5771	11.20	3.50	12.51	109.20	13658	1528	12639	0.4461	3525	212
8	700	5671	11.20	3.49	12.50	109.19	13649	1523	12633	0.4462	3495	247
9	800	5571	11.19	3.48	12.50	109.12	13644	1517	12632	0.4464	3463	281
10	900	5471	11.19	3.48	12.49	109.09	13630	1510	12623	0.4466	3426	316
11	1000	5371	11.19	3.47	12.46	109.22	13609	1499	12610	0.4469	3384	350
12	1100	5271	11.21	3.46	12.39	109.57	13571	1485	12581	0.4472	3339	385
13	1215	5156	11.22	3.46	12.28	109.87	13492	1467	12513	0.4475	3281	423
14	1215	5156	10.14	0.0	12.11	102.91	12460	0	12460	0.5000	3281	423
15	1300	5071	10.15	0.0	12.08	102.99	12444	0	12444	0.5000	3236	450
16	1400	4971	10.15	0.0	12.04	103.06	12411	0	12411	0.5000	3180	482
17	1500	4871	10.14	0.0	11.99	102.85	12334	0	12334	0.5000	3120	514
18	1600	4771	10.12	0.0	11.93	102.39	12219	0	12219	0.5000	3056	546
19	1700	4671	10.07	0.0	11.87	101.47	12042	0	12042	0.5000	2990	578
20	1800	4571	10.00	0.0	11.80	100.08	11805	0	11805	0.5000	2919	609
21	1900	4471	9.93	0.0	11.72	98.65	11561	0	11561	0.5000	2846	640
22	2000	4371	9.86	0.0	11.64	97.14	11307	0	11307	0.5000	2769	671
23	2100	4271	9.78	0.0	11.56	95.59	11048	0	11048	0.5000	2690	701
24	2200	4171	9.70	0.0	11.47	94.00	10785	0	10785	0.5000	2607	731
25	2300	4071	9.62	0.0	11.39	92.57	10542	0	10542	0.5000	2522	760
26	2400	3971	9.55	0.0	11.30	91.23	10309	0	10309	0.5000	2434	790
27	2500	3871	9.46	0.0	11.21	89.51	10032	0	10032	0.5000	2343	818
28	2600	3772	9.35	0.0	11.11	87.49	9718	0	9718	0.5000	2250	846
29	2700	3671	9.24	0.0	11.00	85.35	9388	0	9388	0.5000	2155	874
30	2800	3571	9.11	0.0	10.88	82.92	9023	0	9023	0.5000	2058	901
31	2900	3471	8.96	0.0	10.76	80.21	8628	0	8628	0.5000	1959	928
32	3000	3371	8.79	0.0	10.62	77.30	8209	0	8209	0.5000	1858	954
33	3100	3271	8.63	0.0	10.48	74.41	7797	0	7797	0.5000	1756	979
34	3200	3171	8.46	0.0	10.33	71.62	7400	0	7400	0.5000	1653	1003
35	3300	3071	8.31	0.0	10.19	68.99	7026	0	7026	0.5000	1549	1026
36	3400	2971	8.16	0.0	10.04	66.52	6676	0	6676	0.5000	1444	1049
37	3485	2886	8.02	0.0	9.90	64.36	6373	0	6373	0.5000	1354	1068
38	3485	2886	13.67	7.27	5.58	116.38	6489	2948	4523	0.3027	1354	1068
39	3510	2861	13.67	7.27	5.56	116.35	6466	2934	4510	0.3029	1340	1064
40	3550	2821	13.66	7.26	5.54	116.32	6443	2916	4498	0.3033	1316	1059
41	3625	2746	13.63	7.22	5.50	116.09	6365	2871	4471	0.3045	1272	1049
42	3700	2671	13.57	7.19	5.46	115.28	6294	2822	4412	0.3049	1229	1041
43	3775	2596	13.49	7.16	5.42	113.67	6160	2775	4309	0.3041	1187	1034
44	3850	2521	13.40	7.13	5.38	111.84	6014	2730	4194	0.3029	1145	1027
45	3925	2446	13.31	7.09	5.34	109.99	5870	2686	4079	0.3015	1104	1021
46	4000	2371	13.22	7.06	5.30	108.16	5727	2642	3966	0.3001	1063	1016
47	4075	2296	13.13	7.03	5.26	106.36	5597	2601	3863	0.2988	1023	1011
48	4150	2221	13.03	6.99	5.22	104.68	5469	2555	3765	0.2979	984	1008
49	4225	2146	12.95	6.96	5.19	103.12	5347	2509	3674	0.2971	944	1004
50	4300	2071	12.86	6.92	5.15	101.55	5227	2465	3583	0.2962	905	1001

MODEL B1 (cont.)

I	RADIUS (km)	DEPTH (km)	VP (km/sec)	VS (km/sec)	RHO (gm/cm^3)	PHI (km^2/sec^2)	K (kb)	MU (kb)	LAMBDA (kb)	SIGMA	PRESSURE (kb)	GRAV (cm/sec^2)
51	4375	1996	12.77	6.88	5.11	95.84	5102	2422	3487	0.2951	867	999
52	4450	1921	12.68	6.85	5.07	98.13	4978	2380	3391	0.2938	829	997
53	4525	1846	12.59	6.81	5.04	96.63	4866	2336	3309	0.2931	791	996
54	4600	1771	12.50	6.77	5.00	95.13	4755	2293	3226	0.2923	754	994
55	4675	1696	12.41	6.74	4.96	93.49	4638	2253	3136	0.2909	716	994
56	4750	1621	12.33	6.71	4.92	92.10	4535	2214	3058	0.2901	680	993
57	4825	1546	12.25	6.67	4.89	90.62	4427	2174	2977	0.2890	643	993
58	4900	1471	12.16	6.64	4.85	88.99	4313	2136	2888	0.2874	607	993
59	4975	1396	12.06	6.59	4.81	87.59	4211	2089	2819	0.2872	571	993
60	5050	1321	11.97	6.55	4.77	86.07	4103	2044	2740	0.2864	535	993
61	5125	1246	11.86	6.50	4.72	84.34	3984	1998	2651	0.2851	500	994
62	5200	1171	11.75	6.47	4.68	82.36	3854	1956	2549	0.2829	465	994
63	5275	1096	11.64	6.44	4.64	80.15	3715	1920	2435	0.2796	430	995
64	5350	1021	11.52	6.39	4.59	78.30	3594	1871	2346	0.2781	395	996
65	5425	946	11.39	6.33	4.55	76.31	3469	1824	2253	0.2763	361	997
66	5500	871	11.26	6.28	4.50	74.19	3340	1778	2154	0.2739	327	998
67	5550	821	11.17	6.25	4.47	72.72	3252	1746	2087	0.2722	305	999
68	5600	771	11.07	6.21	4.44	71.18	3162	1712	2020	0.2706	283	1000
69	5650	721	10.97	6.17	4.41	69.71	3075	1677	1957	0.2693	261	1000
70	5700	671	10.88	6.12	4.38	68.39	2996	1642	1901	0.2683	239	1001
71	5700	671	10.08	5.21	4.05	65.37	2644	1098	1911	0.3175	239	1001
72	5725	646	10.01	5.21	4.02	64.03	2575	1092	1846	0.3141	228	1001
73	5750	621	9.95	5.22	4.00	62.62	2503	1088	1777	0.3100	218	1000
74	5775	596	9.88	5.23	3.97	61.16	2430	1086	1706	0.3055	208	1000
75	5800	571	9.81	5.24	3.95	59.66	2355	1084	1632	0.3004	199	1000
76	5825	546	9.75	5.26	3.92	58.13	2280	1084	1558	0.2948	189	999
77	5850	521	9.68	5.27	3.90	56.58	2205	1084	1482	0.2887	179	999
78	5875	496	9.61	5.29	3.87	55.05	2131	1084	1408	0.2825	169	999
79	5900	471	9.54	5.31	3.85	53.55	2060	1083	1338	0.2763	160	998
80	5925	446	9.48	5.32	3.82	52.14	1992	1079	1272	0.2705	150	998
81	5951	420	9.41	5.32	3.80	50.76	1926	1074	1210	0.2649	140	997
82	5951	420	8.75	4.67	3.58	47.61	1706	780	1186	0.3017	140	997
83	5975	396	8.71	4.66	3.57	46.79	1668	775	1151	0.2988	132	997
84	6000	371	8.66	4.66	3.54	46.02	1630	768	1118	0.2965	123	996
85	6050	321	8.56	4.60	3.49	44.96	1569	739	1076	0.2964	105	994
86	6100	271	8.46	4.50	3.44	44.53	1530	695	1067	0.3028	88	992
87	6150	221	8.35	4.37	3.39	44.26	1498	648	1066	0.3110	71	990
88	6175	196	8.30	4.34	3.37	43.79	1473	633	1051	0.3119	63	989
89	6200	171	8.25	4.35	3.35	42.77	1432	633	1009	0.3072	54	988
90	6225	146	8.19	4.37	3.34	41.60	1388	637	962	0.3008	46	987
91	6250	121	8.13	4.44	3.33	39.88	1327	656	889	0.2878	38	986
92	6271	100	8.08	4.53	3.32	38.05	1264	681	810	0.2717	31	986
93	6271	100	8.08	4.53	3.32	38.05	1264	681	810	0.2717	31	986
94	6290	81	8.04	4.62	3.32	36.21	1202	708	730	0.2537	25	985
95	6310	61	8.00	4.72	3.32	34.24	1135	738	643	0.2327	18	984
96	6330	41	7.95	4.80	3.31	32.52	1076	762	568	0.2136	12	984
97	6350	21	7.91	4.83	3.30	31.45	1037	769	524	0.2026	5	983
98	6350	21	6.20	3.40	2.79	23.03	642	322	427	0.2850	5	983
99	6360	11	6.20	3.40	2.79	23.03	642	322	427	0.2850	3	982
100	6371	0	6.20	3.40	2.79	23.03	642	322	427	0.2850	0	981

Table A3.3

MODEL B2

I	RADIUS (km)	DEPTH (km)	VP (km/sec)	VS (km/sec)	RHO (gm/cm^3)	PHI (km^2/sec^2)	K (kb)	MU (kb)	LAMBDA (kb)	SIGMA	PRESSURE (kb)	GRAV (cm/sec^2)
1	1	6370	11.20	3.50	12.58	109.11	13721	1540	12694	0.4459	3613	0
2	100	6271	11.20	3.50	12.58	109.07	13715	1542	12686	0.4458	3609	52
3	200	6171	11.20	3.50	12.57	109.07	13706	1542	12678	0.4458	3601	78
4	300	6071	11.20	3.50	12.55	109.07	13688	1539	12662	0.4458	3589	111
5	400	5971	11.20	3.50	12.55	109.08	13688	1537	12663	0.4458	3573	144
6	500	5871	11.20	3.50	12.54	109.06	13675	1535	12652	0.4459	3553	178
7	600	5771	11.19	3.50	12.52	109.02	13652	1530	12632	0.4460	3528	213
8	700	5671	11.19	3.49	12.51	108.97	13631	1523	12615	0.4461	3500	247
9	800	5571	11.18	3.48	12.51	108.89	13620	1515	12610	0.4464	3466	282
10	900	5471	11.17	3.47	12.49	108.79	13590	1503	12587	0.4466	3429	316
11	1000	5371	11.16	3.46	12.42	108.58	13487	1485	12496	0.4468	3337	350
12	1100	5271	11.16	3.45	12.33	108.66	13397	1466	12418	0.4471	3342	384
13	1215	5156	11.16	3.44	12.24	108.67	13299	1451	12332	0.4474	3285	423
14	1215	5156	10.13	0.0	12.14	102.60	12451	0	12451	0.5000	3285	423
15	1300	5071	10.13	0.0	12.11	102.67	12428	0	12428	0.5000	3240	450
16	1400	4971	10.14	0.0	12.06	102.74	12388	0	12386	0.5000	3183	482
17	1500	4871	10.12	0.0	12.00	102.50	12303	0	12303	0.5000	3123	514
18	1600	4771	10.10	0.0	11.94	102.02	12181	0	12181	0.5000	3060	546
19	1700	4671	10.05	0.0	11.87	101.08	11999	0	11999	0.5000	2993	578
20	1800	4571	9.99	0.0	11.80	99.72	11766	0	11766	0.5000	2923	609
21	1900	4471	9.92	0.0	11.72	98.36	11531	0	11531	0.5000	2849	640
22	2000	4371	9.85	0.0	11.65	96.98	11294	0	11294	0.5000	2772	671
23	2100	4271	9.78	0.0	11.57	95.68	11067	0	11067	0.5000	2693	701
24	2200	4171	9.71	0.0	11.49	94.32	10833	0	10833	0.5000	2610	731
25	2300	4071	9.63	0.0	11.40	92.74	10573	0	10573	0.5000	2525	761
26	2400	3971	9.55	0.0	11.31	91.25	10322	0	10322	0.5000	2437	790
27	2500	3871	9.46	0.0	11.22	89.55	10045	0	10045	0.5000	2346	819
28	2600	3771	9.35	0.0	11.12	87.50	9726	0	9726	0.5000	2253	847
29	2700	3671	9.24	0.0	11.01	85.32	9389	0	9389	0.5000	2158	875
30	2800	3571	9.10	0.0	10.89	82.83	9017	0	9017	0.5000	2060	902
31	2900	3471	8.95	0.0	10.76	80.09	8617	0	8617	0.5000	1961	928
32	3000	3371	8.78	0.0	10.63	77.16	8199	0	8199	0.5000	1861	954
33	3100	3271	8.62	0.0	10.49	74.29	7794	0	7794	0.5000	1759	979
34	3200	3171	8.46	0.0	10.35	71.55	7409	0	7409	0.5000	1655	1004
35	3300	3071	8.31	0.0	10.22	68.98	7049	0	7049	0.5000	1551	1027
36	3400	2971	8.16	0.0	10.08	66.56	6710	0	6710	0.5000	1445	1050
37	3485	2886	8.03	0.0	9.95	64.42	6412	0	6412	0.5000	1355	1069
38	3485	2886	13.46	6.55	6.04	123.91	7485	2589	5759	0.3449	1355	1069
39	3510	2861	13.54	6.85	5.84	120.73	7052	2738	5226	0.3281	1339	1066
40	3550	2821	13.66	7.33	5.52	114.58	6346	2965	4369	0.2979	1315	1061
41	3625	2746	13.63	7.29	5.48	114.86	6294	2915	4350	0.2994	1271	1052
42	3700	2671	13.58	7.25	5.44	114.23	6214	2860	4307	0.3005	1228	1043
43	3775	2596	13.49	7.21	5.40	112.83	6092	2805	4222	0.3004	1186	1035
44	3850	2521	13.40	7.17	5.35	111.23	5961	2752	4126	0.3000	1144	1029
45	3925	2446	13.31	7.12	5.32	109.61	5830	2699	4030	0.2995	1103	1023
46	4000	2371	13.22	7.08	5.28	108.02	5702	2647	3937	0.2990	1063	1017
47	4075	2296	13.13	7.04	5.24	106.43	5577	2596	3846	0.2985	1023	1013
48	4150	2221	13.04	7.00	5.20	104.96	5454	2545	3757	0.2981	983	1009
49	4225	2146	12.96	6.96	5.16	103.38	5338	2498	3673	0.2976	944	1005
50	4300	2071	12.87	6.92	5.13	101.84	5221	2453	3586	0.2969	905	1002

MODEL B2 (cont.)

I	RADIUS (km)	DEPTH (km)	VP (km/sec)	VS (km/sec)	RHO (gm/cm^3)	PHI (km^2/sec^2)	K (kb)	MU (kb)	LAMBDA (kb)	SIGMA	PRESSURE (kb)	GRAV (cm/sec^2)
51	4375	1996	12.78	6.88	5.09	100.16	5099	2410	3492	0.2958	867	1000
52	4450	1921	12.69	6.85	5.06	98.47	4979	2370	3399	0.2946	829	998
53	4525	1846	12.60	6.81	5.02	96.98	4871	2327	3319	0.2939	791	996
54	4600	1771	12.51	6.77	4.99	95.47	4764	2287	3238	0.2930	754	995
55	4675	1696	12.42	6.74	4.96	93.82	4650	2250	3149	0.2916	717	994
56	4750	1621	12.34	6.71	4.92	92.41	4548	2213	3072	0.2906	680	993
57	4825	1546	12.26	6.67	4.89	90.86	4440	2175	2989	0.2894	643	993
58	4900	1471	12.16	6.64	4.85	89.16	4324	2139	2898	0.2877	607	993
59	4975	1396	12.07	6.59	4.81	87.69	4219	2091	2825	0.2873	571	993
60	5050	1321	11.97	6.55	4.77	86.13	4109	2045	2746	0.2865	535	993
61	5125	1246	11.86	6.50	4.73	84.39	3991	1999	2658	0.2854	500	994
62	5200	1171	11.75	6.46	4.69	82.43	3863	1956	2558	0.2833	465	995
63	5275	1096	11.63	6.43	4.64	80.22	3723	1918	2444	0.2802	430	995
64	5350	1021	11.51	6.38	4.60	78.36	3602	1868	2356	0.2789	395	996
65	5425	946	11.39	6.32	4.55	76.38	3475	1819	2262	0.2772	361	997
66	5500	871	11.26	6.28	4.50	74.06	3335	1778	2149	0.2736	327	998
67	5550	821	11.17	6.31	4.47	71.69	3206	1778	2020	0.2659	305	999
68	5600	771	11.07	6.21	4.44	71.11	3158	1714	2014	0.2701	283	1000
69	5650	721	10.97	6.13	4.41	70.40	3104	1655	2000	0.2737	260	1001
70	5700	671	10.88	6.07	4.38	69.32	3034	1611	1960	0.2745	238	1001
71	5700	671	10.10	5.20	4.01	65.93	2644	1083	1922	0.3198	238	1001
72	5725	646	10.03	5.20	3.99	64.55	2574	1076	1855	0.3162	228	1001
73	5750	621	9.96	5.21	3.97	63.09	2502	1076	1765	0.3120	218	1001
74	5775	596	9.90	5.22	3.95	61.56	2429	1075	1711	0.3070	209	1000
75	5800	571	9.83	5.24	3.93	60.00	2355	1077	1637	0.3015	199	1000
76	5825	546	9.76	5.26	3.91	58.43	2282	1079	1562	0.2957	189	999
77	5850	521	9.69	5.28	3.89	56.78	2206	1083	1483	0.2890	179	999
78	5875	496	9.63	5.30	3.87	55.17	2132	1086	1408	0.2822	169	999
79	5900	471	9.56	5.32	3.84	53.59	2060	1089	1334	0.2753	160	998
80	5925	446	9.49	5.34	3.82	52.11	1991	1088	1266	0.2689	150	998
81	5951	420	9.42	5.34	3.80	50.70	1925	1084	1203	0.2630	140	997
82	5951	420	8.75	4.65	3.60	47.66	1717	779	1197	0.3029	140	997
83	5975	396	8.70	4.65	3.58	46.02	1678	775	1161	0.2998	132	997
84	6000	371	8.65	4.65	3.55	46.02	1639	769	1126	0.2972	123	996
85	6050	321	8.55	4.59	3.51	45.02	1579	740	1086	0.2974	105	994
86	6100	271	8.46	4.43	3.45	44.76	1544	691	1083	0.3052	88	992
87	6150	221	8.36	4.35	3.39	44.56	1511	643	1082	0.3136	71	990
88	6175	196	8.31	4.34	3.37	43.88	1478	634	1055	0.3122	63	989
89	6200	171	8.26	4.33	3.35	43.12	1444	628	1025	0.3099	54	988
90	6225	146	8.20	4.36	3.33	41.95	1398	633	976	0.3033	46	988
91	6250	121	8.15	4.44	3.33	40.15	1335	654	899	0.2894	38	987
92	6271	100	8.10	4.54	3.32	38.16	1266	683	811	0.2713	31	986
93	6271	100	8.10	4.54	3.32	38.16	1266	683	811	0.2713	31	986
94	6290	81	8.06	4.65	3.32	36.14	1198	715	721	0.2510	25	985
95	6310	61	8.01	4.76	3.31	34.01	1125	749	626	0.2277	18	984
96	6330	41	7.97	4.84	3.30	32.26	1064	772	549	0.2076	12	984
97	6350	21	7.93	4.84	3.29	31.58	1038	770	524	0.2026	5	983
98	6350	21	6.20	3.40	2.79	23.03	642	322	427	0.2850	5	983
99	6360	11	6.20	3.40	2.79	23.03	642	322	427	0.2850	3	982
100	6371	0	6.20	3.40	2.79	23.03	642	322	427	0.2850	0	981

Table A3.4

Fit of the models to mode data

	Observed Data			Model A1		Model B1		Model B2	
Mode	Period (sec)	S.E.M. (sec)	95% C.I.	Period (sec)	Rel.Error %	Period (sec)	Rel.Error %	Period (sec)	Rel.Error %
${}_0S_0$	1227.65	0.683	1.44	1227.65	0.000	1227.61	-0.002	1227.65	0.000
${}_1S_0$	613.57	0.236	0.54	614.63	0.172	614.09	0.084	614.85	0.205
${}_2S_0$	398.54	0.084	0.16	399.22	0.170	398.49	-0.013	398.65	0.027
${}_3S_0$	305.84	0.129	0.32	305.76	-0.027	305.53	-0.102	305.62	-0.073
${}_4S_0$	243.59	0.067	0.15	243.70	0.043	243.55	-0.018	243.69	0.042
${}_0S_2$	3233.30	0.496	0.98	3231.50	-0.056	3232.45	-0.026	3232.34	-0.030
${}_0S_3$	2133.56	0.380	0.86	2133.50	-0.003	2134.13	0.027	2134.25	0.032
${}_0S_4$	1547.30	0.877	1.76	1545.42	-0.121	1545.82	-0.096	1546.07	-0.080
${}_0S_5$	1190.12	0.432	0.86	1190.19	0.006	1190.42	0.025	1190.65	0.045
${}_0S_6$	963.17	0.292	0.58	963.61	0.046	963.72	0.057	963.88	0.074
${}_0S_7$	811.45	0.246	0.50	812.25	0.099	812.24	0.098	812.32	0.107
${}_0S_8$	707.64	0.135	0.28	707.84	0.028	707.70	0.009	707.71	0.010
${}_0S_9$	633.95	0.102	0.20	633.94	-0.005	633.69	-0.041	633.66	-0.046
${}_0S_{10}$	580.08	0.097	0.18	579.52	-0.096	579.89	-0.154	579.15	-0.161
${}_0S_{11}$	536.56	0.105	0.22	537.21	0.121	536.87	0.057	536.83	0.051
${}_0S_{12}$	502.18	0.073	0.14	502.64	0.092	502.34	0.032	502.32	0.028

Table A3.4 (cont.)

Mode	Observed Data Period (sec)	Observed Data S.E.M. (sec)	Observed Data 95% C.I.	Model A1 Period (sec)	Model A1 Rel.Error %	Model B1 Period (sec)	Model B1 Rel.Error %	Model B2 Period (sec)	Model B2 Rel.Error %
${}_0S_{13}$	473.14	0.070	0.14	473.44	0.063	473.21	0.015	473.21	0.015
${}_0S_{14}$	448.28	0.054	0.10	448.23	-0.011	448.10	-0.040	448.12	-0.036
${}_0S_{15}$	426.24	0.053	0.10	426.19	-0.017	426.16	-0.018	426.20	-0.009
${}_0S_{16}$	406.77	0.050	0.10	406.74	-0.008	406.79	0.005	406.85	0.020
${}_0S_{17}$	389.31	0.068	0.14	389.44	0.032	389.56	0.064	389.64	0.083
${}_0S_{18}$	373.89	0.071	0.14	373.93	0.011	374.10	0.055	374.20	0.083
${}_0S_{19}$	360.20	0.064	0.12	359.96	-0.066	360.14	-0.017	360.26	0.015
${}_0S_{20}$	347.82	0.067	0.14	347.30	-0.150	347.47	-0.102	347.59	-0.066
${}_0S_{21}$	336.00	0.056	0.12	335.75	-0.075	335.88	-0.036	336.02	-0.005
${}_0S_{22}$	325.31	0.060	0.12	325.15	-0.048	325.23	-0.024	325.38	0.020
${}_0S_{23}$	315.43	0.044	0.08	315.38	-0.016	315.38	-0.016	315.53	0.031
${}_0S_{24}$	306.25	0.050	0.10	306.33	0.026	306.24	-0.002	306.40	0.047
${}_0S_{25}$	297.71	0.048	0.10	297.90	0.064	297.72	0.004	297.87	0.055
${}_0S_{26}$	289.69	0.047	0.10	290.02	0.114	289.74	0.019	289.90	0.071
${}_0S_{27}$	282.34	0.066	0.14	282.62	0.098	282.25	-0.033	282.39	0.019
${}_0S_{28}$	275.06	0.052	0.10	275.64	0.210	275.18	0.042	275.32	0.095
${}_0S_{29}$	268.44	0.049	0.10	269.04	0.222	268.49	0.018	268.63	0.071

Table A3.4 (cont.)

Mode	Observed Data Period (sec)	S.E.M. (sec)	95% C.I.	Model A1 Period (sec)	Rel.Error %	Model B1 Period (sec)	Rel.Error %	Model B2 Period (sec)	Rel.Error %
${}_0S_{30}$	262.15	0.051	0.10	262.76	0.236	262.15	-0.000	262.29	0.052
${}_0S_{31}$	256.00	0.062	0.12	256.81	0.315	256.12	0.048	256.26	0.100
${}_0S_{32}$	250.20	0.055	0.12	251.12	0.368	250.38	0.073	250.51	0.125
${}_0S_{33}$	244.95	0.056	0.12	245.68	0.300	244.91	-0.018	245.03	0.033
${}_0S_{34}$	239.70	0.066	0.14	240.48	0.324	239.67	-0.013	239.79	0.037
${}_0S_{35}$	234.69	0.067	0.14	235.48	0.337	234.66	-0.014	234.77	0.035
${}_0S_{36}$	229.74	0.066	0.14	230.66	0.409	229.85	0.048	229.96	0.097
${}_0S_{37}$	225.16	0.052	0.10	226.06	0.400	225.24	0.034	225.35	0.083
${}_0S_{38}$	220.62	0.050	0.10	221.61	0.400	220.80	0.083	220.91	0.131
${}_0S_{39}$	216.43	0.052	0.10	217.32	0.412	216.54	0.049	216.64	0.097
${}_0S_{40}$	212.31	0.090	0.18	213.18	0.410	212.43	0.056	212.53	0.103
${}_0S_{41}$	208.05	0.123	0.24	209.18	0.544	208.47	0.201	208.57	0.249
${}_0S_{42}$	204.57	0.072	0.14	205.32	0.364	204.65	0.038	204.75	0.086
${}_0S_{43}$	200.93	0.080	0.16	201.58	0.321	200.96	0.016	201.06	0.063
${}_0S_{44}$	197.19	0.077	0.16	197.96	0.389	197.40	0.105	197.49	0.153
${}_0S_{45}$	194.03	0.073	0.14	194.45	0.218	193.95	-0.039	194.05	0.008
${}_0S_{46}$	190.59	0.085	0.18	191.06	0.246	190.62	0.017	190.71	0.064
${}_0S_{47}$	187.43	0.054	0.11	187.77	0.180	187.40	-0.018	187.49	0.029

Table A3. 4 (cont.)

Mode	Observed Data			Model A1		Model B1		Model B2	
	Period (sec)	S.E.M. (sec)	95% C.I.	Period (sec)	Rel.Error %	Period (sec)	Rel.Error %	Period (sec)	Rel.Error %
${}_0S_{48}$	184.25	0.090	0.19	184.58	0.177	184.27	0.019	184.36	0.059
${}_0S_{49}$	181.30	0.106	0.23	181.48	0.101	181.24	-0.031	181.33	0.017
${}_0S_{50}$	178.35	0.118	0.25	178.48	0.072	178.83	-0.023	178.39	0.025
${}_0S_{51}$	175.42	0.030	0.06	175.56	0.082	175.46	0.023	175.54	0.071
${}_0S_{52}$	172.64	0.030	0.06	172.73	0.054	172.70	0.033	172.78	0.082
${}_0S_{53}$	169.97	0.030	0.06	169.98	0.008	170.01	0.026	170.10	0.074
${}_0S_{54}$	167.38	0.030	0.06	167.31	-0.041	167.41	0.016	167.49	0.065
${}_0S_{55}$	164.85	0.030	0.06	164.71	-0.082	164.87	0.015	164.95	0.063
${}_0S_{56}$	162.41	0.030	0.06	162.19	-0.135	162.41	0.001	162.49	0.050
${}_0S_{57}$	160.01	0.030	0.06	159.74	-0.172	160.02	0.004	160.09	0.053
${}_0S_{58}$	157.70	0.040	0.08	157.35	-0.224	157.69	-0.009	157.76	0.040
${}_0S_{59}$	155.45	0.040	0.08	155.02	-0.275	155.42	-0.021	155.49	0.028
${}_0S_{60}$	153.24	0.040	0.08	152.76	-0.313	153.21	-0.020	153.28	0.029
${}_0S_{61}$	151.12	0.040	0.08	150.56	-0.371	151.06	-0.041	151.13	0.008
${}_0S_{62}$	149.07	0.040	0.08	148.42	-0.439	148.96	-0.072	149.04	-0.020
${}_0S_{63}$	147.09	0.050	0.11	146.33	-0.519	146.92	-0.115	146.99	-0.067

Table A3.4 (cont.)

Mode	Observed Data Period (sec)	S.E.M. (sec)	95% C.I.	Model A1 Period (sec)	Rel.Error %	Model B1 Period (sec)	Rel.Error %	Model B2 Period (sec)	Rel.Error %
${}_1S_2$	1470.85	1.227	2.60	1468.52	-0.158	1469.05	-0.122	1469.39	-0.099
${}_1S_3$	1060.83	0.993	2.05	1062.41	0.149	1062.76	0.182	1063.09	0.213
${}_1S_4$	852.68	0.374	0.74	851.48	-0.140	851.75	-0.109	852.11	-0.067
${}_1S_5$	730.56	0.437	1.00	729.16	-0.191	729.30	-0.172	729.67	-0.122
${}_1S_6$	657.61	0.201	0.41	656.99	-0.094	656.94	-0.102	657.27	-0.052
${}_1S_7$	603.93	0.306	0.63	604.40	0.078	604.25	0.053	604.54	0.100
${}_1S_8$	555.83	0.156	0.16	556.37	0.098	556.22	0.070	556.45	0.112
${}_1S_9$	509.58	0.197	0.43	509.97	0.076	509.86	0.056	510.03	0.088
${}_1S_{10}$	465.45	0.287	0.63	466.23	0.169	466.20	0.161	466.29	0.180
${}_1S_{14}$	337.00	0.084	0,16	336.57	-0.128	336.64	-0.107	336.55	-0.135
${}_1S_{15}$	316.06	0.076	0.17	315.55	-0.162	315.59	-0.150	315.64	-0.132
${}_1S_{16}$	299.87	0.145	0.33	299.59	-0.094	299.47	-0.135	299.63	-0.079
${}_1S_{17}$	285.97	0.129	0.29	286.38	0.142	286.10	0.044	286.29	0.112
${}_2S_1$	1058.09	0.892	2.06	1057.79	-0.029	1057.92	-0.016	1057.75	-0.032
${}_2S_2$	904.23	0.487	1.04	903.92	-0.034	904.50	0.029	904.57	0.038
${}_2S_3$	804.17	0.511	1.10	804.66	0.061	805.04	0.109	805.21	0.130
${}_2S_4$	724.87	0.234	0.45	724.76	-0.016	725.02	0.021	725.20	0.045

Table A3.4 (cont.)

	Observed Data			Model A1		Model B1		Model B2	
Mode	Period (sec)	S.E.M. (sec)	95% C.I.	Period (sec)	Rel.Error %	Period (sec)	Rel.Error %	Period (sec)	Rel.Error %
${}_2S_5$	660.41	0.111	0.23					657.67	-0.112
${}_2S_6$	594.71	0.137	0.29			594.60	-0.018	594.82	0.018
${}_2S_8$	488.02	0.151	0.33	487.28	-0.151	487.65	-0.076	487.90	-0.024
${}_2S_9$	448.36	0.133	0.29	448.02	-0.076	448.37	0.002	448.63	0.061
${}_2S_{10}$	415.67	0.163	0.33	415.56	-0.026	415.89	0.052	416.15	0.114
${}_2S_{11}$	388.27	0.229	0.55	388.27	0.000	388.54	0.071	388.80	0.136
${}_2S_{12}$	365.12	0.188	0.40	364.92	-0.054	365.13	0.002	365.37	0.067
${}_2S_{13}$	344.88	0.186	0.44	344.59	-0.083	344.71	-0.050	344.91	0.010
${}_2S_{14}$	326.26	0.124	0.25	326.43	0.053	326.44	0.056	326.57	0.094
${}_2S_{15}$	309.20	0.055	0.15	309.02	-0.058	308.95	-0.081	308.87	-0.106
${}_3S_2$	580.80	0.700	1.40	580.61	-0.034	580.49	-0.054	580.47	-0.057
${}_3S_3$	489.05	0.359	0.82	488.02	-0.211	488.00	-0.215	487.94	-0.227
${}_3S_4$	439.18	0.476	1.05	439.08	-0.023	438.79	-0.088	438.90	-0.063
${}_3S_5$	415.11	0.221	0.51	415.17	0.047	414.87	-0.059	414.88	-0.055
${}_3S_6$	392.32	0.114	0.22	392.70	0.097	392.42	0.025	392.36	0.010
${}_3S_7$	372.05	0.126	0.28	372.72	0.180	372.45	0.108	372.38	0.090
${}_3S_8$	354.57	0.106	0.23	355.07	0.141	354.86	0.083	354.80	0.064

Table A3.4 (cont.)

Mode	Observed Data Period (sec)	S.E.M. (sec)	95% C.I.	Model A1 Period (sec)	Rel.Error %	Model B1 Period (sec)	Rel.Error %	Model B2 Period (sec)	Rel.Error %
${}_3S_9$	339.14	0.145	0.32	339.15	0.004	339.02	-0.034	338.98	-0.048
${}_3S_{10}$	323.80	0.111	0.23	324.45	0.201	324.41	0.187	324.39	0.181
${}_3S_{11}$	310.77	0.075	0.20	310.64	-0.043	310.68	-0.029	310.68	-0.028
${}_4S_1$	505.82	0.211	0.45	504.36	-0.288	504.14	-0.333	504.47	-0.267
${}_4S_2$	479.33	0.186	0.38	478.11	-0.255	478.00	-0.277	478.29	-0.217
${}_4S_3$	460.78	0.146	0.30	461.14	0.077	460.93	0.033	461.14	0.077
${}_4S_4$	420.10	0.089	0.19	420.19	0.021	420.22	0.029	420.14	0.009
${}_4S_5$	369.72	0.074	0.15	369.83	0.029	369.88	0.044	369.80	0.022
${}_4S_6$	332.11	0.082	0.18	332.08	-0.009	332.15	0.011	332.09	-0.005
${}_4S_7$	303.97	0.091	0.19	303.87	-0.033	303.95	-0.006	303.95	-0.007
${}_4S_8$	283.56	0.098	0.21	283.73	0.061	283.83	0.095	283.87	0.011
${}_4S_9$	269.66	0.058	0.13	269.81	0.054				
${}_4S_{10}$	258.86	0.049	0.10	258.94	0.032	259.03	0.064	258.96	0.038
${}_5S_2$	397.36	0.157	0.36	396.48	-0.221	396.78	-0.147	397.06	-0.075
${}_5S_3$	353.52	0.170	0.42	354.34	0.233	354.22	0.197	354.33	0.228

Table A3.4 (cont.)

Mode	Observed Data Period (sec)	S.E.M. (sec)	95% C.I.	Model A1 Period (sec)	Rel.Error %	Model B1 Period (sec)	Rel.Error %	Model B2 Period (sec)	Rel.Error %
${}_6S_1$	348.41	0.046	0.10	348.83	0.119	348.32	-0.027	348.37	-0.012
${}_6S_4$	293.19	0.132	0.28	293.21	0.006	293.13	-0.021	293.29	0.033
${}_6S_5$	273.52	0.046	0.11	273.54	0.009	273.35	-0.019	273.52	0.001
${}_7S_2$	310.07	0.079	0.17	309.97	-0.031	309.58	-0.158	309.67	-0.130
${}_7S_3$	281.37	0.113	0.25	281.33	-0.014	281.22	-0.053	281.23	-0.050
${}_7S_5$	239.96	0.028	0.06	240.21	0.103	239.90	-0.026	240.00	0.015
${}_8S_1$	272.10	0.144	0.31	271.57	-0.194	271.44	-0.244	271.77	-0.123
${}_8S_2$	247.74	0.022	0.05	246.77	-0.393	248.71	0.390	249.05	0.528

Table A3.4 (cont.)

Mode	Observed Data Period (sec)	Observed Data S.E.M. (sec)	Observed Data 95% C.I.	Model A1 Period (sec)	Model A1 Rel.Error %	Model B1 Period (sec)	Model B1 Rel.Error %	Model B2 Period (sec)	Model B2 Rel.Error %
${}_0T_2$	2640.63	10.104	23.84	2630.62	-0.379	2630.81	-0.372	2631.36	-0.351
${}_0T_3$	1705.83	2.529	5.47	1702.30	-0.213	1702.43	-0.205	1702.91	-0.177
${}_0T_4$	1305.45	0.926	1.91	1303.42	-0.155	1303.53	-0.147	1303.98	-0.113
${}_0T_5$	1075.97	0.820	1.68	1075.20	-0.072	1075.30	-0.062	1075.73	-0.022
${}_0T_6$	925.83	0.530	1.11	925.16	-0.072	925.26	-0.062	925.67	-0.018
${}_0T_7$	819.31	0.680	1.41	817.68	-0.199	817.76	-0.189	818.15	-0.142
${}_0T_8$	736.86	0.339	0.68	736.06	-0.109	736.13	-0.099	736.48	-0.051
${}_0T_9$	671.80	0.369	0.74	671.48	-0.047	671.53	-0.040	671.86	0.008
${}_0T_{10}$	618.98	0.294	0.58	618.82	-0.026	618.84	-0.023	619.13	0.025
${}_0T_{11}$	574.62	0.469	0.96	574.84	0.039	574.82	0.035	575.09	0.082
${}_0T_{12}$	536.84	0.337	0.70	537.44	0.112	537.37	0.099	537.62	0.145
${}_0T_{13}$	504.94	0.411	0.84	505.15	0.041	505.02	0.016	505.24	0.060
${}_0T_{14}$	475.73	0.363	0.75	476.91	0.247	576.73	0.209	576.92	0.251
${}_0T_{15}$	450.97	0.255	0.54	451.95	0.216	451.71	0.164	451.89	0.204
${}_0T_{16}$	429.19	0.270	0.56	429.68	0.115	429.40	0.049	429.56	0.085
${}_0T_{17}$	407.95	0.195	0.42	409.68	0.424	409.35	0.342	409.48	0.376
${}_0T_{18}$	390.94	0.283	0.58	391.58	0.163	391.20	0.066	391.32	0.096
${}_0T_{19}$	374.75	0.168	0.36	375.10	0.093	374.68	-0.019	374.78	0.008

Table A3.4 (cont.)

Mode	Observed Data Period (sec)	S.E.M. (sec)	95% C.I.	Model A1 Period (sec)	Rel.Error %	Model B1 Period (sec)	Rel.Error %	Model B2 Period (sec)	Rel.Error %
${}_0T_{20}$	359.59	0.291	0.62	360.03	0.121	359.57	-0.007	359.65	0.017
${}_0T_{21}$	345.82	0.296	0.65	346.17	0.100	345.67	-0.042	345.74	-0.022
${}_0T_{22}$	332.57	0.220	0.49	333.38	0.242	332.85	0.086	332.91	0.102
${}_0T_{23}$	321.21	0.291	0.63	321.52	0.097	320.98	-0.071	321.02	-0.058
${}_0T_{24}$	310.18	0.252	0.55	310.51	0.106	309.95	-0.075	309.98	-0.065
${}_0T_{25}$	299.51	0.206	0.51	300.24	0.244	299.66	0.051	299.68	0.057
${}_0T_{26}$	290.26	0.156	0.39	290.64	0.130	290.05	-0.072	290.06	-0.069
${}_0T_{27}$	281.21	0.444	1.13	281.64	0.153	281.05	-0.057	281.05	-0.058
${}_0T_{28}$	272.75	0.274	0.61	273.19	0.161	272.59	-0.057	272.58	-0.061
${}_0T_{29}$	264.53	0.324	1.01	265.24	0.267	264.64	0.041	264.62	0.034
${}_0T_{30}$	257.29	0.375	1.01	257.73	0.171	257.14	-0.060	257.11	-0.070
${}_0T_{31}$	249.85	0.239	0.59	250.64	0.316	250.05	0.080	250.02	0.067
${}_0T_{32}$	242.97	0.251	0.59	243.93	0.396	243.35	0.155	243.31	0.139
${}_0T_{33}$	236.71	0.235	0.62	236.71	0.365	237.00	0.120	236.95	0.102
${}_0T_{34}$	231.29	0.227	0.64	231.54	0.107	230.97	-0.140	230.92	-0.161
${}_0T_{35}$	224.93	0.346	0.86	225.79	0.384	225.24	0.137	225.18	0.112
${}_0T_{36}$	219.69	0.247	0.64	220.33	0.292	219.79	0.043	219.73	0.017
${}_0T_{37}$	213.89	0.214	0.67	215.13	0.578	214.59	0.328	214.53	0.298

Table A3.4 (cont.)

Mode	Observed Data Period (sec)	S.E.M. (sec)	95% C.I.	Model A1 Period (sec)	Rel.Error %	Model B1 Period (sec)	Rel.Error %	Model B2 Period (sec)	Rel.Error %
${}_0T_{38}$	209.83	0.593	2.54	210.16	0.157	209.65	-0.087	209.57	-0.124
${}_0T_{39}$	204.27	0.098	0.43	205.42	0.561	204.92	0.316	204.85	0.282
${}_0T_{40}$	199.96	0.381	1.06	200.88	0.460	200.39	0.216	200.32	0.180
${}_0T_{41}$	195.88	0.434	1.20	196.54	0.336	196.05	0.088	195.99	0.056
${}_0T_{42}$	191.26	0.254	0.70	192.38	0.585	191.91	0.338	191.83	0.297
${}_0T_{43}$	187.40	0.490	0.21	188.39	0.528	187.93	0.283	187.85	0.240
${}_0T_{44}$	183.78	0.270	0.75	184.57	0.431	184.12	0.182	184.03	0.138
${}_0T_{45}$	180.25	0.056	0.19	180.90	0.358	180.45	0.112	180.37	0.065
${}_0T_{46}$	176.85	0.056	0.19	177.36	0.289	176.93	0.046	176.84	-0.003
${}_1T_2$	756.57	0.625	1.36	757.47	0.118	756.80	0.030	756.99	0.055
${}_1T_3$	695.18	0.515	1.10	694.92	0.037	694.41	-0.109	694.52	-0.092
${}_1T_4$	629.98	0.627	1.74	630.87	0.014	630.50	0.083	630.56	0.092
${}_1T_6$	519.09	0.297	0.68	519.60	0.098	519.46	0.072	519.52	0.083
${}_1T_8$	438.50	0.230	0.59	438.94	0.099	438.89	0.088	439.01	0.117
${}_1T_{10}$	381.58	0.148	0.33	382.17	0.155	382.07	0.129	382.24	0.173
${}_2T_4$	421.81	0.363	0.78	420.29	-0.359	420.62	-0.283	421.05	-0.180
${}_2T_7$	363.66	0.283	0.62	363.72	-0.010	363.47	-0.053	363.59	-0.020
${}_2T_8$	343.46	0.219	0.50	343.75	-0.085	343.48	0.004	343.49	0.010

Table A3.5

Fit of the model to differential travel time data

Phase combination	Observed Data Δ (deg)	T (sec)	S.E.M. (sec)	95% C.I.	Model A1 T (sec)	ΔT (sec)	Model B1 T (sec)	ΔT (sec)	Model B2 T (sec)	ΔT (sec)
PcP - P	30.00	181.9	0,18	0.39	181.5	-0.5	181.0	-0.9	181.1	-0.8
surface	35.00	151.4	0.14	0.30	151.4	-0.0	151.3	-0.1	151.3	-0.1
focus	40.00	125.1	0.22	0.46	124.5	-0.7	124.5	-0.6	124.5	-0.6
	45.00	100.7	0.22	0.43	100.6	-0.1	100.8	0.1	100.7	-0.0
	50.00	79.9	0.19	0.39	79.8	-0.2	79.9	0.0	79.9	-0.0
	55.00	62.3	0.45	1.02	61.6	-0.7	61.8	-0.5	61.8	-0.5
	60.00	46.1	0.45	0.99	46.0	-0.1	46.1	0.0	46.2	0.1
	65.00	33.0	0.43	0.95	32.8	-0.3	32.8	-0.2	33.0	-0.0
	70.00	22.1	1.11	2.72	22.0	-0.2	21.8	-0.3	22.1	-0.0
	75.00	13.4	0.76	2.12	13.6	0.2	13.3	-0.8	13.6	0.2
PcP - P	30.00	162.2	0.27	0.69	161.9	-0.3	161.7	-0.5	161.7	-0.6
deep	35.00	133.1	0.78	2.17	134.1	1.0	134.1	1.0	134.0	0.9
focus	40.00	109.1	0.81	2.58	109.3	0.2	109.4	0.3	109.3	0.2
	45.00	87.3	0.28	0.61	87.7	0.4	87.8	0.5	87.7	0.4
	50.00	68.8	0.06	0.13	68.7	-0.1	68.8	0.0	68.8	-0.0
	55.00	52.5	0.19	0.53	52.3	-0.2	52.4	-0.1	52.4	-0.1
	60.00	37.5	0.23	0.49	38.2	0.7	38.3	0.8	38.4	0.9
	65.00	25.9	0.27	0.59	26.6	0.7	26.5	0.6	26.7	0.8
	70.00	17.2	0.25	0.59	17.3	0.7	17.0	-0.2	17.3	0.1

Table A3.5 (cont.)

	Observed Data				Model A1		Model B1		Model B2	
Phase combination	Δ (deg)	T (sec)	S.E.M. (sec)	95% C.I.	T (sec)	ΔT (sec)	T (sec)	ΔT (sec)	T (sec)	ΔT (sec)
P'(AB)	147.50	7.7	0.24	0.51	7.3	0.3	7.8	-0.1	7.0	0.7
-P'(DF)	152.50	20.6	0.28	0.58	20.5	0.1	20.9	-0.3	20.3	0.3
deep	157.50	35.1	0.19	0.39	35.3	-0.2	35.7	-0.6	35.2	-0.1
focus	165.00	60.8	0.31	0.64	60.3	0.5	60.7	0.1	60.4	0.4
	175.00	100.1	0.31	0.69	-	-	-	-	99.0	1.1
P'(BC)	146.25	2.5	0.30	0.71	2.4	0.1	2.5	0.0	2.1	0.5
-P'(DF)	148.75	4.9	0.11	0.23	5.3	-0.4	5.3	-0.4	5.0	-0.1
deep	151.25	7.6	0.20	0.42	8.0	-0.4	7.9	-0.3	7.6	-0.0
focus	153.75	9.0	0.24	0.58	10.4	-1.4	10.3	-1.3	10.1	-1.1
	156.25	10.8	0.34	0.77	12.7	-1.9	12.6	-1.8	12.4	-1.6

Table A3.5 (cont.)

	Observed Data				Model A1		Model B1		Model B2	
Phase combination	Δ (deg)	T (sec)	S.E.M. (sec)	95% C.I.	T (sec)	ΔT (sec)	T (sec)	ΔT (sec)	T (sec)	ΔT (sec)
ScS - S	30.00	311.3	0.80	1.77	309.7	-1.6	308.3	-3.0	309.4	-1.9
deep	35.00	259.4	0.71	1.53	258.7	-0.7	259.0	-0.4	259.1	-0.3
focus	40.00	215.7	0.66	1.62	213.4	-2.3	214.6	-1.1	214.4	-1.3
	45.00	174.3	0.52	1.11	173.4	-0.9	175.0	0.7	174.6	0.3
	50.00	138.6	0.69	1.44	138.6	-0.0	139.4	0.8	139.2	0.6
	55.00	108.5	0.58	1.25	108.7	0.2	108.7	0.2	108.7	0.2
	60.00	82.0	0.52	1.07	82.5	0.5	82.2	0.2	82.3	0.3
	65.00	59.7	0.44	0.92	60.0	0.3	59.4	-0.3	59.5	-0.2
	70.00	40.6	0.46	0.96	41.1	0.5	40.6	-0.0	40.6	0.0
	75.00	25.5	0.60	1.25	26.2	0.7	25.6	0.1	25.7	0.2
	80.00	14.0	0.37	0.80	14.6	0.6	14.4	0.4	15.0	1.0

Table A3.6

Fit of the models to absolute travel time data

Phase	Δ (deg)	J.B. (sec)	'68 Tables (sec)	A1 (sec)	B1 (sec)	B2 (sec)
P (surface focus)	30	372.5	369.5	370.5	370.9	370.6
	35	416.1	413.3	414.5	414.4	414.2
	40	458.1	455.7	456.8	456.5	456.4
	45	498.9	497.4	497.3	497.0	496.8
	50	538.0	535.2	536.0	535.6	535.5
	55	575.4	572.2	573.0	572.6	572.5
	60	610.7	607.4	608.3	608.0	607.7
	65	644.0	640.9	642.0	641.7	641.4
	70	675.4	672.7	673.7	673.6	673.2
	75	705.0	702.6	703.5	703.5	703.1
	80	732.7	730.6	731.4	731.5	731.0
	85	758.5	756.6	757.4	757.4	756.9
	90	782.7	780.7	781.7	781.5	781.1
	95	805.7	803.9	804.9	804.6	804.2
PcP (surface focus)	30	554.9	552.1	552.1	551.9	551.7
	35	568.6	565.9	565.9	565.7	565.5
	40	583.9	581.1	581.2	581.0	580.8
	45	600.5	597.7	597.9	597.7	597.5
	50	618.3	615.5	615.8	615.6	615.4
	55	637.0	634.3	634.6	634.4	634.3
	60	656.6	653.9	654.3	654.1	654.0
	65	676.9	674.2	674.7	674.5	674.4
	70	697.8	695.1	695.7	695.5	695.3
	75	719.1	716.5	717.1	716.9	716.7
	80	740.6	738.0	738.8	738.5	738.5
	85	762.3	759.9	760.8	760.5	760.5
	90	784.2	781.9	782.9	782.7	782.7

Table A3.6 (cont.)

Phase	Δ (deg)	J.B. (sec)	'68 Tables (sec)	A1 (sec)	B1 (sec)	B2 (sec)
PKP (surface focus)	180 A	1330.6	1327.8	-	-	1328.5
	170	1286.3	1283.7	1284.0	1283.4	1283.6
	160	1242.7	1239.7	1239.9	1239.3	1239.3
	150	1200.2	1196.9	1197.3	1196.8	1196.6
	145 B	1180.4	1178.0	1178.0	1177.4	1177.3
	145 B	1179.3	1174.4	1178.0	1177.4	1177.3
	150	1190.7	1188.1	1192.7	1191.8	1192.0
	155 C	1201.7	1201.0	1205.3	1204.3	1204.6
	110 D	1113.2	1113.0	1114.8	1114.0	1114.9
	120	1132.7	1132.1	1133.6	1132.7	1133.0
	130	1152.0	1151.3	1152.3	1151.4	1151.8
	140	1170.5	1170.1	1170.4	1169.5	1170.0
	150	1187.4	1186.8	1187.2	1186.2	1186.8
	160	1200.8	1200.0	1200.9	1200.0	1200.4
	170	1209.2	1208.4	1209.8	1208.9	1209.3
	180 F	1212.2	1211.0	1212.9	1212.1	1212.4
PKiKP (surface focus)	10		996.9*	996.9	996.2	996.3
	20		1000.1	1000.3	999.6	999.6
	30		1005.7	1005.8	1005.1	1005.1
	40		1013.2	1013.4	1012.7	1012.8
	50		1022.8	1023.0	1022.3	1022.4

* Data for PKiKP from Engdahl et.al. [1970, Table 1].

Table A3.6 (cont.)

Phase	Δ (deg)	J.B. (sec)	H&R [1970a] (sec)	A1 (sec)	B1 (sec)	B2 (sec)
S (surface focus)	30	670.2	669.5	672.0	675.0	671.7
	35	748.2	749.0	751.5	752.8	751.9
	40	824.5	825.7	829.5	828.8	828.6
	45	897.9	899.5	704.2	902.5	903.1
	50	968.6	970.5	975.9	973.9	974.6
	55	1036.8	1038.7	1044.4	1043.2	1043.8
	60	1102.6	1104.1	1109.7	1109.2	1109.6
	65	1165.5	1166.7	1172.4	1172.5	1172.9
	70	1225.6	1226.4	1233.1	1233.2	1233.7
	75	1282.6	1283.2	1290.4	1290.6	1291.1
	80	1336.5	1337.3	1344.9	1344.8	1345.3
	85	1387.3	1388.5	1395.8	1395.7	1395.5
	90	1435.5	1436.9	1444.2	1443.7	1442.0
	95	1478.2	1482.4	1489.1	1488.6	1490.6
ScS (surface focus)	30	1011.0		1016.6	1016.4	1016.7
	35	1036.4		1042.2	1042.0	1042.4
	40	1064.6		1070.6	1070.5	1070.8
	45	1095.1		1101.7	1101.5	1101.9
	50	1127.8		1135.1	1134.8	1135.2
	55	1162.5		1170.2	1169.9	1170.3
	60	1198.8		1207.0	1206.6	1207.1
	65	1236.4		1245.1	1244.7	1245.2
	70	1275.2		1284.2	1283.9	1284.5
	75	1315.0		1324.2	1323.9	1324.5
	80	1355.5		1364.9	1364.6	1365.4
	85	1396.5		1406.3	1405.8	1406.8
	90	1437.8		1447.9	1447.3	1448.5
	95	1479.2		1489.5	1489.0	1490.6

Table A3.7

Fit of the models to auxillary differential travel time data

Phase Combination	Δ (deg)	H&R (sec)	A1 (sec)	B1 (sec)	B2 (sec)
SKKS-SKS (surface focus)	85	8.2*	6.4	6.4	6.3
	90	15.4	13.4	13.4	13.2
	95	23.9	23.0	22.8	22.7
	100	33.9	34.1	33.9	33.9
	105	45.2	46.7	46.2	46.1
	110	57.9	59.8	59.4	59.3
	115	72.0	73.9	73.5	73.6
	120	87.6	88.8	88.5	88.6
	125	104.8	104.7	104.5	104.2
SKS-S (surface focus)	85	6.4†	6.4	7.0	6.3
	90	22.0	24.8	24.9	22.7
	95	39.4	42.5	42.6	44.1

* SKKS-SKS data from Hales and Roberts [1971, Eqn.3].

† SKS-S data from Hales and Roberts [1970a, Table 4].